DGU

DANMARKS GEOLOGISKE UNDERSØGELSE · SERIE A · NR. 19

MILJØMINISTERIET · Geological Survey of Denmark

Geochemical investigation of Potassium-Magnesium Chloride mineralization of Zechstein 2 salt, Mors Dome, Denmark

Microthermometry on solid inclusions in quartz crystals

BY

JOHANNES FABRICIUS

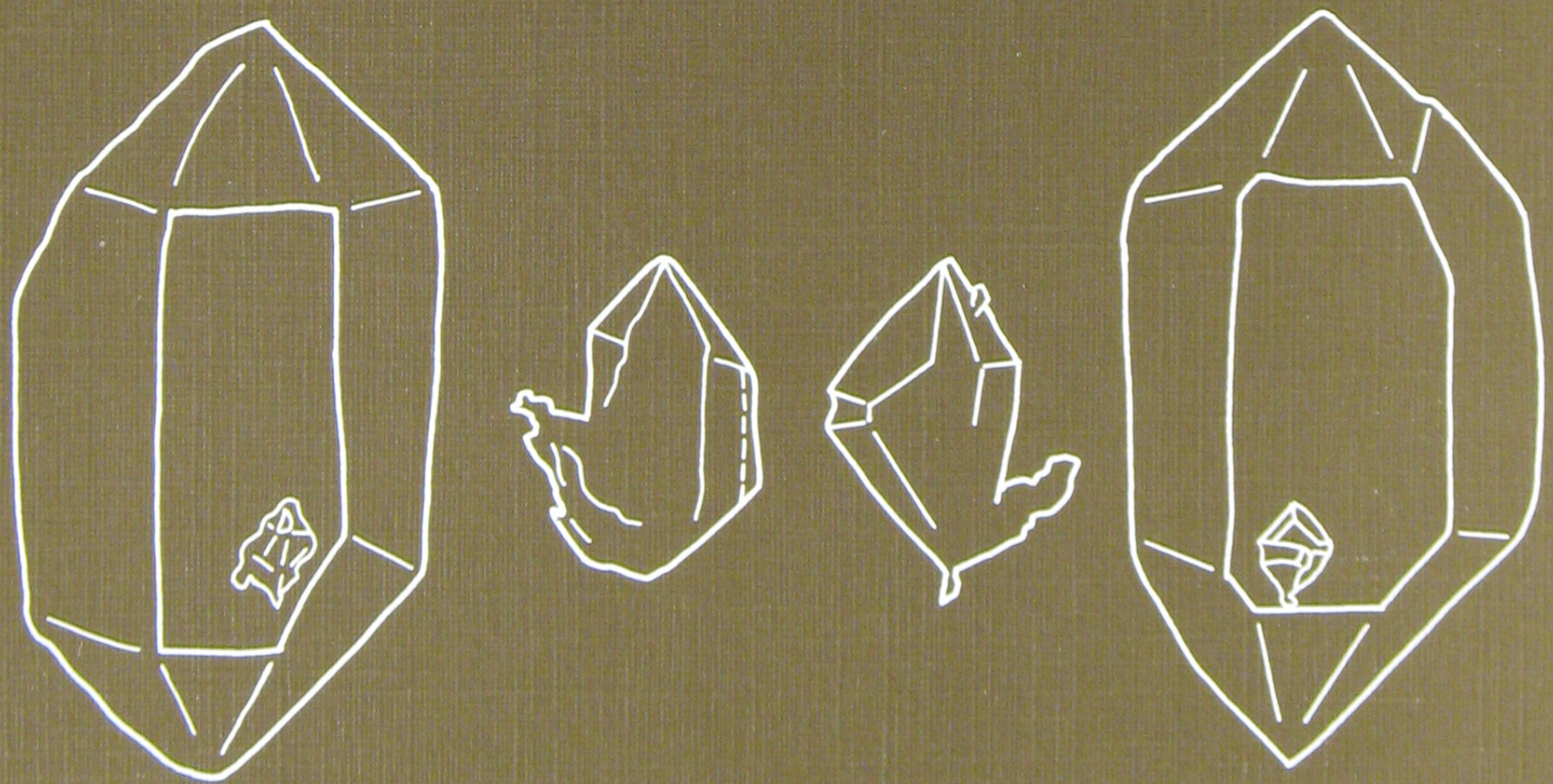

I kommission hos C. A. Reitzels forlag · København 1987

DANMARKS GEOLOGISKE UNDERSØGELSE · SERIE A · NR. 19
MILJØMINISTERIET · Geological Survey of Denmark

Geochemical investigation of Potassium-Magnesium Chloride mineralization of Zechstein 2 salt, Mors Dome, Denmark

Microthermometry on solid inclusions in quartz crystals

BY
JOHANNES FABRICIUS

I kommission hos C. A. Reitzels forlag · København 1987

Key words:
Quartz, Chemical composition, Carnallite, P,T conditions, Salt domes.

With 5 plates

DGU Serie A nr. 19
ISBN 87-421-0751-2
ISSN 0901-0270
Oplag: 1200
Tryk: AiO Tryk as, Odense
Tegning: Eva Melskens
Dato: 15-12-1987
Johannes Fabricius, DGU
Thoravej 8, 2400 København NV
Redaktion: Leif Banke Rasmussen

Contents

Abstract

Solid-rich inclusions at 20°C of the Na-K-Mg-Cl-H_2O system, found in euhedral quartz from the top of Zechstein 2 salt in the Mors dome, Denmark, were objects of microthermometrical investigation.

The quartz crystals, all of the long prismatic, slender type, average length of 750 μm, are genetically closely connected to the intercalated clay in the deck halite Na2r.

The inclusions are faceted negative crystals, crystallographically orientated with the host quartz. Carnallite ($KMgCl_3 \cdot 6H_2O$) is the main daughter mineral, followed by tetrahydrate ($MgCl_2 \cdot 4H_2O$) and minor sylvite (KCl). Halite (NaCl) is found as grains in suspension in the trapped solutions. The trapped solutions represent melts of carnallite or tetrahydrate saturated with NaCl. The concentrations range from 167 mol $MgCl_2$ + 83 mol K_2Cl_2 +3 mol Na_2Cl_2 per 1000 mol H_2O to 250 mol $MgCl_2$ + 5 mol K_2Cl_2 + 0 mol Na_2Cl_2 per 1000 mol H_2O, corresponding to salinities from 52 to 62 weight%. Melting temperatures measured, 170-185°C, and estimated pressures, 80-110 MPa, are minimum trapping values.

In a few cases highly irregular, "dry" grains of carnallite, containing dissolved high-pressure gas, were observed to have been trapped.

In this study it is shown that the melting temperature of carnallite in a closed space, where evaporation is prevented, depends on the prevailing pressure. It is also shown that high-pressure gas is dissolved in trapped grains of carnallite or halite, but not in the solutions.

Finally, the results lead to the proposal of a model, related to time and space, of the metamorphism of an original carnallitic potash bed and subsequent K-Mg-Cl mineralization of the deck halite. The original paragenesis kieserite-halite-carnallite, sedimented in the deeper parts of the basin, was altered to the present kieseritic hard salt by means of progressive geothermal metamorphism from Upper Triassic to Lower Cretaceous. The hanging wall of the potash bed, the deck halite, was mineralized by the metamorphic solutions, squeezed out from the potash bed, possibly during the diapiric penetration phase in Upper Jurassic – Lower Cretaceous.

Introduction and previous studies

The present work is an amplification of an earlier study (Fabricius 1987) concerning solid-rich inclusions with compositions belonging to the Na-K-Mg-Cl-H_2O system.

The main topic of the previous work was microthermometrical studies of fluid inclusions in euhedral quartz crystals found in the deck halite of Zechstein 2 from the well Erslev-1 in the Mors salt dome. These fluid inclusion contain carnallite as a daughter mineral at room temperature. The carnallite dissolves congruently during heating runs either under the vapour pressure of the highly saline solution (type I) or in the interval 0.1 – c. 75 MPa (type II). Both types are small primary irregular fluid inclusions situated on a crystallographic *m*-interface. The solid:liquid ratio ranges from very small (type I) to slightly larger than 1 (type II).

The salinity of the equilibrium solution, type I and II, at the total dissolution temperature of carnallite, T_m car., obtained in these previous studies, is illustrated in fig. 1. The shaded area outlines schematically the carnallite stability field (fig. 6A). The dots on fig. 1 represent the concentrations of $MgCl_2$ and KCl in inclusions also containing a cube of sylvite. The outermost left dot represents 29.2 weight% $MgCl_2$ plus 7.4 weight% KCl. The outermost right dot represents 42.4 weight% $MgCl_2$ plus 9.2 weight% KCl.

Fig. 2 illustrates the concentrations of Na_2Cl_2, K_2Cl_2 and $MgCl_2$ in mole per cent of the equilibrium solution at the total dissolution temperature of carnallite in 35 inclusions. The mean concentrations of type I, type II, and their mutual mean value are also plotted.

The type II inclusions allow construction of a proposed pressure-dependent melting curve of carnallite, melting incongruently to sylvite and solution. Some measurements of the present study support the proposal (fig. 11). The proposed melting curve is verified by autoclave experiments (Fabricius and Rose-Hansen, in prep., fig. 8).

In the present study only solid inclusions (at room temperature) are dealt with, fourteen selected solid inclusions from the previous studies and eleven new ones.

The previous and the present studies are part of a paragenesis/geochemistry project concerning K-Mg zones in the Danish Zechstein salt. The main purpose of the investigation is to elucidate the relations between the chemical and mineralogical compositions of the K-Mg-Cl rocks and the metamorphic pressure-temperature conditions occuring in salt deposits.

Fig. 1. The salinity of the equilibrium solution versus the dissolving temperature of daughter carnallite, type I and II inclusions. The dots represent the concentrations of $MgCl_2$ and KCl ranging from 29.2 wt.% $MgCl_2$ + 7.4 wt.% KCl (outermost left) to 42.4 wt.% $MgCl_2$ + 9.2 wt.% KCl (outermost right). After Fabricius (1987, Fig. 7 and Table 2).

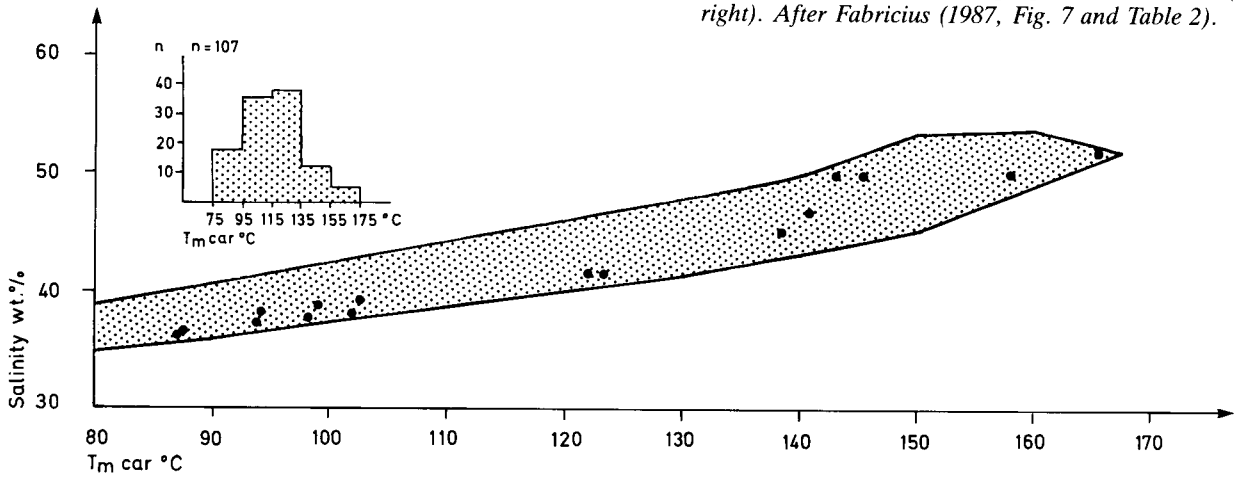

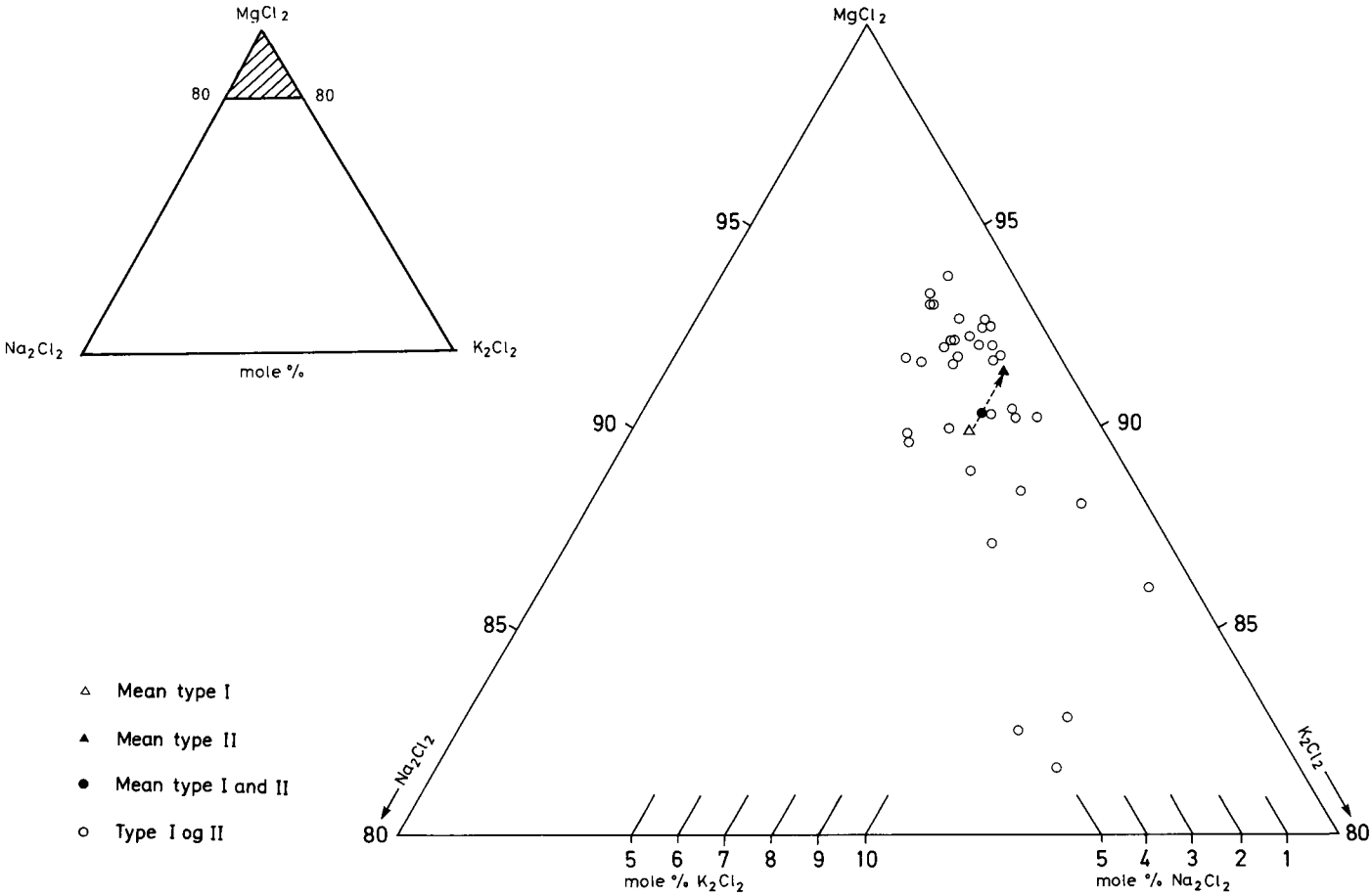

Fig. 2. Estimated compositions of the equilibrium solutions at the temperature of total dissolution of carnallite in 35 inclusions. Based on measurements from Fabricius (1987).

Geological setting

The Danish Subbasin forms the south-eastern branch of the Northern Permian Basin (Ziegler 1981, fig. 10). During Zechstein time 4 evaporite cycles (Z1-Z4) precipitated in the Danish Subbasin. Fig. 3 shows the extension of the Zechstein sediments, the main dome area, and depth contours to the pre-Zechstein reflector. It is seen that the Mors dome is situated centrally in the basin and that a 8000 m depth contour is found close to the Mors dome in a southern direction.

The stratigraphy of the Danish Zechstein evaporites is given in table 1 and fig. 5A. The four Zechstein cycles correspond to the North German Zechstein 1 – 4 cycles. The symbols used in table 1 and fig. 5 are those proposed by Richter-Bernburg (1953, p. 852) and refer to the main minerals in the layer: Na – halite, A – anhydrite, Ca – carbonate, (K) – potassic salt, K – potash zone (mainly sylvite), T – (Salz-) Ton = salt clay. The Veggerby Potash Zone K2 corresponds to the famous German Flöz Stassfurt (Richter-Bernburg 1962, p. 71).

The interpretation of the stratigraphy (table 1 and fig. 5A) is based on the works of Richter-Bernburg (1962, 1981) and Jacobsen (1984).

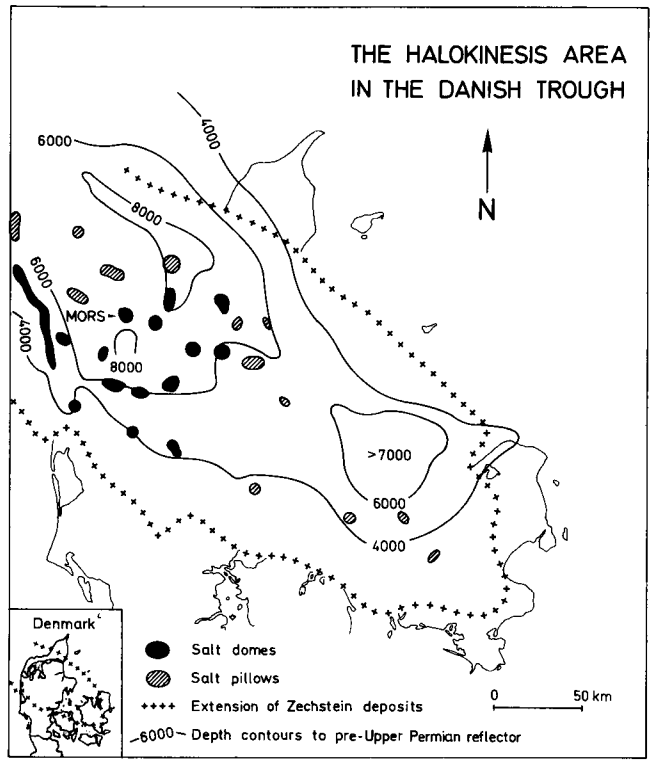

Fig. 3. The Zechstein basin with the halokinesis area. Simplified after Michelsen et al. (1981, Fig. 1).

Table 1. Stratigraphy of the Danish Zechstein.

Cycle	Symbol	Depth m	Lithology
Z4	Na4	20	*rock salt,* light grey to pale orange, clayey.
	T4	30–40	*salt clay,* medium olive brown to olive grey to greyish black, silty clay and claystone, with rock salt.
Z3	Na3	c.100	*rock salt,* red to brownish to greyish, coarse crystalline, with disseminated anhydrite and two thin potash zones and one thin bed of anhydrite.
	T3	15–60	*salt clay,* sand-, silt-, claystone, red and green to greyish black, with rock salt.
Z2	Na2r	15	*deck halite,* yellowish red to orange red, kieseritic, potassic, with disseminated carnallite and anhydrite, clayey.
	K2	10	*hard salt,* kieserite, halite, sylvite, and anhydrite, clayey. *Veggerby Potash Zone.*
	Na2(K)	20	*rock salt,* reddish to brownish red, potassic and kieseritic.
	Na2	c.600	*rock salt,* light to medium grey, occ. colourless, translucent, coarse crystalline with disseminated anhydrite.
	Ca2	12–14	*anhydrite-dolomite zone,* alternating layers of anhydrite, dolomite, and limestone, medium grey.
Z1	A1r	1	*anhydrite,* bluish grey, compact.
	Na1	c.400	*rock salt,* light to medium grey, occ. colourless, translucent, coarse crystalline with disseminated anhydrite.

Fig. 4 shows the profile NNE-SSW of the Mors dome according to seismic measurements (Richter-Bernburg 1981, p. 34). The stratigraphy of the well Erslev-1 is seen to be very complicated with inverted, interfolded, and overthrusted layers. The bottom part, shown on fig. 5B, is even more complicated, especially below the Veggerby Potash Zone K2 at a depth of c. 2690 – c. 2740 m. K2 is not repeated but the deck halite Na2r is repeated three times, and the salt clay T3 with the rock salt Na3 four times. At a depth of 3000 m the youngest cycle Z4 appears, also inverted. Z4 (= T4+Na4) is repeated twice.

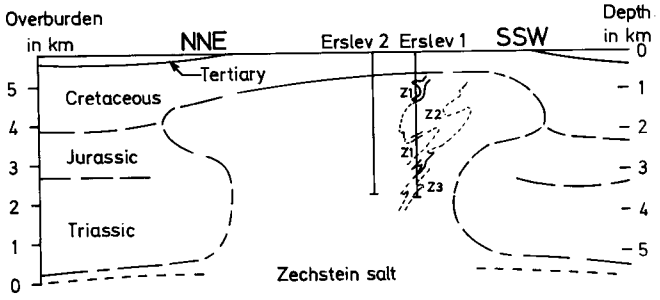

Fig. 4. The Mors dome with the two wells Erslev 1 and 2. The stratigraphy and tectonics of Erslev 1 as interpreted by Richter-Bernburg (1981). Note the depths of the overburden outside the dome at various times.

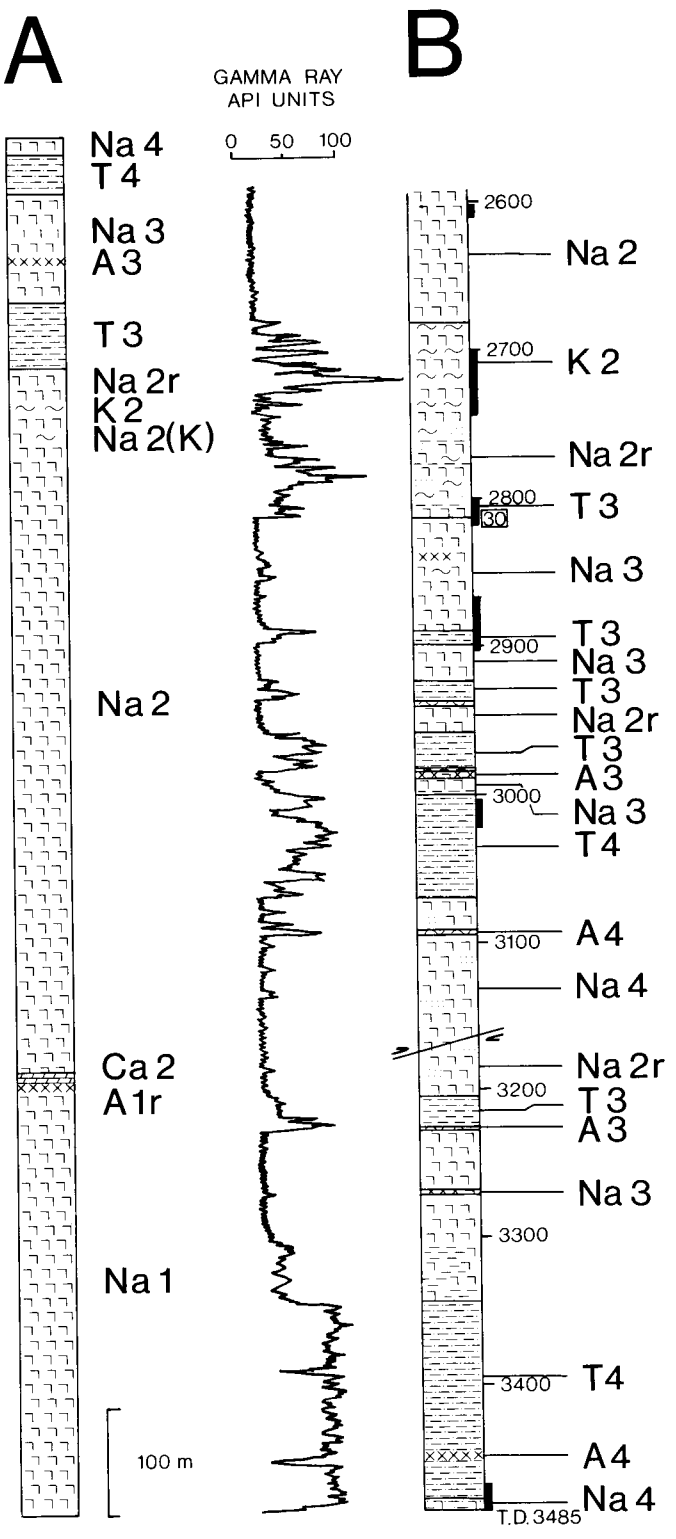

Fig. 5 A. Idealized stratigraphic column of the Danish Zechstein evaporites. B. The bottom part of the well Erslev 1, interpreted by Jacobsen (1981).

Materials and methods

Abbreviations

T	Temperature, °C.
T_b	Disappearence T of the liquid shrinkage bubble.
T_m	Melting/dissolving T.
T_r	Re-formation or formation T.
T_n	Nucleation T of gas bubble, high-pressure (HP) or shrinkage.
tot.	Totally.
part.	Partly.
inc.	Incipient.
HP	High-pressure gas bubble.
car.	Carnallite, $KMgCl_3 \cdot 6H_2O$.
sy.	Sylvite, KCl.
ha.	Halite, NaCl.
tet.	Tetrahydrate, $MgCl_2 \cdot 4H_2O$.
hex.	Bischofite, $MgCl_2 \cdot 6H_2O$.
oct.	Octahydrate, $MgCl_2 \cdot 8H_2O$.
dod.	Dodecahydrate, $MgCl_2 \cdot 12H_2O$.
Com.	Comments.

Materials

Core No. 30 from the well Erslev-1 drilled at a depth of 2800 m in the Mors dome (fig. 5B and 13) consists of mixed deck halite Na2r and salt clay T3. From the top of the core a piece of approximately 500 g salt and clay was cut. The salt was dissolved and the residue was examined. The quartz crystals were separated from the residue by the aid of heavy liquids and by hand picking with a small brush. The crystals were examined under the microscope and the usable crystals (1-2%) with solid inclusions of the Na-K-Mg-Cl-H_2O system were eventually studied by the aid of a ChaixMeca cooling heating device.

The quartz crystals

The quartz crystals are all of the long-prismatic, doubly terminated form $m + r + z$. The length of the crystals ranges from a few μm to 1.2 – 1.4 mm. The average length of the usable crystals, i.e. longer than 0.3 – 0.5 mm, is approximately 0.7 mm. The number of crystals per 500 g core material is very great compared with the number of crystals from the "grey salt" Na1 and Na2 (Fabricius 1985, p. 251).

No twins are found. The *m* faces are often developed with a mosaic structure (pl. III, fig. 4) which is never found on the *r* or z faces. The *m* faces are very rarely horizontally striated.

As a rule, one large crystal is intergrown with a few other, much smaller crystals. Alternatively, the crystals form aggregates of one or two large crystals intergrown with many small crystals, which occasionally form irregular thin plates similar to the crystal lining in vugs. The intergrown crystals and the aggregates often prevent a proper study of the inclusions, because the upside *m* face should be perpendicular to the optic axis of the microscope in order to prevent optical distortion of the inclusion.

The large number of crystals in the examined core compared with the grey salt suggests another source of silica than seawater. Thick sections of the Na2r-T3 salt very clearly show that the quartz crystals are found always in connexion with clay, intercalated in the salt.

In many of the crystals a large irregular hole is to be found in one or both of the pyramids or, rarely, in the prism (pl. I and II). In connexion with these holes there is always a "front" of small fluid inclusions (pl. III, figs. 5, 7). The front follows the contours of the hole at a distance of 40-75 μm, either as a thin waving veil of extremely small inclusions, or a waving curtain of larger fluid inclusions a size of up to 30 × 15 μm.

The inclusions, the vapour bubble, and released high-pressure gas

The inclusions studied in the present work are large and isolated, primary inclusions. A few of the inclusions have 1-3 much smaller neighbouring fluid inclusions.

All the inclusions are classified as solid inclusions at room temperature with an extremely large solid:liquid (S:L) ratio. Two of the inclusions – x-29.1 and x-67.1 – have a S:L ratio of approximately 5:1. These two inclusions are the only two that reacted upon freezing, forming ice and various $MgCl_2$ hydrates.

Regular inclusions with shapes ranging from spheroids over more or less elongated ellipsoids and box-like forms to negative crystals. Practically all the inclusions are faceted with crystal faces. Most, or perhaps all, of the negative crystals actually occur on lineage bounda-

ries, i.e. in the crystallographically orientated mosaic structure of the *m* faces (Buerger 1932, p. 229, Skinner 1953, p. 548) (pl. III, fig. 4). The present shapes of the inclusions have not necessarily been inherited from the time of their formation. They may have been irregular inclusions, which have been modified through geologic time in the direction of lowest possible energy level, i.e. bounded by crystal planes (Tuttle 1949, p. 335, Roedder 1971, p. 332, 1981b, p. 123).

In H_2O-rich inclusions, where the net decrease in SiO_2 solubility with temperature allows the precipitation of silica in the edges of pre-existing negative crystals, rounded equilibrium shapes may form (Swanenberg 1980, p. 83).

A few of the inclusions terminate in a small "tail" in the direction of the c-axis of the host quartz. The "tail" is connected with the main inclusion through a narrow short tube (pl. I and II). The "tail" was possibly formed in connexion with the modelling of the faceted inclusion, perhaps by liquid "in excess".

The average size of the inclusions is approximately 35 x 25 x 25 μm with the shortest dimension down to c. 15 μm and the longest dimension up to c. 100 μm.

The liquid shrinkage vapour bubble is very small at room temperature compared with the volume of the inclusion because of the large S:L ratio. The liquid is concentrated in a small void or hollow formed by the liquid on the surface of the solids filling up the inclusion (pl. III, fig. 2).

In some of the inclusions the bubble is a liquid shrinkage vapour bubble containing no high-pressure gas. During heating runs no Brownian bubble movements are observed, indicating highly viscous brines. The brines are syropy in consistency (Holser 1979, p. 230). The dynamic viscosity of a bischofite solution is c. 5 poises at 20°C, i.e. 500 times higher than the viscosity of water (Sonnenfeld 1984, pp. 50-51).

It is very important to measure the bubble disappearance temperature T_h during the first heating run, because HP gas is released, as a rule, when trapped grains of carnallite, sylvite, or halite are totally melted or dissolved during the run.

During the first heating run, where all solid phases are melted/dissolved, a certain amount of fluid is released, and the S:L ratio decreases. The liquid shrinkage bubble will then be larger, at room temperature, than before the first heating run. But the disappearence temperature T_h will be the same in the following runs, if no HP gas is released from the solid phases.

The vapour pressure of a saturated $MgCl_2$ solution is 3.4 mm Hg at 20°C, 80.5 mm Hg at 100°C, and 774.5 mm Hg at 160°C (Grube and Bräuning 1938, table 1). As the vapour pressure is high at high temperatures, the shrinkage bubble contains significant amounts of $MgCl_2$ and KCl (Roedder 1981a, p. 11, Ramboz et al. 1982, p. 38).

Irregular inclusions. Two of the inclusions (x-1.3, pl. II, fig. 5 and x-33.1, pl. II, fig. 6) are large, highly irregular, solid inclusions with no vapour bubble before the first heating run. A grain consisting of carnallite and intergrown sylvite was trapped during the crystallization of the host quartz. As no liquid is visible, the inclusions are classified as being "dry" in spite of the presence of a saturated H_2O dipole film (Kühn 1952, pp. 150, 155).

At the total melting of the carnallite component, HP gas was released, proving the trapping of solid carnallite. Consequently, the melting temperature T_m car.tot. is a *maximum* trapping temperature T_t , i.e. the maximum formation temperature of the host quartz.

Also in these two cases more HP gas was released, when the sylvite component was brought to solution.

Released high-pressure gas. Fluid inclusions and gas inclusions are frequently present in secondary salt minerals which formed deep below the surface under certain geological conditions, and in recrystallized salt rocks (Baar 1977, p. 32).

The solubility of gases in salt solutions decreases rapidly as the salinity increases. The solubility also decreases with increasing temperature (Discussion). As the trapping temperature (175-180°C) and the salinities (50-60 weight%), measured in the present work, are high, only negligible amounts of gas can dissolve in the bitterns. Therefore, released gas proves the trapping of solid salt grains suspended in the solutions. These accidentally trapped salt grains are not daughter minerals.

The gas is bounded interstitially between the salt crystals (pl. III, fig. 6) and/or in the lattice interstices or where the lattice is disordered or has vacancies (Müller and Heymel 1956, p. 315, Baar 1958, p. 139, 1960, p. 132, Giesel 1968, 1972, p. 235).

Carnallite commonly contains a large amount of gases under high confining pressure in very fine, microscopic pore spaces that are not interconnected. Potash salts, in general, contain many times the quantity of gas found in halite (Sonnenfeld 1985, pp. 260-261). Therefore, if an inclusion before the first heating run contains grains of carnallite and halite and no gas is released during the melting of the carnallite grains during the first heating run, the total melting temperature of the carnallite grains, T_m car.tot., is a *minimum* trapping temperature of this particular inclusion. The trapped grain of halite dissolves totally at a much higher temperature (275-300°C) in the highly saline K-Mg-Cl solution formed, whereby HP gas is released.

PLATE I

The black signature on the quartz crystals at Figs. 2, 4, 5, 8, and 12 illustrates holes in the crystals after now dissolved carnallite. The solid:liquid ratio in all the inclusions is extremely large, i.e. the solid phase practically fills up the entire inclusion with the liquid and a shrinkage bubble gathering in a small void in the surface of the solid phase. Note on Figs. 7 and 8 the small "tails" in the direction of the crystallographic c-axis. The inclusion x-71.1 (Fig. 12) is weakly faceted on the side not shown.

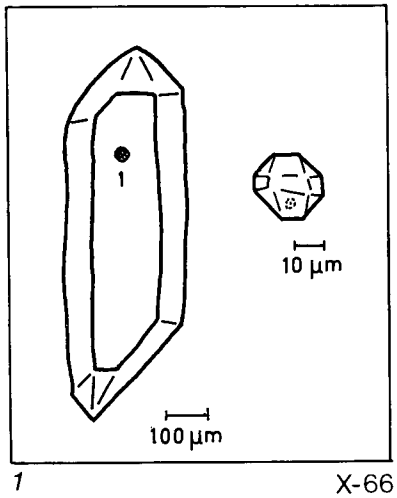

1 X-66

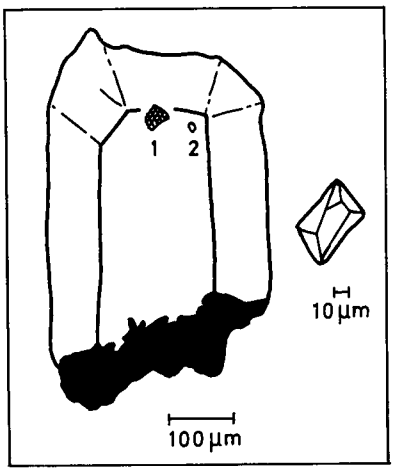

2 X-16

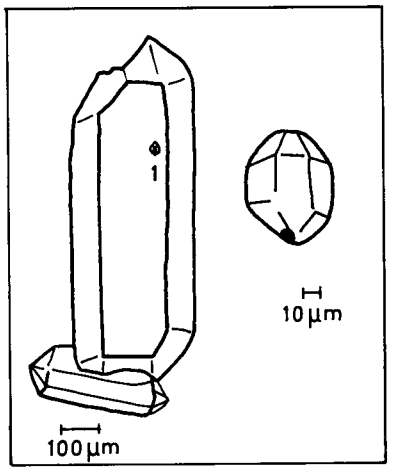

3 X-41

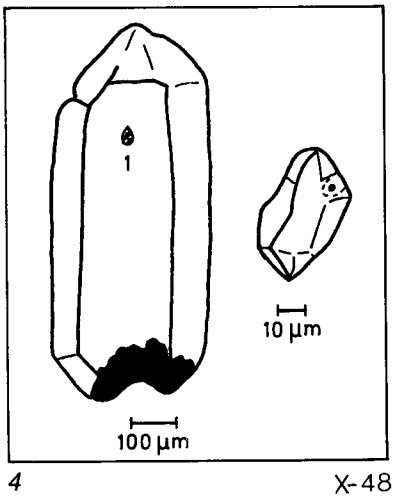

4 X-48

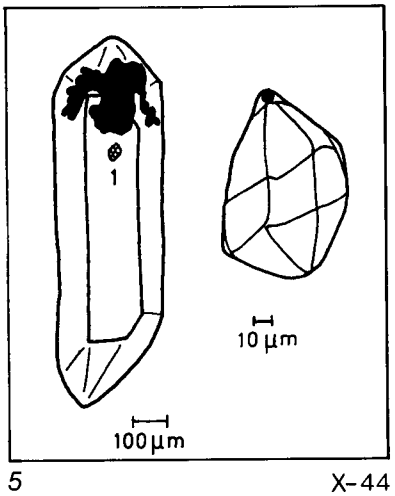

5 X-44

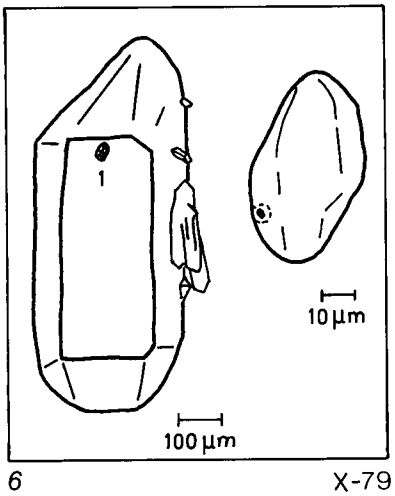

6 X-79

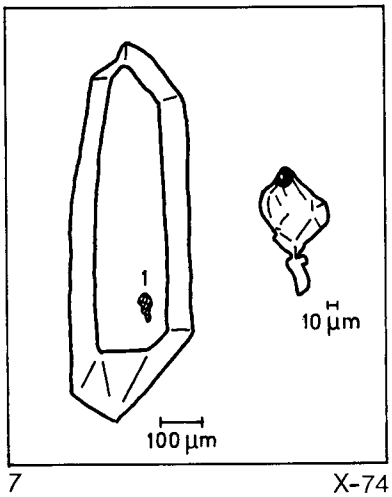

7 X-74

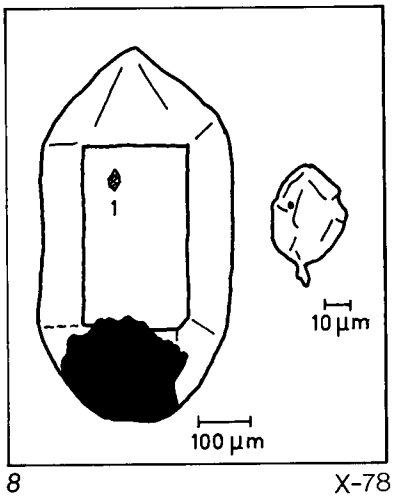

8 X-78

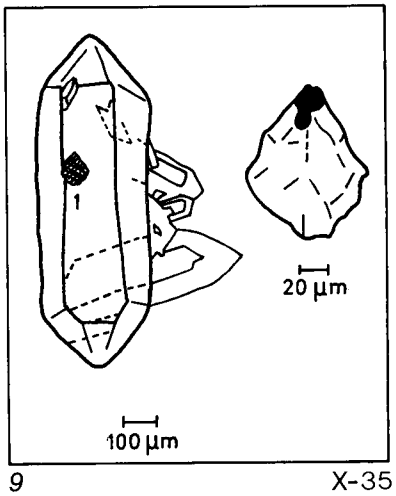

9 X-35

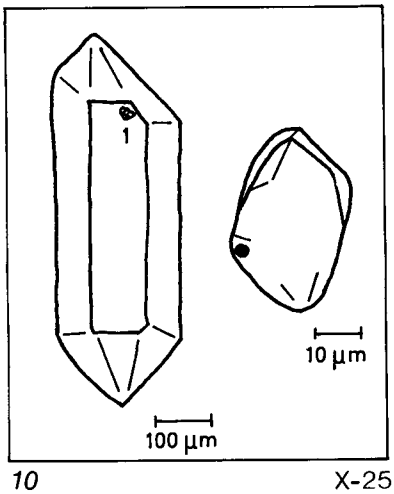

10 X-25

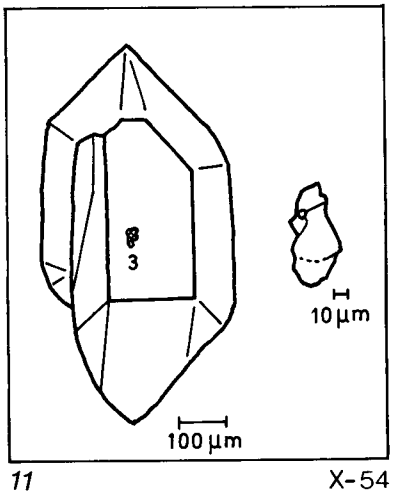

11 X-54

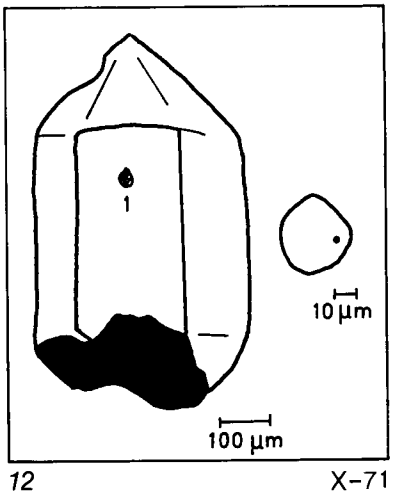

12 X-71

PLATE II

Figs. 2, 3, and 6 show holes (black) after now dissolved carnallite. The triangular prisms on both sides of the up-turned m face refract the vertical beam of light, so no light from these prisms enters the objective of the microscope. The prisms are more or less opaque. On Fig. 6 we see inclusion x-33.1. When the inclusion is observed through the m face $(10\bar{1}0)$, the m face $(1\bar{1}00)$ is practically opaque, and the inclusion is almost invisible, Fig. 6, right.

Note the large hole after now dissolved carnallite in the prism at Fig. 6. The inclusion x-33.1 consists of a trapped grain of carnallite with an intergrown grain of sylvite.

The inclusion x-51.1 (Fig. 1) is very weakly faceted.

Fig. 7 exhibits the inclusion x-67.1 seen through four different prism faces. The inclusion was studied in position C and D, because the positions A and B were optically distorted by the quartz wedge formed by the rhombohedron faces.

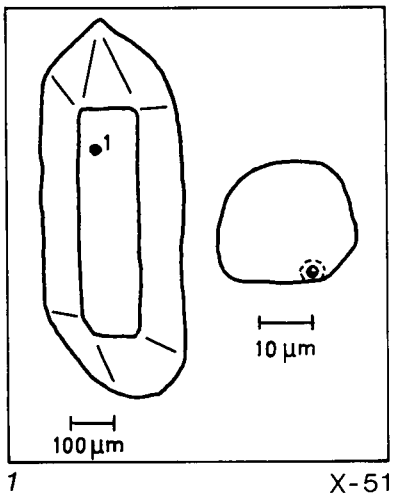

1 X-51

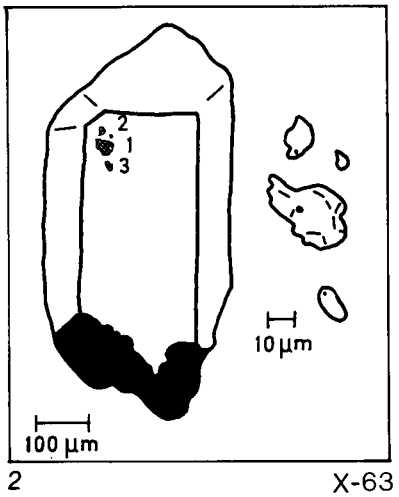

2 X-63

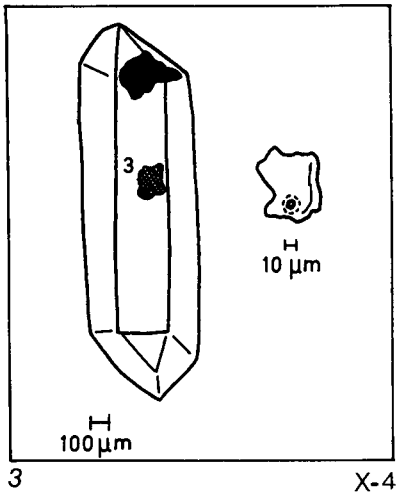

3 X-4

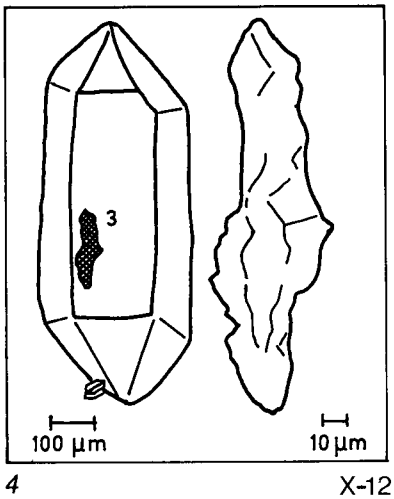

4 X-12

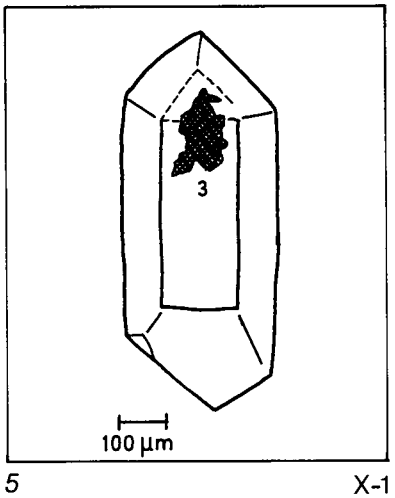

5 X-1

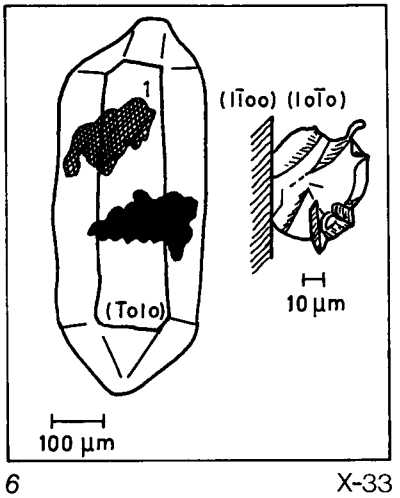

6 X-33

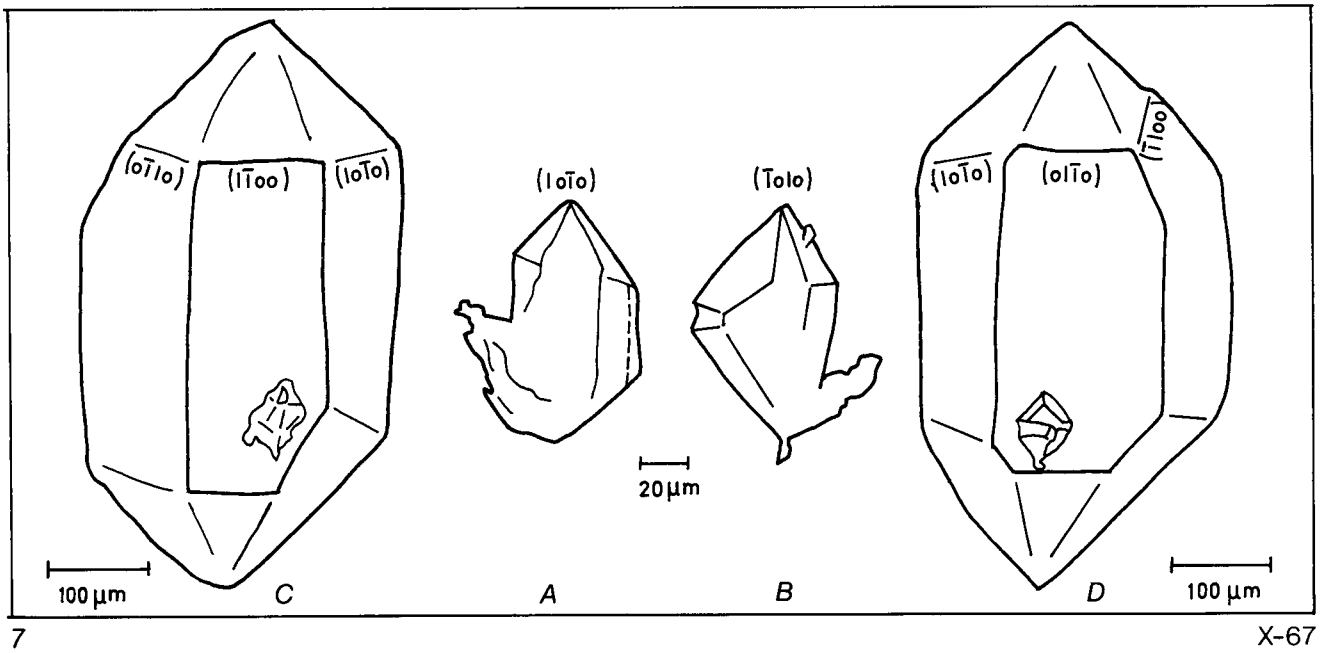

7 X-67

Phase diagrams of the Na-K-Mg-Cl-H_2O system

The phase diagram of fig. 6A is a simplified diagram after d'Ans and Sypiena (1942, fig. 2). The construction of the diagram is based on results obtained at atmospheric pressure and the solutions saturated with NaCl.

The stability fields of KCl, $KMgCl_3 \cdot 6H_2O$, $MgCl_2 \cdot 6H_2O$, $MgCl_2 \cdot 4H_2O$, and $MgCl_2 \cdot 2H_2O$ are marked with thick lines. The isotherms are drawn with thin full lines. These isotherm curves show a minimum solubility of KCl in a solution with a concentration of c.

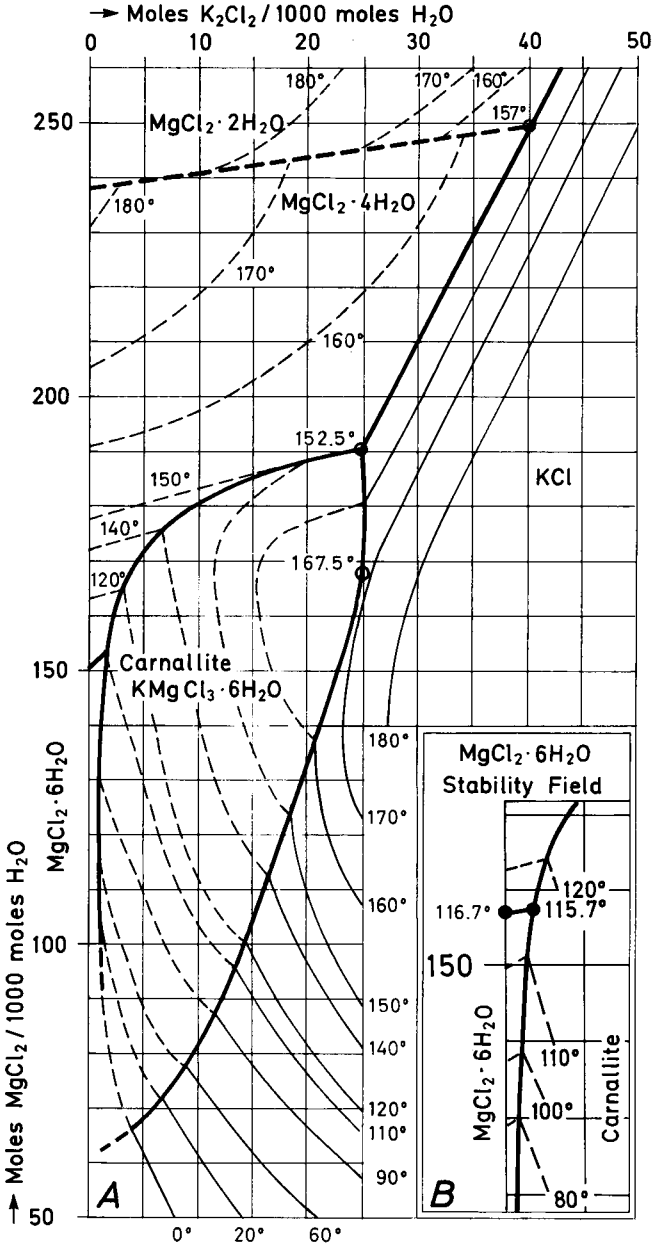

Fig. 6 A and B. Phase diagram of the system KCl-$MgCl_2$-H_2O, saturated with NaCl at atmospheric pressure. The temperatures are degrees centigrade. After d'Ans and Sypiena (1942, Fig. 2).

135 mol $MgCl_2$ per 1000 mol H_2O. The KCl-isotherms in the $KMgCl_3 \cdot 6H_2O$ (carnallite), $MgCl_2 \cdot 4H_2O$ (tetrahydrate), and $MgCl_2 \cdot 2H_2O$ (dihydrate) stability fields are drawn with thin dashed lines, because of lack of systematic determinations.

The point marked 167.5°C is the temperature of incongruent melting of carnallite under atmospheric pressure as determined by van't Hoff and Meyerhoffer (1899). The isotherms in the vicinity of this point in the carnallite stability field curve around the point. The melting point 167.5°C is a temperature maximum on the equilibrium melting curve of KCl and $KMgCl_3 \cdot 6H_2O$, whereby a KCl-isotherm is a tangent in the melting point.

In the transition point marked 152.5°C, 120 mol $KMgCl_3 \cdot 6H_2O$ plus 70 mol $MgCl_2 \cdot 4H_2O$ give 70 mol KCl plus an equilibrium solution consisting of 25 mol KCl plus 190 mol $MgCl_2$ per 1000 mol H_2O (d'Ans and Sypiena 1942, p. 93).

D'Ans (1961, p. 126) notes that two dissolution curves intersect in the transition point 152.5°C:

1. Carnallite (s) + $MgCl_2 \cdot 4H_2O$ (l)
2. KCl (s) + $MgCl_2 \cdot 4H_2O$ (l),

where the liquid systems are saturated with NaCl.

It is worth having in mind that the consequences are that dry carnallite transforms to KCl and $MgCl_2 \cdot 4H_2O$ at 152.5°C during liberation of water vapour, and a melt must form above 152.5°C, besides the precipitates. Serowy and Tittel (1959, p. 24) mention experiments, which confirm these consequences.

Presence of KCl in the solution depresses the temperature of 181.5°C for the tetrahydrate-dihydrate transition with 1°C per 1.5 mol K_2Cl_2/1000 mol H_2O. The transition temperature was found to be 157°C, marked in the diagram at c. 249 mol $MgCl_2$ and 40 mol K_2Cl_2 (d'Ans and Sypiena 1942, p. 93).

The upper part of the $MgCl_2 \cdot 6H_2O$ (bischofite) stability field is shown on fig. 6B. The transition temperature bischofite-tetrahydrate is 116.7°C. With 1.5 mol K_2Cl_2 in solution, this temperature is lowered 1°C to 115.7°C, also given in the diagram.

The block diagram of fig. 7 shows the stability fields of sylvite, carnallite, and the $MgCl_2$ hydrates at atmospheric pressure. The transition temperatures are taken partly from fig. 6 and partly from table 2. The concentrations of $MgCl_2$ and K_2Cl_2 are mol per 1000 mol H_2O.

Solid phases in the inclusions, characterizations and identification

As the inclusions derive from metamorphism solutions penetrating the deck halite Na2r, the solutions must be saturated with NaCl at the moment of trapping by the quartz crystals.

The daughter minerals and trapped minerals noted below are found in the inclusions. The refractive in-

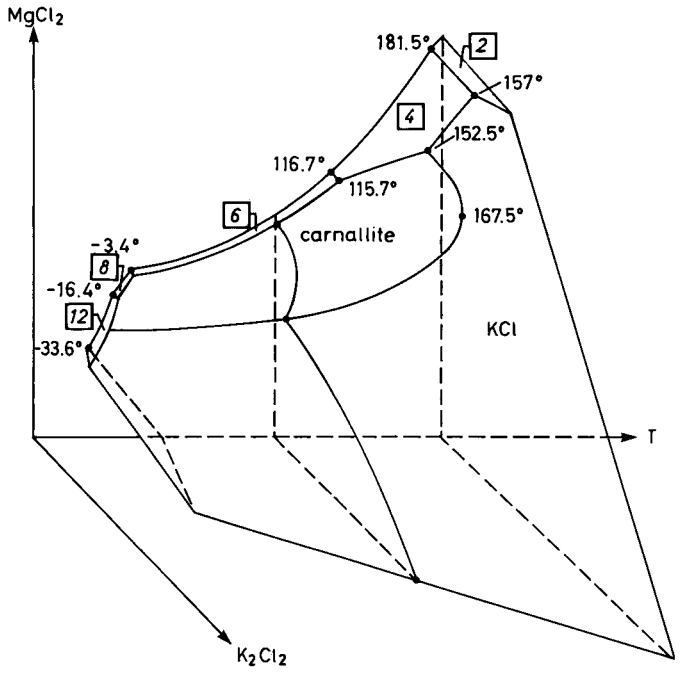

Fig. 7. Three-dimensional phase diagram of the system KCl-$MgCl_2$-H_2O, saturated with NaCl, atmospheric pressure. The numbers in the open squares refer to the various $MgCl_2$ hydrates. Note the vaulted surface of the carnallite stability field. After Findlay (1907).

dices are measured at 20°C, except for dodecahydrate: -25°C. The indices at the actual, much higher dissolving/melting temperatures are unknown.

Simple salts

Halite, NaCl, is cubic and isotropic with a refractive index of 1.5443, very close to n_o of quartz: 1.5442. D = 2.168 g/cm^3. The Temperature Coefficient of Solubility TCS = 0.015 (Borisenko 1978, table 2).

A solution with a concentration of 36 weight% $MgCl_2$ contains only 0.33 wt.% NaCl at 35°C (Meyer et al. 1949, p. 1237).

Zdanovskij (1949, p. 585, fig. 5) found at 105°C that the solubility of NaCl decreased dramatically from c. 28 wt.% to very small values close to zero, when the concentration of $MgCl_2$ increased from zero to c. 43 wt.%, equals c. 140 mol/1000 mol H_2O.

Fig. 8 shows the NaCl polytherms at fixed $MgCl_2$ concentrations, after d'Ans and Sypiena (1942, fig. 5, table 2). 166 2/3 mol $MgCl_2$/1000 mol H_2O correspond to the concentration of $MgCl_2$ in carnallite (6 mol H_2O). The concentration of Na_2Cl_2 is 4.4 mol/1000 mol H_2O at 180°C in a solution containing 166 2/3 mol $MgCl_2$/1000 mol H_2O, corresponding to 1.5 wt.% NaCl and 46.2 wt.% $MgCl_2$. At 20°C the concentration of Na_2Cl_2 is extremely small, so the daughter halite represents 1.5 wt.% NaCl. The halite precipitates on the surface of the trapped grain of halite and no cube of daughter halite is visible.

The curve of 166 2/3 mol $MgCl_2$ is extrapolated to 300°C, the approximate dissolving temperature of halite in suspension in solutions of the present work. The concentration of Na_2Cl_2 at 300°C is between 25 and 30 mol/1000 mol H_2O, giving a concentration of 8-9 wt.% NaCl and 43-42 wt.% $MgCl_2$. Therefore, the trapped grain of halite represents 6-7 wt.% NaCl or 20-25 mol Na_2Cl_2/1000 mol H_2O at 180°C. But the actual solutions contain an appreciable amount of dissolved KCl (c. 30 mol K_2Cl_2 at 180°C), which diminishes the solubility of NaCl due to the "common ion effect" and to the fact that KCl being much more soluble than NaCl in $MgCl_2$ solutions. Consequently, the trapped grain of halite is somewhat overestimated.

The solubility of NaCl increases by 10 per cent in the system NaCl-H_2O during an increase of pressure from atmospheric pressure to 70 MPa, corresponding to the hydrostatic pressure at a depth of 5000 m (Holser 1979, p. 242-243). It is assumed that the pressure-dependent

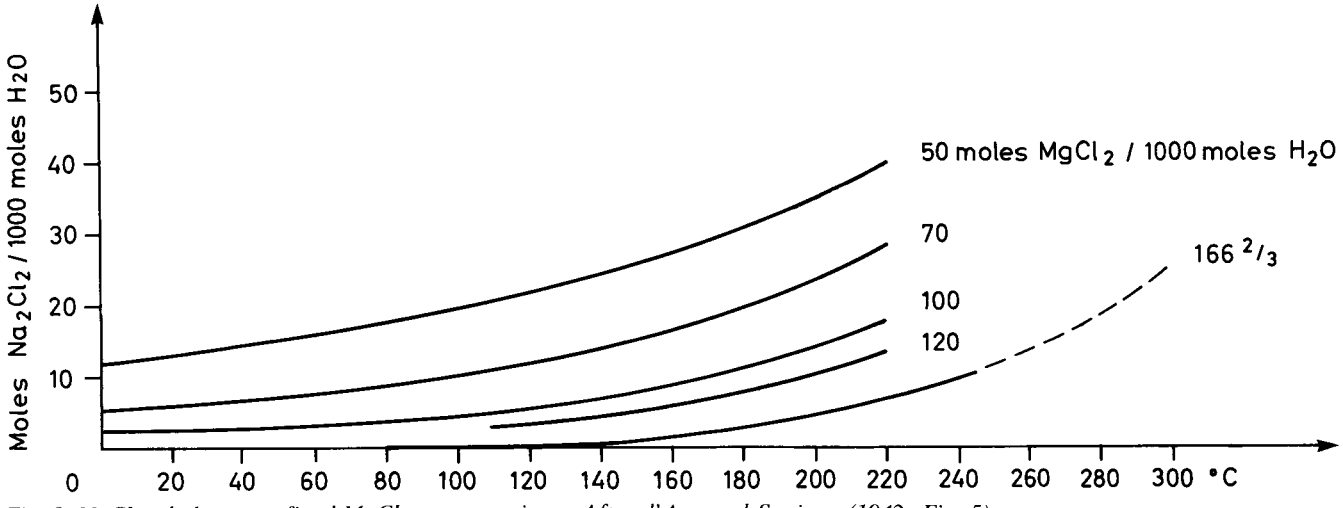

Fig. 8. NaCl-polytherms at fixed $MgCl_2$ concentrations. After d'Ans and Sypiena (1942, Fig. 5).

solubility of NaCl in the actual highly concentrated bitterns is of the same order of magnitude.

The grains of halite in the inclusions were trapped under pressures of 75 – 125 MPa (table 15). The pressure in the inclusions at room temperature equals the vapour pressure of the bitterns. Consequently, the solubility of NaCl drops more than 10 per cent, resulting in precipitation of NaCl on the surfaces of the trapped grain of halite. Therefore, the pressure effect causes an overestimate of the size of the trapped grain of halite.

The volumetric expansion of halite is 2.3 % from 25°C to 200°C (Skinner 1966, p. 80). This pressure increase is negligible, because NaCl dissolves with a small volume reduction, and because the solubility increases with increasing pressure.

In the vast majority of the inclusions, small grains of halite were suspended in the solutions during the trapping. These grains normally dissolved totally within a temperature interval of 275-300°C. High-pressure gas is released after total dissolution, which, in connexion with the high dissolving temperatures, proves the trapping of solid grains of halite, i.e. the halite is not a daughter mineral. During a test run the dissolved NaCl re-forms spontaneously, being the first solid phase during the following cooling period. The re-formation temperature $T_r$ha is normally within the range of 160-140°C, i.e. the solution is strongly supercooled. The formation of crystallization seeds calls for supersaturation with NaCl (Buckley 1934, p. 228, Tollert 1956, p. 247).

Halite re-forms characteristically in a reticulate pattern (pl. III, figs. 11, 12), which recrystallizes to one or two oblate grains, rarely to cubes or octahedrons. In strongly supersaturated solutions, NaCl crystallizes as octahedrons, not as cubes (Hartman 1979, p. 146). Comment No. 6 on table 13.

Sylvite, KCl, is cubic and isotropic with a refractive index of 1.490, close to n_z of carnallite: 1.494. D = 1.99 g/cm^3. TCS = 0.16, much greater than TCS of halite (Holser 1979, p. 284). Because of their significantly different solubilities, sylvite and halite are easily differentiated during heating tests. During heating of the ternary system from room temperature to 100°C, KCl solubility increases rapidly, whereas NaCl solubility actually decreases a small amount (Sterner and Bodnar 1984, p. 2661). Sylvite is more cryophilic than halite in a $MgCl_2$ solution (Borchert and Muir 1964, fig. 7.2).

In the present work, in very few cases a suspended grain of sylvite was accidentally trapped with the solution. The total melting temperature T_m sy.tot. of these grains is within the interval of 290 – 300°C. These grains are not daughter minerals.

In inclusions, containing solutions with a $MgCl_2$ -concentration higher than 190 mol/1000 mol H_2O, cubes of KCl are often found at room temperature. These cubes are true daughter minerals, because T_m sy.tot. of the cubes vary from c. 120°C up to the trapping temperatures. T_m sy combined with the final melting temperature T_m tet.tot. of the $MgCl_2 \cdot 4H_2O$ gives the concentration of KCl of the trapped solution, fig. 10.

With a concentration of 166 2/3 mol $MgCl_2$/1000 mol H_2O in the solution, the concentration of K_2Cl_2 drops approximately 25 mol at a temperature decrease from 180°C to 20°C, corresponding to c. 10 wt.% KCl (fig. 6A).

During a heating run sylvite re-forms during the cooling period after total melting of the last solid phase in connexion with the re-formation of halite. Sylvite forms instantaneously as small round grains ("pearls"), much less supercooled (20-40°C) than the halite (130-150°C). This feature is caused by the much higher TCS value of sylvite than that of halite (Kühn 1950/51, p. 112). The "pearls" recrystallize slowly into a few large round grains. This recrystallization is not as fast as the recrystallization of halite, which may be due to the higher solubility of sylvite than that of halite.

Finally, sylvite is formed during the incongruent melting of carnallite, which is the main identification of carnallite in contrast to $MgCl_2 \cdot 4H_2O$. This incongruently formed sylvite dissolves in the interval 185-215°C.

Magnesium chloride hydrates. $MgCl_2 \cdot nH_2O$

Rising brine temperatures cause a progressive dehydration of hydrated solute species (Sonnenfeld 1984, p. 73). Stability fields for hydrates in the $MgCl_2$-H_2O system are given in table 2.

Table 2. Temperature (°C) stability fields of $MgCl_2 \cdot nH_2O$.

$MgCl_2 \cdot nH_2O$	van't Hoff und Meyerhoffer 1898	Strakhov 1962
$MgCl_2 \cdot 12H_2O$	−33.6 – −16.4	−33.6– −16.4
$MgCl_2 \cdot 8H_2O$ (β)	−17.4 – −9.6	−40.0– −15.0
$MgCl_2 \cdot 8H_2O$ (α)	−16.4 – −3.4	−15.0– −3.4
$MgCl_2 \cdot 6H_2O$, metastable	/	−15.0– −5.0
$MgCl_2 \cdot 6H_2O$	−3.4 – 116.67	±0– 116.0
$MgCl_2 \cdot 4H_2O$	116.67– 181	116.0– 181.5
$MgCl_2 \cdot 2H_2O$	>181 – (182)	181.5– 300.0

Fig. 9 shows the temperature-solubility curve of the $MgCl_2$-H_2O system below zero °C based on measurements by Bergman and Luzhnaya (1951). The transition temperatures deviate very little from the temperatures of van't Hoff and Meyerhoffer (table 2).

Dodecahydrate, $MgCl_2 \cdot 12H_2O$, crystallizes in the monoclinic system. D=1.241 g/cm^3 (Sasvari and Jeffrey 1966, p. 875). The refractive indices n_x = 1.423, n_y = 1.427, n_z = 1.432 are lower than the indices of carnallite. TCS=2.2 (Borisenko 1978, table 2).

The dodecahydrate is well known combined with $CaCl_2$ hydrates from fluid inclusions in quartz crystals from the grey salt Na1 and Na2 (Fabricius 1984, fig. 6).

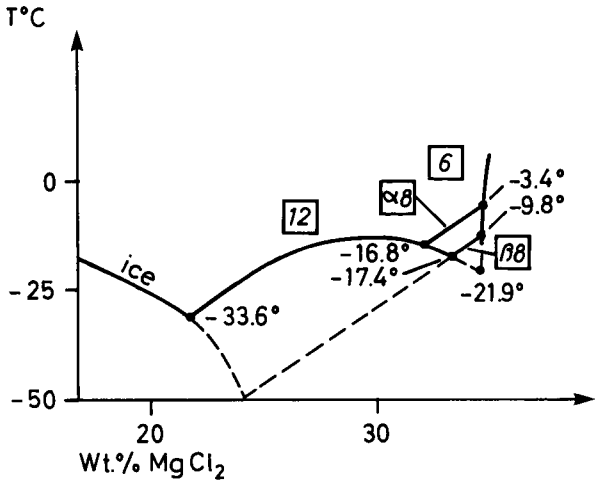

Fig. 9. The temperature-solubility curve of the $MgCl_2$-H_2O system below zero °C. The numbers in the open squares refer to the hydrate. After Strakhov (1962, Fig. 117).

The freezing point depression of the dodecahydrate gives the $CaCl_2$:$MgCl_2$ ratio (weight%) of the NaCl saturated solution (Luzhnaya and Verescetina 1964, figs. 3, 5, and 7).

Octahydrate, $MgCl_2 \cdot 8H_2O$, is dimorphic (van't Hoff and Meyerhoffer 1898). According to Grube and Bräuning (1938, p. 134) $MgCl_2 \cdot 8H_2O$ may form an unstable phase between -17.4°C and -9.6°C. The refractive indices of α-octahydrate are smaller than 1.5442, n_o of quartz.

Bischofite, hexahydrate, $MgCl_2 \cdot 6H_2O$, crystallizes in the monoclinic system, pseudotrigonal. Colourless, vitreous. The refractive indices $n_x = 1.495$, $n_y = 1.507$, $n_z = 1.528$ are higher than the indices of carnallite and sylvite. D = 1.604 g/cm³, (e.g. Braitsch 1962, 1971, table 3). TCS = 0.2 (Borisenko 1978, table 2).

According to Dietzel and Serowy (1959, p. 9), Derby and Ingve (1916) have measured the upper limit of the stability field to be 117.2°C, by means of vapour pressure measurements. Dietzel and Serowy (1959, p. 16) observed the same temperature by a radiographic method and different solubility methods. The equilibrium solution contains 164.9 mol $MgCl_2$/1000 mol H_2O, equals 46.6 wt.%, having a density of 1.4325 g/cm³ at 117.25°C (fig. 10). And at 25°C with 35.54 wt.% $MgCl_2$ the density is 1.341 g/cm³ (Lee and Egerton 1923, table III).

At a temperature of about 117°C (depending on water content and impurity level) bischofite melts incongruently into a saturated solution of tetrahydrate, $MgCl_2 \cdot 4H_2O$, with about 1 wt.% tetrahydrate in the solid phase. These crystals of tetrahydrate dissolve at 129°C (van Eekelen et al. 1981, p. 390).

Under atmospheric pressure, the melting point (116.7°C) is lowered 1°C per 1.5 mol K_2Cl_2/1000 mol H_2O in the solution (d'Ans and Sypiena 1942, p. 93).

The melting temperature of bischofite is pressure-dependent with an increase of 1°C per 10 MPa. The pressure-dependent melting curve is practically linear up to 500 MPa (Geller 1930, p. 151).

During the cooling in a closed system after total melting of bischofite the vapour pressure above 117°C is the vapour pressure of a solution saturated with tetrahydrate. Below 117°C, the vapour pressure is at first the pressure of a solution supersaturated with tetrahydrate. But at 102°C the tetrahydrate in excess suddenly precipitates, resulting in a dilution of the solution from its supersaturated equilibrium to a normal saturation, now having the vapour pressure of a solution saturated with bischofite. Eventually, bischofite precipitates, coating the precipitated tetrahydrate and thereby preventing the tetrahydrate from forming bischofite (Haug 1933, p. 19). Urai (1983, p. 126) observed that molten bischofite, when cooled from above 130°C, between 120°C and 117°C becomes saturated with $MgCl_2 \cdot 4H_2O$. Precipitation of this phase occured very unpredictably in the form of a few vol.% of needle shaped crystals.

Through vapour pressure measurements of pure bischofite, Grube and Bräuning (1938, p. 138) observed that bischofite re-formed spontaneously at 98.5°C, forming a wet crystal mush. Between 117°C and 98.5°C the system is unstable and the vapour pressure is higher than the vapour pressure of the stable bischofite at 98.5°C. The vapour pressure of the saturated solution at 98.5°C increases from 93.8 to 167.0 mm Hg within several days. During heating of bischofite, the vapour pressure has its maximum at 110°C, resulting in a rapidly increasing solubility.

Bischofite forms by alteration of carnallite in water (Sonnenfeld 1984, p. 456). In the Stassfurt potash zone (K2), Germany, d'Ans and Kühn (1960, p. 79) and Richter and Klarr (1984, p. 98) have observed secondary bischofite deriving from the high-temperature incongruent decomposition of carnallite. This secondary bischofite is found intergrown in the carnallite masses (Herrmann 1980, p. 442).

Bischofite was not observed in any inclusion of the present work before the first heating run. But after total melting of the carnallite, secondary bischofite was observed in most of the inclusions. The bischofite reforms spontaneously but incomplete as diffuse clouds and coatings on the inclusion walls or, very rarely, as a wet crystal mush. The re-formation temperature is always below 100°C and the crystallization continues several degrees below the re-formation temperature. This behaviour may be due to the consuming of heat (-19.19 KJ/cm³) during the crystallization contrary to halite (+11.64 KJ/cm³), sylvite (+36.91 KJ/cm³), and carnallite (+20.76 KJ/cm³) (Sonnenfeld 1984, table 3-1).

Identification of bischofite:

i. Optical properties: anisotropic; refractive indices

larger than the indices of carnallite, but smaller than the indices of quartz within the stability field of bischofite.

ii. Precipitation properties: after re-formation of carnallite, precipitation below 100°C.

iii. Melting properties: melts incongruently at 117°C ± depending on pressure and concentration of KCl.

Tetrahydrate, $MgCl_2 \cdot 4H_2O$. Crystal system and refractive indices are unknown. Dietzel and Serowy (1959, p. 15) measured the transition temperature tetrahydrate-dihydrate to be 181.0°C in a $MgCl_2$ solution with a concentration of 237.5 mol $MgCl_2$/1000 mol H_2O. Fig. 10 shows the concentration of the equilibrium solution *versus* the temperature from 70°C to 200°C (Dietzel 1959, Annex I), combined with the density of the solution (Dietzel 1959, fig. 2).

The $MgCl_2$ polytherm of the equilibrium solution (fig. 10) changes markedly above 152.5°C (the dashed curve), when KCl is present in the solution, because KCl strongly lowers the transition temperature tetrahydrate-dihydrate (d'Ans and Sypiena 1942, p. 93). In the point marked 152.5°C the solution consists of 25 mol K_2Cl_2, 190 mol $MgCl_2$, and 1000 mol H_2O and in the point marked 157.0°C: 40 mol K_2Cl_2, 249 mol $MgCl_2$, and 1000 mol H_2O (d'Ans and Sypiena 1942, p. 93, fig. 3).

A concentration of 1.5 mol K_2Cl_2 lowers the transition temperature by 1°C in accordance with the lowering of the melting temperature of bischofite.

The dashed curve of fig. 10 corresponds to the line 152.5°-157° on fig. 6A.

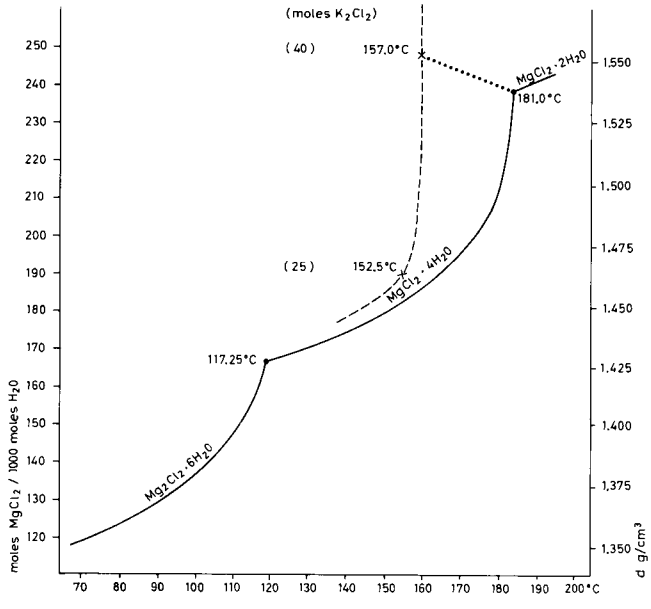

Fig. 10. Concentration and density of the equilibrium solution of the $MgCl_2$-H_2O system. After Dietzel (1959). The dashed curve shows the influence of KCl in the solution, see text. The density scale is only valid for the full curve – the pure $MgCl_2$-H_2O system.

Due to the high concentrations of $MgCl_2$ and the moderate temperatures, the full curve of fig. 10 is also valid for the NaCl-$MgCl_2$-H_2O system (Dietzel and Serowy 1959, p. 8).

If a melt of carnallite in a natural salt body is squeezed away from contact with the reaction sylvite from the incongruent melting of carnallite, the solution ($MgCl_2$ + 0.25KCl + $6H_2O$) first precipitates carnallite, when cooled down. Reaching a temperature of c. 130°C also tetrahydrate may form, which below 117°C is transformed to bischofite (Braitsch 1962, 1971, p. 192, Knipping and Herrmann 1985, p. 115). This process is seen in the inclusions of group C (table 9).

The re-formation after total melting of the tetrahydrate takes place in the temperature interval 135-125°C, 20-25°C lower than the re-formation temperatures of carnallite. And the re-formation is not as spontaneous as carnallite, and is only partial. The re-formed grains are larger and precipitation and recrystallization take place down to c. 115°C. Tetrahydrate is found as a daughter mineral only.

Identification of tetrahydrate:

i. Re-formation properties after total melting: reforms after supercooling to 135 – 125°C, c. 20°C lower than the re-formation temperature of carnallite in the same inclusion.

ii. Stability properties: metastable below 117°C, forming bischofite below 100°C.

Dihydrate, $MgCl_2 \cdot 2H_2O$, is not observed with certainty in the present study.

The double salt carnallite

Carnallite, $KMgCl_3 \cdot 6H_2O$, crystallizes in the orthorhombic system, pseudotrigonal. D = 1.60 g/cm³. Colourless to white, greasy. The refractive indices n_x = 1.466, n_y = 1.475, n_z = 1.494 are smaller than the indices of bischofite, (e.g. Borchert and Muir 1964, table 1). Polysynthetic twinning after {001} is common. Sometimes carnallite forms hexagonal tablets parallel to {001}.

The upper stability limit of carnallite under atmospheric pressure is 167.5°C (van't Hoff and Meyerhoffer 1899). The lower stability limit is -21°C (d'Ans 1933, Kühn 1952, p. 160).

When carnallite is heated in a closed system, where formation of vapour is prevented, an incongruent melting takes place, forming sylvite and a concentrated $MgCl_2$ solution (Jänecke 1915, pp. 41-42). Under these conditions at 167.5°C, carnallite decomposes into 75% sylvite and a solute consisting of the $MgCl_2$ + 25% KCl in the water of crystallization (Serowy and Tittel 1959, p. 12, Braitsch 1962, 1971, table 13). The salinity of this equilibrium solution is 43 wt.% $MgCl_2$ + 8 wt.% KCl.

The KCl solubility (347 g/l, 20°C) is much smaller than that of carnallite (645 g/l, 20°C) and decreases with an increasing magnesium chloride content of the brine (Schwerdtner 1964, p. 1113). During decreasing temperature sylvite precipitates first, because carnallite solutions are never congruently saturated (Campbell et al. 1934, pp. 2508, 2509).

If bischofite is present in solutions of the ternary system KCl-$MgCl_2$-H_2O, carnallite is almost completely insoluble (Lightfoot and Prutton 1948, p. 4112).

According to Klockmann (1978/1980, p. 492) Na may replace K to some extent. The melting temperature may possibly be slightly lowered by such replacement.

The volume of most solutions is less than the sum of the solute and solvent, so that decrease in pressure may be expected to cause precipitation of the solute (Bain 1936, p. 515). This is not the case concerning carnallite. The molecular volume of the double salt carnallite is 4.78% larger than the sum of the molecular volumes of the starting salts sylvite and bischofite (Lepeschkow 1958, pp. 109-110, table 3). This means that an equivalent pressure drop occurs in the inclusion during the melting of "dry" carnallite.

In inclusions of the present work containing trapped grains of carnallite, no vapour bubble or visible liquid is present before the first heating run. The inclusions are "dry" with the solid carnallite surrounded by a saturated film of H_2O (Kühn 1952, p. 150). The pressure in these inclusions during the first heating run is temperature-dependent and equals the vapour pressure of dry carnallite up to the incipient melting temperature. According to Grube and Bräuning (1938, table 4) the vapour pressure of solid carnallite ranges from 0.8 mm Hg at 22°C to 547.2 mm Hg at 160°C. The pressure increases strongly above 140°C (258.7 mm Hg), which is interpreted as a tighter bond of the water of crystallization.

After total melting carnallite precipitates spontaneously within the interval 155 – 145°C, using most of the reaction sylvite. The remaining sylvite is sealed off from the solution by the precipitated carnallite like an armoured relict. Secondary tetrahydrate then precipitates in the interval 135 – 125°C. Bischofite forms below 100°C.

The reaction sylvite is the main identification of carnallite, especially combined with tetrahydrate in the same inclusion.

Carnallite melts incongruently in a closed system, where evaporation is prevented, after the formulae T_m°C = 167.5°C + (dT/dP)(P_m – 0.1)°C, where dT/dP = 0.1°C/MPa above 0.1 MPa, or P_m MPa = 0.1 MPa + (dP/dT)(T_m – 167.5) MPa, where dP/dT = 10 MPa/°C above 167.5°C, (fig. 11) (Fabricius and Rose-Hansen, in prep., fig. 4).

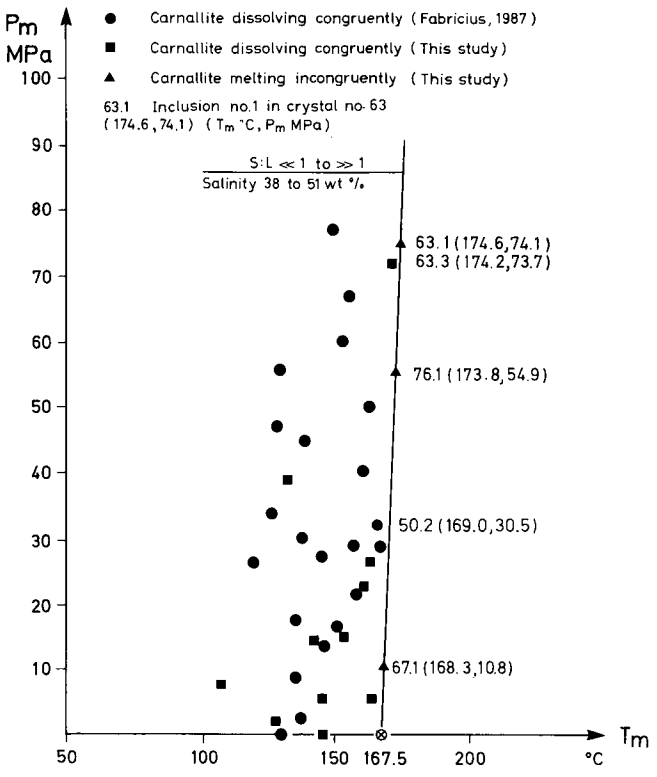

Fig. 11. The lower, practically linear part of the pressure-dependent melting curve of carnallite melting incongruently in a closed system.

Identification of carnallite:

i. Optical properties: anisotropic; refractive indices smaller than n_o of quartz at all temperatures within its stability field.

ii. Melting properties: melts incongruently at pressure-dependent temperatures higher than 167.5°C, forming a melt and solid KCl.

iii. Re-formation properties after total melting: reforms spontaneously after supercooling to 155 – 145°C. In the stability field of bischofite, also bischofite precipitates, even no bischofite was present before the first heating run.

The mineral almeraite: KCl·NaCl·$MgCl_2$·H_2O is very closely connected to carnallite (Klockmann 1978/1980, p. 492). Comment No. 4 on table 3.

The chemical combination E

In many inclusions an anisotropic homogeneous chemical combination, named E after the well Erslev-1, was found before the first heating run. The solid:liquid ratio is extremely large with a very small shrinkage vapour bubble (pl. I and II). Normally no liquid is visible and the solid phase fills up the entire inclusion. The refractive index is smaller than 1.5442, n_o of quartz.

E melts in the temperature interval approximately 180-195°C. In a few of the inclusions halite and sylvite

precipitate simultaneously at the total melting temperature of E. In other inclusions halite and sylvite precipitate during the succeeding cooling period. Halite and sylvite are present in all the inclusions and the concentration of $MgCl_2$ is very high – 190 mol per 1000 mol H_2O or higher. The grain of halite is a trapped grain in suspension in the trapped $MgCl_2$ solution, whereas the sylvite is either a daughter mineral or reaction sylvite after incongruent melting of carnallite. The $MgCl_2$ component of E is carnallite or tetrahydrate or both carnallite and tetrahydrate.

In very few cases E re-formed during the cooling period after total melting in the first heating run. Only in one case (x-82.1) E re-formed in all the cooling periods.

Other important solid inclusions

Anhydrite, $CaSO_4$, orthorhombic tabular prisms, abundant as inclusions in the quartz crystals and in the water insoluble residue from the salt. The crystals normally have rounded corners and edges in contrast to the euhedral crystals of the grey salt Na1 and Na2. The crystals seem to have suffered a slight dissolution, possibly from the NaCl solutions from the alteration of the salt clay before the crystallization of the quartz crystals.

Kieserite, $MgSO_4 \cdot H_2O$, monoclinic, characteristically as rounded twins. Kieserite is abundant in the water insoluble residue, but very rare as inclusions in the quartz crystals – three cases, e.g. crystal no. 63 with two dry twins, ∅ 15 and 17 μm. The main mass of kieserite in the deck halite is of a secondary origin formed after the formation of the quartz crystals.

Magnesite, breunerite, $(Mg,Fe)CO_3$, trigonal brown rhombohedrons. Magnesite is not rare, neither in the residue nor in the quartz crystals. The magnesite possibly formed by the heavy $MgCl_2$ solutions in the deeper parts of the basin. Magnesite is not found at the margins of the basin or on barriers (Backmann 1985, p. 136).

Pyrite, FeS_2, cubic octahedrons. Pyrite is abundant in the residue. However, it is extremely rare as inclusions in the quartz – only one case observed – and therefore is interpreted as in general postdating the quartz crystals.

Hematite, Fe_2O_3, red to yellowish red, hexagonal thin crystals. In places abundant in the residue, but extremely rare as inclusions in the quartz crystals – one case, doubtful. The scales of hematite possibly derive from 1st generation of carnallite in the deck halite. Petrographic investigations of primary carnallite show that hematite is intergrown crystallographically orientated with the host carnallite, which is interpreted as an exsolution process (Marr 1958, p. 89). Hematite is not found in the inclusions of carnallite, which indicates a secondary origin of the carnallite (Borchert and Muir 1964, p. 200, Braitsch 1962, 1971 p. 185).

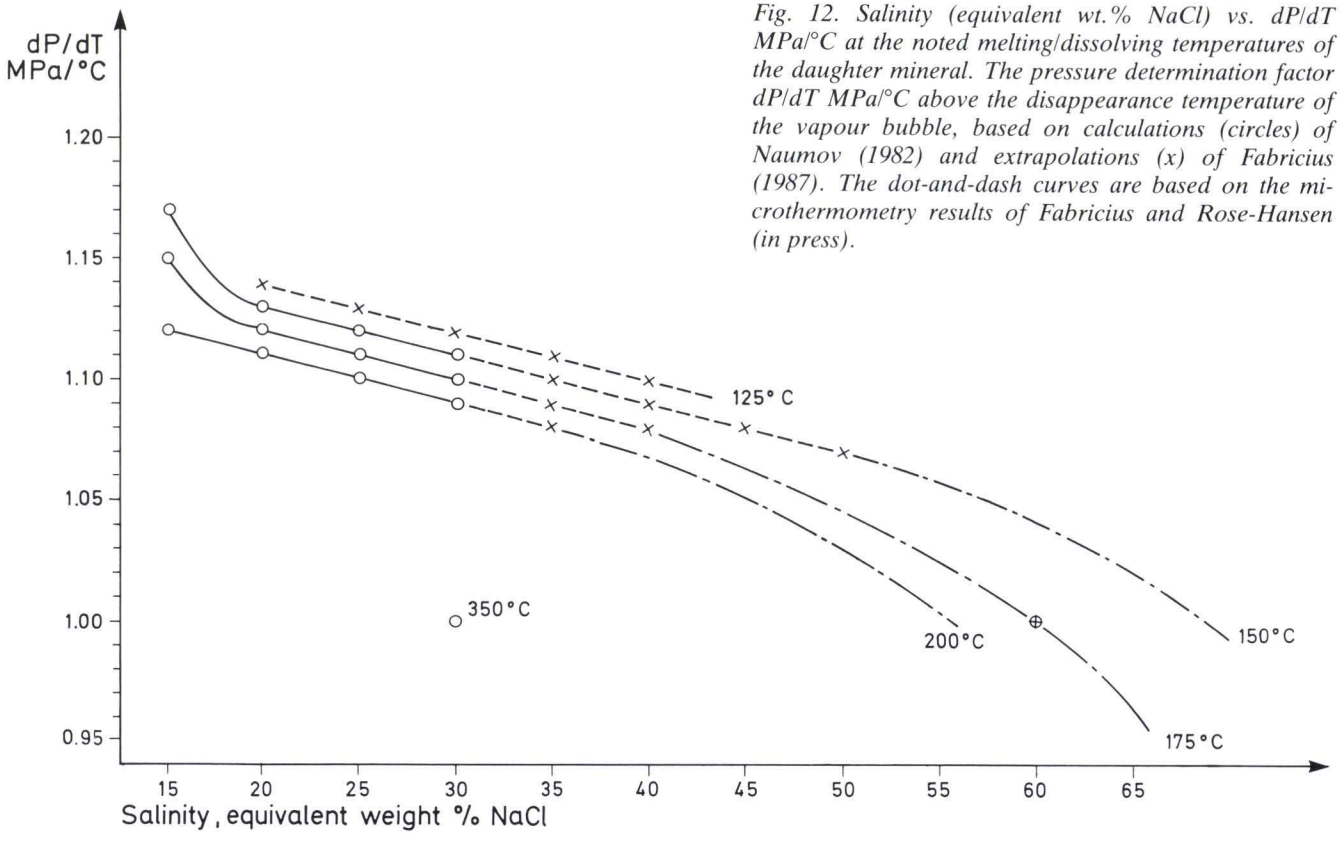

Fig. 12. Salinity (equivalent wt.% NaCl) vs. dP/dT MPa/°C at the noted melting/dissolving temperatures of the daughter mineral. The pressure determination factor dP/dT MPa/°C above the disappearance temperature of the vapour bubble, based on calculations (circles) of Naumov (1982) and extrapolations (x) of Fabricius (1987). The dot-and-dash curves are based on the microthermometry results of Fabricius and Rose-Hansen (in press).

Determination of the melting/dissolving pressure P_m

The melting pressure of daughter carnallite melting incongruently:

$$P_m \text{ MPa} = 0.1 \text{ MPa} + 10(T_m - 167.5) \text{ MPa}.$$

If a daughter mineral dissolves/melts on a higher temperature T_m than the disappearance temperature T_b of the liquid shrinkage vapour bubble, the pressure is calculated from

$$P_m \text{ MPa} = (dP/dT)(T_m - T_b) \text{ MPa}.$$

The factor dP/dT MPa/°C is found in the diagram, fig. 12 (Fabricius and Rose-Hansen, in prep., fig. 8).

Stability and metastability

The time spent on the study of the very complicated natural chemical system Na-K-Mg-Cl-H_2O in the inclusions is infinitesimal compared with geologic time. So, a high degree of metastability is to be expected in the laboratory.

Transformations can go from a metastable phase to another metastable phase, but never from a stable phase to a metastable phase (Kühn 1952, p. 149, Holser 1979, p. 248). But the metastable state is a characteristic feature of the natural processes concerning precipitation of salts (Waljaschko 1958, p. 204).

As the inclusions are small, exceedingly clean systems, both homogeneous and heterogeneous nucleation of new phases are frequently retarded, and a variety of metastable states may result (Roedder 1971, p. 327, 1981a, p. 11).

In order to prevent metastability during the runs and in order not to overstep the many phase change boundaries, the heating or cooling rate must be kept very low (Crawford 1981, p. 77).

During the course of a complete heating run, some phase transitions can be metastable or, more often, concern stable but local (partial) equilibirum processes (Ramboz et al. 1982, p. 31). These phenomenons are often seen on the transition boundaries bischofite-tetrahydrate during heating (115-120°C) and during cooling tetrahydrate-bischofite (100-85°C) in the very large inclusions of the present study.

After the heating runs, an equilibration time of at least 24 hours is required. In a few cases much longer time must be spent on the stabilizing of the inclusion. At pl. III, figs. 13-15, is shown x-82.1 at 20°C before the first heating run and after equilibration in 24 and 48 hours after the third run. The demonstrated metastability may be caused by the very dense (fig. 10) and highly viscous tetrahydrate solution (Pichavant et al. 1982, p. 24).

Measurements and calculations

All the inclusions of this study are solid inclusions at room temperature before the first heating run. The solid: liquid ratio is extremely large. The liquid is disclosed by the very small liquid shrinkage vapour bubble.

The inclusions are classified by their contents of daughter minerals at 20°C after total melting/dissolving of the solid phases:

A. Carnallite + sylvite (+ bischofite).
B. Carnallite + sylvite + bischofite.
C. Carnallite + tetrahydrate + sylvite + bischofite.
D. Tetrahydrate ± sylvite ± bischofite.

In many of the inclusions small grains of halite were in suspension in the trapped, highly saline solutions. In none of the inclusions bischofite was present before the first heating run.

In order to obtain the most accurate measurements of the total dissolving/melting temperatures of the polycrystalline daughter minerals, especially of bischofite, the method of Potter and Clynne (1978, pp. 702-3) was used: The heating run is interrupted before the last grain or "cloud" disappears. The inclusion is cooled slowly, whereby the dissolved mineral precipitates on the remaining small grain. The measurements are then continued on a single larger grain.

A. Carnallite + sylvite (+ bischofite)

The inclusion No. x-67.1 is the only one in this group. The inclusion is a large negative crystal, crystallographically orientated with the host quartz (pl. II, figs. 7A-D). The most perfect negative crystal is seen through the *m* face (10$\bar{1}$0) or the opposite *m* face ($\bar{1}$010). Unfortunately, the edge between *m* face (10$\bar{1}$0) and *r* face (10$\bar{1}$1) goes right over the inclusion, whereby the "quartz wedge" formed by the *r* face and the opposite *z* face spoils the optical picture of essential parts of the inclusion. The two pictures not shown are also poor, whereas the two pictures seen through the *m* faces (1$\bar{1}$00) and (01$\bar{1}$0), respectively, are of a high quality, because the main plane of the pictures practically is perpendicular to the optic axis of the microscope. It is not possible, with the available methods, to measure the volumes of the inclusion or the different phases.

Before the first heating run the inclusion contained solids and liquid with a ratio of approximately 5:1 (pl. IV, fig. 1). The main solid phase is carnallite with more than 90 vol.% of the total amount of solids, which are exposed during the melting of the carnallite: a crystal of the chemical combination A and a small grain of sylvite. No bischofite or halite is present before the first heating run. The small vapour bubble is a true liquid shrinkage bubble with vapour pressure of the equilibrium solution at 20°C. No high-pressure gas is present.

Table 3. Inclusion x-67.1 observed through the m face (1$\bar{1}$00).

Com.	Events	1st run	2nd run	3rd run	Plate/ figs.
	$T_m$car.inc.	144.1	148.3	145	
1	T_b	157.5	/	/	IV/3
2	$T_m$car.tot.	168.1	168.5	168.6	IV/5
3	$T_m$sy.tot.	190	/	188.2	IV/6
4	T_mA.tot.	293.1	/	/	IV/7
4,5	T_rA;$T_r$ha.;T_nHP.	246	/	/	IV/8
4	$T_m$ha.tot.	277.9	292.8	/	
4	T_mA.tot.	292.3	/	/	
6	T_bHP.	293.1	294.7	/	
	T_nHP.	259.1	267.3	/	
	$T_r$ha.	254	257.3	/	
	$T_r$car.	/	/	154.5	IV/9
7	T_mA'.	/	180.9	/	

Comments on table 3:

1. A pure liquid shrinkage bubble did not reappear after the first heating run, where all the solid phases were melted/dissolved, whereby dissolved high-pressure gas (HP) was released.
2. After total melting of carnallite in the first heating run, the remaining solids in the inclusion were the mineral A as euhedral (pseudotetragonal?) crystal (28 x 20 μm) projecting from the inclusion wall and a grain of sylvite (8 x 4 μm). No halite or other solids were present. The composition of the equilibrium solution at 168°C is c. 167 mol $MgCl_2$ plus 25 mol K_2Cl_2 per 1000 mol H_2O (fig. 6A). The content of Na_2Cl_2 is approximately 1.5 mol (fig. 8). The salinity is c. 52 weight%.
3. In the third run, which was interrupted just after T_m sy.tot. = 188.2°C, car. re-formed at 154.5°C. T_m car.tot. was checked during renewed heating: T_m car.tot. = 168.1°C.
   Reaction sylvite did not form during the melting of the carnallite, and the volume of the grain of sylvite did not seem to increase. The carnallite possibly melted congruently, and the KCl component went into solution.
4. After total melting/dissolving of the mineral A at 293.1°C, A partly re-formed in connection with a crystal of halite at 246°C. During renewed heating first the crystallized halite dissolved at 277.9°C, and then the mineral A at 292.3°C. In the second run A did not reform, and the halite dissolved at a much higher T than in

the first run, indicating a higher concentration of $MgCl_2$ in solution and a somewhat larger crystal of halite.

The mineral A may be the hydrate $NaCl{\cdot}MgCl_2{\cdot}H_2O$ (Titov 1949, p. 458) or, if also KCl is present, the mineral almeraite: $KCl{\cdot}NaCl{\cdot}MgCl_2{\cdot}H_2O$.

The mineral A must have crystallized prior to the carnallite, because the euhedral A projects from the inclusion wall and is impinged on by the polycrystalline, anhedral carnallite.

5. No high-pressure gas was released during the melting of the carnallite. But after dissolving/melting of the mineral A, high-pressure gas was released. The gas was possibly dissolved in the grain of halite, which later formed the mineral A combined with $MgCl_2$ solution before precipitation of the carnallite. The mineral A and the carnallite are daughter minerals, whereas the grain of halite was in suspension in the trapped solution.
6. Possibly the high-pressure gas condensates at T_h HP = 293.1°C due to the very high pressure build-up in the inclusion.
7. In the first run, a new solid phase A' formed during the cooling period at 153.6°C as a small round grain. A' may be identical with the mineral A, comment No. 9 on table 4.

Run Nos. 4, 5, and 6, table 4

After the third run the crystal was turned, so the inclusion was observed through the prism face (01$\bar{1}$0). The composition before run No. 4: car. + ha. + sy. + A' + solution. The solid:liquid ratio is very large, and a large high-pressure gas bubble is present. No bischofite is present.

The crystal was cooled down very slowly to -100°C, (run 4 and 6).

The measurements from the fourth, the fifth, and the sixth run, are noted in table 4.

Table 4. Inclusion x-67.1 observed through the m face (01$\bar{1}$0).

Com.	Events	4th run	6th run	Plate/ figs.
1	car. colour change	−72.2	/	
2	$T_f$ice	−32	−75	
3	$T_f$hyd.	/	−64.7	
4	$T_m$ice,tot.;$T_m$ice,part.	−29	−48	V/3
5	$T_f$dod.	−31.5	−33	
5	$T_f$oct.	/	−18	V/4
5,6	$T_f$hex.	+4	−2.8	V/5
7	equilibration	5th run	+20	V/2
	$T_m$hex.inc.	64.5	67.5	IV/13
8	$T_m$hex.tot.	87.2	91.2	IV/14;V/7
	$T_m$car.inc.	141.6	151	IV/15
	$T_m$car.tot.	168.2	168.0	
9	T_mA'.tot.	/	180.8	
	$T_m$sy.tot.	181.4	/	

Comments on table 4:

1. During the cooling down to -100°C in the fourth run, the carnallite got a bluish tint at c. -20°C. This bluish tint was intensified into a bluish colour down to -100°C. From -100°C the temperature was raised very slowly, and the bluish colour of the carnallite changed to a yellowish colour at -72.2°C.
2. The inclusion and the crystal became dark, indicating the formation of ice.
3. During freezing runs, saturated chloride solutions are transformed into a dark fine-grained aggregate, whereas saturated sulphate and carbonate solutions freeze without appreciable darkening (Borisenko 1978, pp. 15-16). The hydrate formed at -64.7°C in the sixth run might be the fine-grained aggregate mentioned above.
4. In the fourth run, the inclusion and the host crystal suddenly became bright at -29°C, indicating formation of melt (Crawford 1981, p. 82). In the sixth run the inclusion brightened slightly at -48°C and totally at -22°C.
5. The identification of the different hydrates: dodecahydrate, octahydrate and hexahydrate (bischofite), is based on the transition temperatures noted in table 2. The transition is easily observed, because a certain amount of solution suddenly is released, and the remaining aggregate becomes more coarse-grained. The dodecahydrate recrystallized slightly at -26°C in the fourth run, and at -28°C in the sixth run.
6. After the formation of bischofite the solid:liquid ratio is extremely large, but large high-pressure gas bubbles are still present. The present sylvite formed a perfect cube with the length of an edge of 6.5 µm. The bischofite recrystallized slowly up to 13.2°C in the fourth run and to c. 12°C in the sixth run. As a large cube of sylvite is present side by side with bischofite, a high degree of metastability is present, because sylvite and bischofite form carnallite, the "carnallite synthesis" (Kühn 1952, p. 154).

   The concentration of KCl in the solution is approximately 1.5 mol K_2Cl_2 per 1000 mol H_2O (fig. 6B).
7. After the fourth run the inclusion was held on 20°C for equilibration through 24 hours. In the sixth run the equilibration time at 20°C was c. 3 hours.
8. The equilibrium solution at 90°C consists of c. 130 mol $MgCl_2$, 1.5 mol K_2Cl_2 (fig. 6A), and c. 5 mol Na_2Cl_2 (fig. 8) per 1000 mol H_2O. The salinity is approximately 42 weight%. Bischofite did not re-form during the succeeding cooling periods, neither in the fifth run nor in the sixth run. This is not a phenomenon of metastability, but it shows that the concentration of KCl in the solution increased, and thereby again follows the right border line of the carnallite stability field (fig. 6A) as was the case in the first three runs.
9. After total dissolving of A' at 180.8°C, A' re-formed at 136.5°C during the succeeding cooling period. A' forms an angular grain 10 x 5 µm. A' seems to be a stable daughter mineral. A' cannot be tetrahydrate due to the high dissolving temperature combined with the high concentration of KCl in the solution.

B. Carnallite + sylvite + bischofite

In table 5 are noted the sizes and shapes of the inclusions of this group. The solid:liquid ratio before the first heating run is extremely large.

Table 5. Inclusion size and shape.

x–	Size µm	Plate/ fig.	Shape
1.3	150×100	II/5	amoeboidal, "dry"
4.3	70×54×20	II/3	orientated negative crystal
35.1	48×42×42	I/9	orientated negative crystal
66.1	22×22×22	I/1	orientated negative crystal

In table 6 is given the results of the heating runs.

Table 6. Measured temperatures, mean values.

Com.	x-	T_h	T_mE	$T_m$car.	$T_m$hex.	$T_m$sy.	$T_m$ha.
1	1.3	206.1	/	172.4	?	215	/
2	4.3	147.8	/	176.3	98.9	190.8	272.4
2	35.1	178.3	/	182.8	?	295.8	/
3	66.1	147.2	191.7	176.3	113.2	211.6	289.8

PLATE III

Fig. 1. Deck halite Na2r with intercalated clay and a quartz aggregate. A grain of carnallite is trapped partly in the pyramid of the quartz and partly in the surrounding salt. High-pressure gas bubbles are seen on the grain boundaries. Crossed Nicols and gypsum plate.

Fig. 2. Twinned crystal of carnallite in the deck halite Na2r. The solid:liquid ratio is extremely large. Note the small liquid shrinkage vapour bubble, 20°C. Not autoclaved. Crossed Nicols.

Fig. 3. Polycrystalline aggregate of carnallite at 20°C after 192°C and 102.6 MPa in the autoclave. Longest dimension c. 110 μm. Note the high-pressure gas bubble. Grains of secondary bischofite: blue with high relief. Crossed Nicols and gypsum plate.

Fig. 4. Mosaic structure on the prism face of a quartz from the deck halite Na2r. Crossed Nicols and gypsum plate.

Fig. 5. Hole after now dissolved carnallite in one end of quartz crystal No. 47 from the deck halite Na2r. The depth of the hole is c. 140 μm. Note the veil of very small fluid inclusions following the contours of the hole. Crossed Nicols.

Fig. 6. Gas inclusions on the surface of grains of halite from the deck halite Na2r. The length of the stocking shaped inclusion: c. 50 μm. Plane polarized light.

Fig. 7. Quartz crystal No. 69, x-69, from the deck halite Na2r. 670x300 μm. Bitter almond oil, n = 1.60, 20°C. Partly crossed Nicols and gypsum plate.
Note the large hole after now dissolved carnallite and the inclusion x-69.1.

Fig. 8. X-69.1, negative crystal (48 x 29 μm) with a solid:liquid ratio larger than 1:1. Note the vapour bubble, 20°C. Partly crossed Nicols and gypsum plate. At least six different solid phases are present. The inclusion was not further studied.

Fig. 9. X-44.1 (48 x 38 μm). 20°C before the first heating run. The solid:liquid ratio is extremely large. The content is the chemical combination named E. Crossed Nicols.

Fig. 10. X-44.1. During the first heating run incipient melting of E: T_mE,inc. = 190°C. The vapour bubble disappeared at T_b = 124.4°C.

Fig. 11. X-44.1. Total melting of E: T_mE.tot. = 193.3°C. Simultaneously, precipitation of halite and sylvite, characteristically in a reticulate pattern (ha.) and small "pearls" (sy.).

Fig. 12. X-44.1. T = 196.9°C. Recrystallization of halite and sylvite.

Fig. 13. X-82.1 (61 x 42 μm). 20°C at the end of the third heating run. The content: much tetrahydrate, half as much halite, a small grain of carnallite and a few small grains of secondary bischofite, solution, and a large high-pressure gas bubble. The solid:liquid ratio c. 1:4.

Fig. 14. X-82.1. Equilibration at 20°C, 24 hours after the third run. The tetrahydrate almost totally dissolved and replaced by a large composite grain of bischofite. The carnallite recrystallized to an angular grain. The HP gas bubble has disappeared. The solid:liquid ratio c. 1:1.

Fig. 15. X-82.1. Equilibration at 20°C, 48 hours after the third run. The same solid content as in Fig. 14, but the HP gas bubble has re-formed and the solid:liquid ratio somewhat larger than 1:1.

Fig. 16. X-82.1. The fourth heating run. Total melting of the bischofite: $T_m$hex.tot. = 117.1°C. The gas bubble has grown larger.

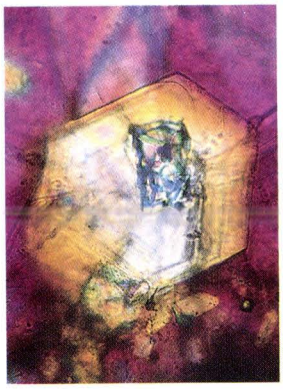
1 100 µm

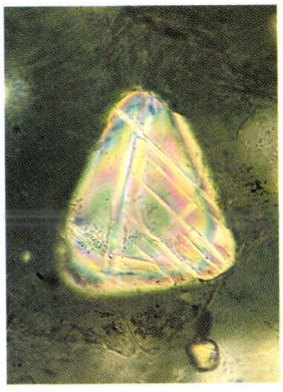
2 100 µm

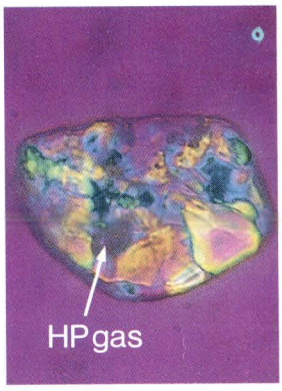

3 50 µm


4 20 µm


5

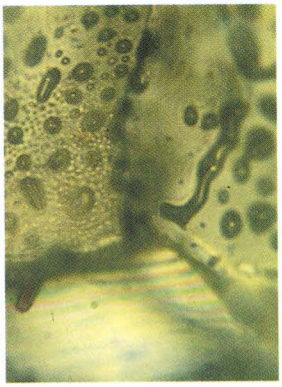
6

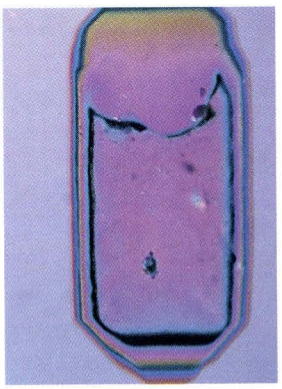
7 100 µm


8 10 µm

x-44.1

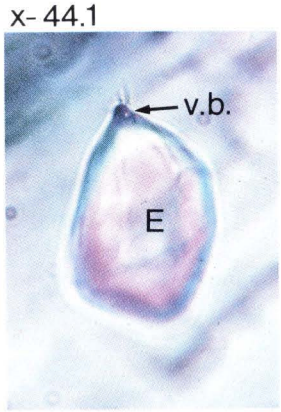

9 10 µm

10

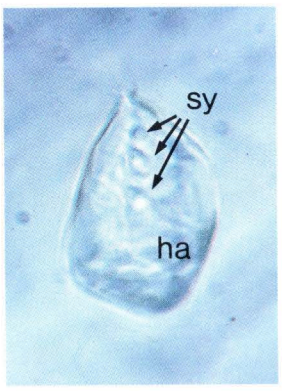

11


12

x-82.1

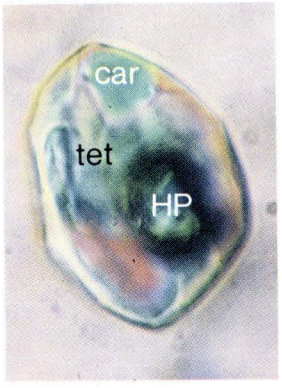

13 10 µm

14

15

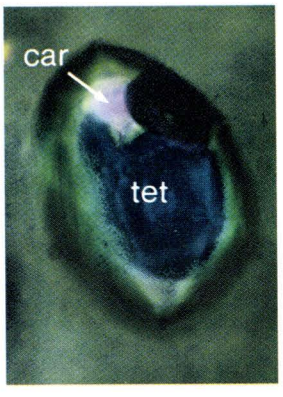

16

PLATE IV

Figs. 1-9. Inclusion x-67.1 seen through the m face ($1\bar{1}00$).

Figs. 10-16. Inclusion x-67.1 seen through the m face ($01\bar{1}0$).

Fig. 1. 20°C before the first heating run. XN + gypsum plate. Carnallite, sylvite, the mineral A, liquid shrinkage bubble. Solid:liquid ratio c. 5:1.

Fig. 2. $T_m$car.part. = 153.6°C. Note the mineral A with tetragonal configuration.

Fig. 3. T_b = 157.5°C. A: 28x20 μm.

Fig. 4. $T_m$car.part. = 164.0°C.

Fig. 5. $T_m$car.tot. = 168.1°C. The rest: the mineral A, sylvite, and solution. No halite.

Fig. 6. $T_m$sy.tot. = c. 195°C. T_mA,inc. = 203°C. ∅: 24 μm.

Fig. 7. T_mA,tot. = 293.1°C. Only solution left.

Fig. 8. (Cooling from 293.1°C). T_rA = $T_r$ha. = T_nHP = c. 246°C. Repeated heating until dissolving of A at 292.3°C.

Fig. 9: (Cooling from $T_m$sy = 188.2°C). $T_r$car. = 154.5°C.

Fig. 10. 20°C after the third heating run. Carnallite, sylvite, HP bubble. Halite covered by the carnallite. No bischofite.

Fig. 11. + 7.8°C after freezing to –100°C. Bischofite recrystallizing. The grain of carnallite is seen faintly below the bischofite.

Fig. 12. 20°C. Recrystallized bischofite. Note the polysynthetic twin of bischofite and the cube of sylvite.

Fig. 13. $T_m$hex.part. = 64.5°C.

Fig. 14. $T_m$hex.tot. = 87.2°C.

Fig. 15. $T_m$car.part. = 166.7°C. Note the cube of sylvite and the large, very thin crystal of halite.

Fig. 16. $T_m$car.tot. = 168.2°C. Note the sylvite and the halite.

x-67.1 (1$\bar{1}$00)

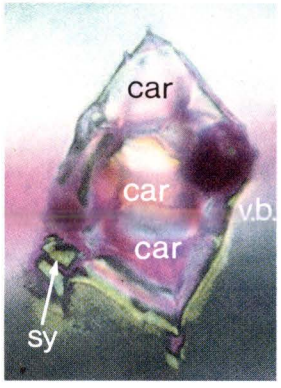

1 25 µm

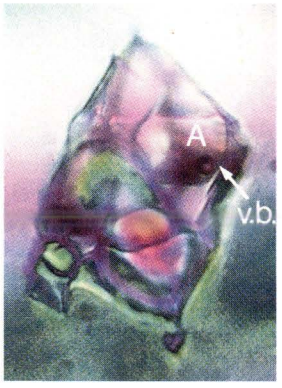

2

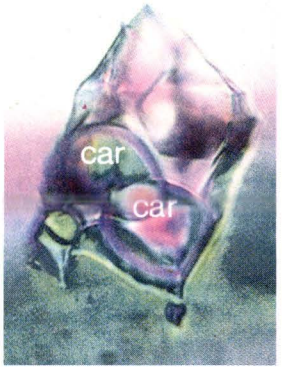

3

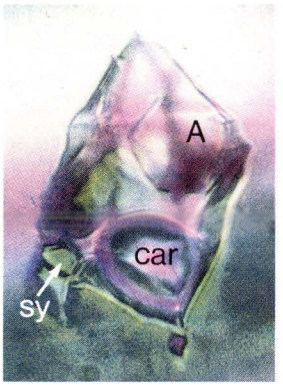

4

5

6

7

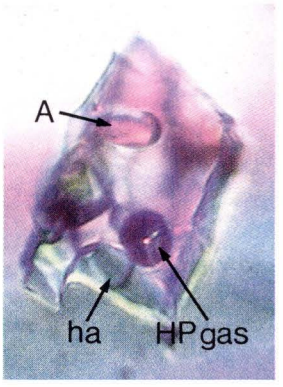

8

x-67.1 (01$\bar{1}$0)

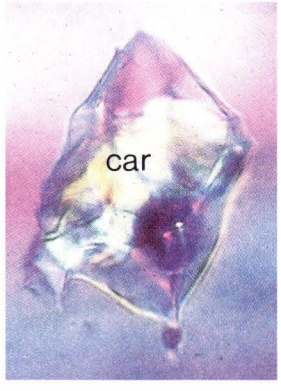

9

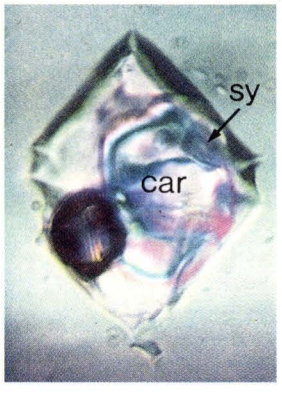

10 25 µm

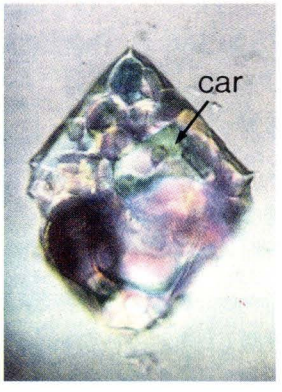

11

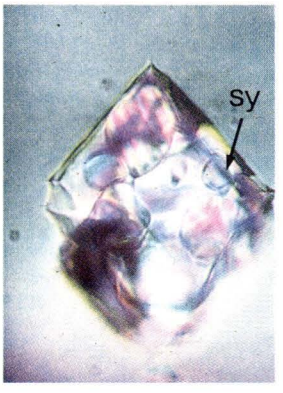

12

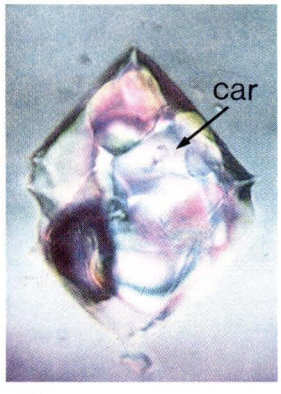

13

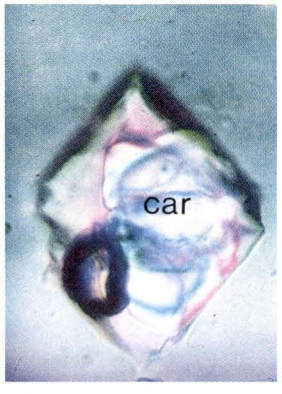

14

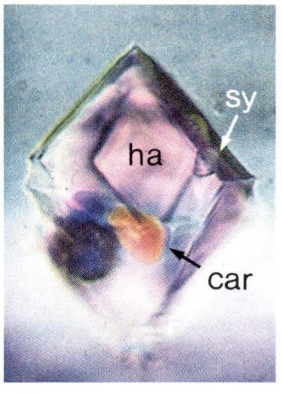

15

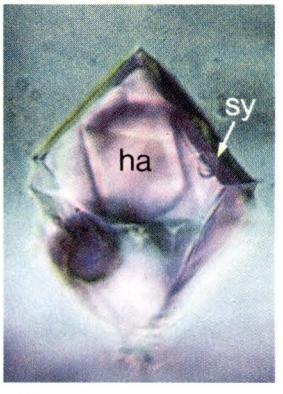

16

PLATE V

Figs. 1-8: Inclusion x-67.1 seen through the m face ($01\bar{1}0$).

Figs. 9-16: Inclusion x-82.1

Fig. 1. $T_m$sy.tot = 181.4°C. The rest: halite, HP gas bubble, and solution.

Fig. 2. 20°C. Equilibration in 24 hours after the fifth run.

Fig. 3. $T_m$ice = -48°C after freezing to -100°C. Formation of unknown hydrated aggregate.

Fig. 4. Transition from dodecahydrate to octahydrate.$T_r$oct. = -18°C after $T_r$dod. = -33°C.

Fig. 5. Transition from octahydrate to hexahydrate (bischofite). $T_r$hex. = -2.8°C.

Fig. 6. 20°C. Equilibration for 3 hours. The content mainly bischofite covering carnallite, halite, A'. S:L extremely large.

Fig. 7. $T_m$hex.part. = 88.5°C.

Fig. 8. $T_m$hex.tot. = 91.2°C. The rest: carnallite, A', halite.

Fig. 9. X-82.1. 20°C before the first heating run. The content: the chemical combination E. S:L extremely large.

Fig. 10. T_mE,inc. = 178.9°C.

Fig. 11. T_mE,tot. = 182.7°C. Simultaneous formation of halite, 19x19 μm, and a "pearl" of sylvite.

Fig. 12. Decreasing T. $T_r$car. = 154.8°C. HP gas bubble developed.

Fig. 13. $T_r$tet. = 127.3°C.

Fig. 14. 20°C. Equilibration 24 hours after the first heating run. The content: bischofite, carnallite, HP gas bubble, liquid shrinkage bubble.

Fig. 15. $T_m$hex.tot. = 117.3°C. Incongruently formed tetrahydrate at 117.9°C.

Fig. 16. $T_m$tet.tot. = 148.1°C. The rest: carnallite, HP gas bubble, solution.

x-67.1 (0ī1ī0)

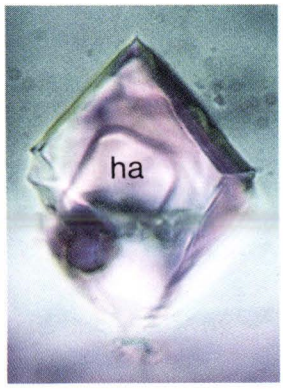

1

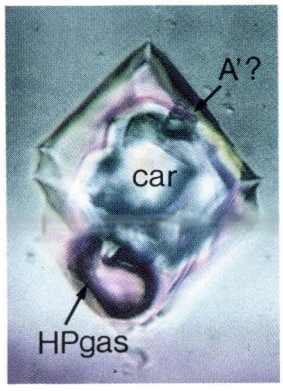

2

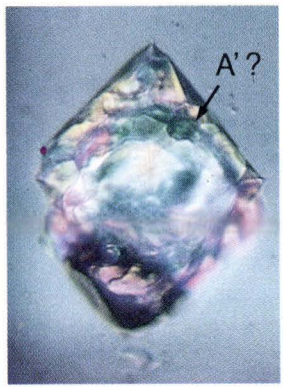

3

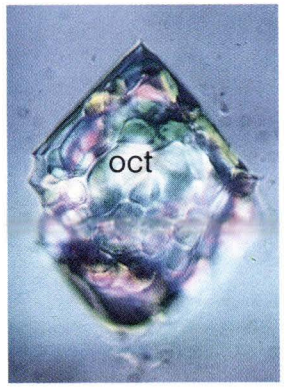

4

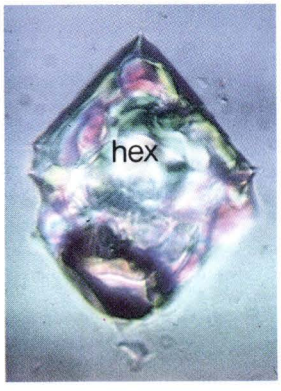

5

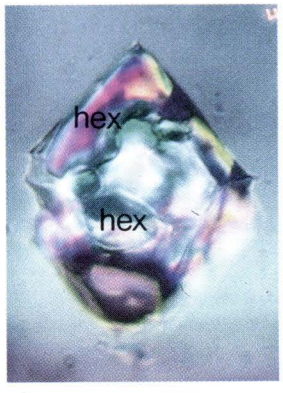

6

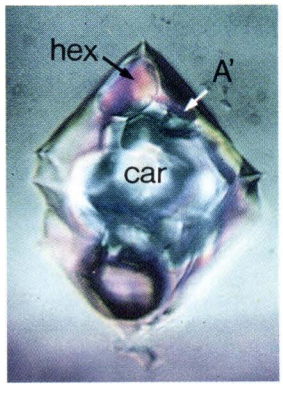

7

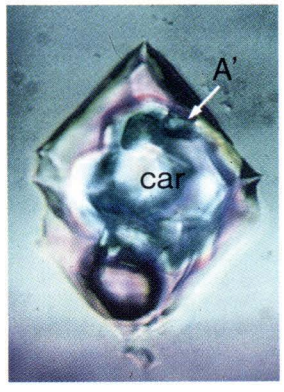

8

x-82.1

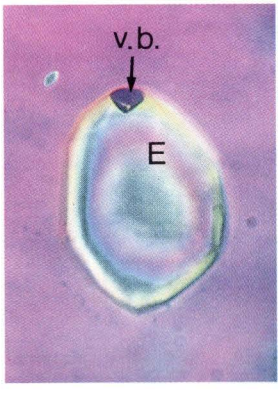

9

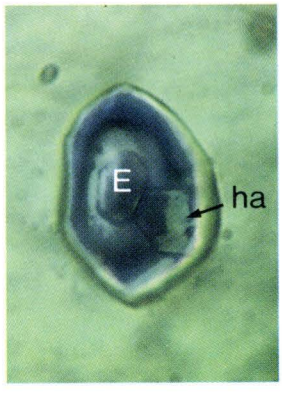

10

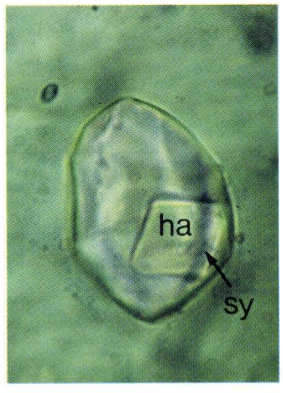

11

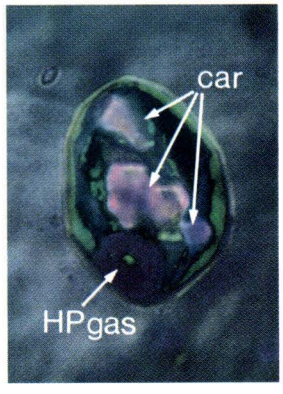

12

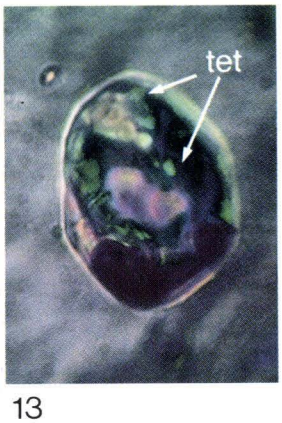

13

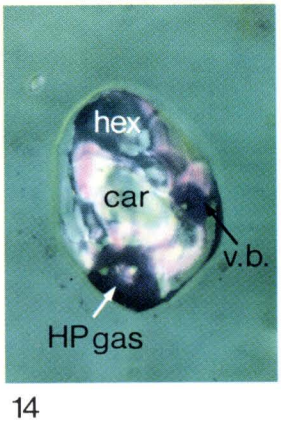

14

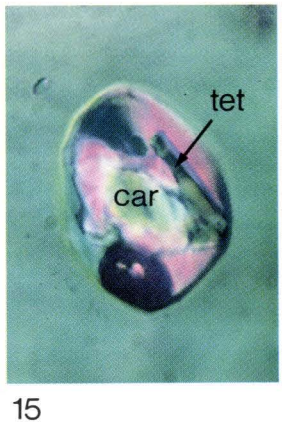

15

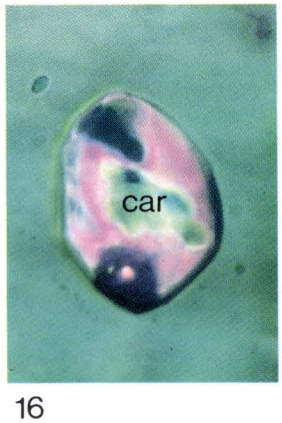

16

Comments on table 6

1. The inclusion x-1.3 is highly irregular. High-pressure gas was released after total melting of the carnallite. Therefore, the inclusion must be a trapped grain of carnallite. After total melting of the carnallite a very small amount of bischofite (hex.) precipitated as thin clouds here and there on the surface of the re-formed carnallite and on the inclusion walls.
2. The chemical combination E was not present in x-4.3 or x-35.1 before the first heating run, indicating the trapping of a melt of carnallite with grains of sylvite or halite in suspension. High-pressure gas was released after dissolution of the grains of halite (x-4.3) or sylvite (x-35.1). The total melting temperature of the carnallite is a minimum trapping temperature.
3. The shape of x-66.1 is very close to a perfect short prismatic negative crystal. Before the first heating run, the solid:liquid ratio is extremely large with the liquid gathering in a small void in the surface of the chemical combination E.
   E consists of carnallite + sylvite + halite. E does not re-form after the heating runs. TCS = 0.026, calculated from T_m E,inc. = 153.4°C and T_m E,tot. = 191.7°C.
   The main component carnallite plus a cube of halite with the length of an edge of 8.5 μm practically fill up the inclusion at room temperature. The high dissolving temperature of the reaction sylvite indicates the presence of a small trapped grain of sylvite. The amount of bischofite, secondarily formed after the melting of the carnallite component, is very small. T_m car.tot. = 176.3°C is a minimum trapping temperature of the melt of carnallite with suspended grains of halite and sylvite. The melt consists of 166.67 mol $MgCl_2$ + 83.33 mol K_2Cl_2 + c. 3 mol Na_2Cl_2 per 1000 mol H_2O at 212°C. These concentrations equal 34 weight% $MgCl_2$ + 27 weight% KCl + less than 1 weight% NaCl, also valid for x-4.3 and x-35.1.

C. Carnallite + tetrahydrate + sylvite + bischofite

In table 7 are noted the sizes and shapes of the inclusions of this group. The solid:liquid ratio before the first heating run is extremely large.

In table 8 is given the results of the heating runs.

Table 7. Inclusion size and shape.

x-	Size μm	Plate/ fig.	Shape
33.1	140×130	II/6	highly irregular, dry
54.3	33×15×15	I/11	orientated irregular ellipsoid
63.1	32×22×22	II/2	irregular ellipsoid
44.1	48×38×38	I/5	orientated faceted ellipsoid
48.1	50×26×26	I/4	orientated faceted ellipsoid
79.1	56×32×32	I/6	orientated faceted ellipsoid
57.1	26×22×22	-/-	orientated faceted ellipsoid
60.1	17×15×15	-/-	orientated negative crystal
82.1	61×42×42	V/9	orientated negative crystal

Comments on table 8

1. An irregular grain of carnallite with an intergrown grain of sylvite was trapped during the crystallization of the host quartz. Solid halite was not present. During the melting/dissolving of the solid carnallite and sylvite, dissolved high-pressure gas was released. During the cooling period, after total melting of the carnallite, much bischofite (hex.) formed. In the next heating runs, the bischofite melted incongruently at 120.9°C, forming tetrahydrate, which in turn melted totally at 135.4°C. The high melting temperature 120.9°C shows a certain metastability.
2. During all the heating runs, a solid phase crystallized spontaneously in the temperature interval 182.6 – 185.7°C. The phase, which consists of NaCl, $MgCl_2$, and H_2O, and possibly also little KCl, dissolved totally in the temperature interval 293.4 – 297.2°C. The refractive index n is smaller than n of the surrounding solution.
3. The chemical combination E re-formed spontaneously at 144.7°C during the cooling period of the first heating run. During the next heating run, E melted totally at 175.3°C, c. 6°C lower than in the first run.
4. Before the first heating run the inclusion consisted of a composite grain of carnallite and tetrahydrate with an extremely high S:L ratio, E was not present. In the quartz crystal x-63 two solid inclusions of kieserite twins, ∅ 15 and 17 μm, are found. Possibly E did not form in x-63.1 due to a certain minor concentration of sulphate in the trapped solution.
5. In the first run, halite and sylvite crystallized simultaneously with the total melting of E: T_m E,tot. = T_r ha.+sy. = 192.8°C. The halite crystallized in the characteristical reticulate pattern, later recrystallising into a thin "cube" with a volume of c. 500 μm^3. The sylvite formed a much smaller rounded grain. The composition of E: much solution of carnallite and tetrahydrate + much halite + little sylvite.
6. The heating runs of x-82.1 are expounded in detail below. See also pl. V, figs. 9-16.

Heating runs of x-82.1, table 9

Comments on table 9

General comments. In order to avoid metastability before the beginning of a new heating run, the inclusion was stabilized at 20°C for at least 24 hours. Nevertheless, some of the measured temperatures reflect a high degree of metastability, especially in run 4 and 5 (Com. No. 6).

Just after the third run, the inclusion consisted of much tetrahydrate, approximately one fifth of the volume of the inclusion, half

Table 8. Measured temperatures, mean values.

Com.	x-	T_b	T_mE	$T_m$tet.	$T_m$car.	$T_m$hex.	$T_m$sy.	$T_m$ha.	HP gas
1	33.1	191.6	183.9	135.4	179.6	120.9	298.9	/	+
	44.1	124.4	192.9	155	175.9	116.3	185.4	294.3	+
2	48.1	105.5	185.4	138.4	178.7	114.7	188.4	216	–
	54.3	143.8	172.5	152.1	170.6	118.4	175.6	273.9	+
3	57.1	163.8	181.4	156.4	174.4	?	214.4	288.6	+
	60.1	114.3	193.2	133.1	175.7	117.2	190.4	?	+
4	63.1	144.8	/	157.8	174.6	119.1	195	275.7	+
5	79.1	117	192.8	158.5	176.3	113.3	226.0	293.4	+
6	82.1	182.4	182.5	156.8	171.6	116.6	263.5	292.1	+

Table 9. Measured temperatures on x-82.1.

Com.	Events	1st run	2nd run	3rd run	4th run	5th run	Plate V, figure
1	T_b	182.4	/	/	/	112.6	9
2	T_mE,inc.	182.4	/	172.2	169	/	10
2	T_mE,tot.	182.5	/	174.7	175.2	173.7	11
3	$T_m$sy.tot.	263.5	/	/	176	/	/
3	$T_m$ha.tot.	292.1	/	/	/	/	/
	$T_t$car.	154.8	151.8	150.9	153.2	119.7	12
4	$T_t$tet.	127.3	127.8	128.9	153.2	125.5	13
	$T_t$hex.	75.3	73.6	69.1	95.1	85.2	14
5	$T_m$hex.tot.	/	117.3	115.9	117.1	116.5	15
6	$T_m$tet.tot.	/	148.1	156.2	152.8	169.9	16
6	$T_m$car.tot.	/	172.8	173.3	159.6	168.7	/

as much halite, and a small grain of carnallite (pl. III, figs. 13-16). In addition, a few small grains of bischofite and a large high-pressure gas bubble were present. 24 hours later, the tetrahydrate has dissolved almost totally, and was replaced by a large composite grain of bischofite, intergrown with a few small crystals of tetrahydrate. The carnallite had recrystallized into a somewhat larger angular grain. The large HP gas bubble has disappeared. The crystal of halite was incorporated into the chemical combination E. The solid-liquid ratio increased from c. 1:4 to c. 1:1. Due to these conditions, the inclusion was given 24 hours more for equilibration. After this equilibration time, the HP gas bubble had re-formed and the solid:liquid ratio was somewhat larger than 1:1.

In the following heating run (run No. 4), the gas bubble grew larger during the melting of the bischofite, indicating dissolved gas in the polycrystalline bischofite.

This inclusion is the only one, in which E re-forms after each heating run.

1. The liquid shrinkage vapour bubble contained high-pressure gas before the first heating run. The bubble reduces appreciably up to c. 150°C and then slowly up to 182.4°C = T_b = T_m E,inc. In the fifth run, besides the very large HP gas bubble, also a small liquid shrinkage bubble was present, T_b of which is 112.6°C.
2. In the first heating run, E melts within one tenth of a degree. The heating run was interrupted and the temperature was lowered to 160°C. E re-formed, and, during renewed heating, E melted totally at 182.7°C. Simultaneously, a thin "cube", 19 x 19 µm, of halite and a small grain of sylvite formed. In the third run, E was hidden under the carnallite. During the melting of E, the grain of halite increased in size into a thin rectangular grain, 35 x 19 µm. In the fourth run, a small grain of sylvite formed at 172.6°C during the melting of E.
3. In the first heating run, T_m sy.inc. = 258°C, which gives TCS,sy. = 0.2; T_m ha.inc. = 240°C, giving TCS,ha. = 0.019.
4. After the re-formation of tetrahydrate of 127.3°C in the first heating run, a weak but distinct dissolution of the tetrahydrate takes place from 115°C to 105°C.
5. In the second run, the bischofite melts incongruently, forming tetrahydrate crystallization seeds, which in the locally supersaturated solution form tetrahydrate at 117.9°C. In the third run, bischofite melts incongruently at 115.9°C, resulting in formation of tetrahydrate at 120°C.
6. The melting temperatures of carnallite and tetrahydrate in the 4th and the 5th runs, respectively, reflect a high degree of metastability and the temperatures T_m tet.tot. = 169.9°C and T_m car. tot. = 159.6°C are not reliable.

D. Tetrahydrate ± sylvite ± bischofite

In table 10 are noted the sizes and shapes of the inclusions of this group. The solid:liquid ratio before the first heating run is extremely large.

The inclusions are divided into two groups, differing in whether the chemical combination E is present before the first heating run, or not.

Table 10. Inclusion size and shape.

x-	Size µm	Plate/ fig.	Shape
71.1	∅ 32	I/12	± regular spheroid
16.2	25×16×16	I/2	orientated faceted spheroid, dry
51.1	26×19×19	II/1	orientated faceted spheroid
74.1	58×32×32	I/7	orientated faceted ellipsoid
78.1	35×26×20	I/8	orientated faceted ellipsoid
81.1	54×38×38	–/–	orientated faceted ellipsoid
16.1	42×32×32	I/2	orientated slightly irregular neg. cryst.
12.3	150×48×48	I/4	orientated faceted irregular neg. cryst.
29.1	77×38×32	–/–	orientated boxlike negative crystal
73.1	42×20×20	–/–	orientated boxlike negative crystal
80.1	45×32×20	–/–	boxlike negative crystal, not orientated

In table 11 are noted the measured temperatures from inclusions, where E was not present, and in table 12 are noted the measured temperatures from inclusions where E was present before the first heating run.

Table 11. E not present. Measured temperatures, mean values.

Com.	x-	T_b	$T_m$tet. inc.	$T_m$tet. tot.	$T_m$sy.	HP gas
	12.3	?	180	181.2	/	?
1	16.1	135.4	178.3	181.5	177.0	–
2	16.2	/	180.6	181.9	/	–
3	29.1	144.9	161.1	171.3	122.0	–

Comments on table 11

General comments. None of the inclusions contained grains of halite. Bischofite did not form after the heating runs. No high-pressure gas was released after melting of the solid phases, indicating trapping of solutions only. The melting temperatures of the tetrahydrate are minimum trapping temperatures.

1. The inclusion is consanguineous with x-16.2, but the trapped solution contains a certain amount of KCl.
2. No liquid shrinkage vapour bubble developed during the cooling periods after melting of the tetrahydrate, i.e. "stretched" fluid (Roedder 1967). The trapped solution is a pure melt of tetrahydrate: 250 mol $MgCl_2$/1000 mol H_2O.
3. At 20°C the solid:liquid ratio is approximately 5:1. In a freezing run the solution reacted at -26°C after cooling down to -95°C. The solution formed a fine-grained aggregate, possibly $MgCl_2 \cdot 12H_2O$, which recrystallized into larger grains, possibly $MgCl_2 \cdot 8H_2O$, at -16°C. Simultaneously, a small amount of water was released. The aggregate continued the recrystallization with increasing temperature. The inclusion was kept at 20°C throughout 24 hours for equilibration. After the equilibration the inclusion had re-established into the state before the first heating run. No bischofite formed during the runs due to a certain concentration of KCl in the solution: c. 15 mol K_2Cl_2/1000 mol H_2O at 122.0°C (fig. 6A).

Table 12. E present before first heating run. Measured temperatures, mean values.

Com.	x-	T_b	T_mE	$T_m$tet.inc.	$T_m$tet.tot.	$T_m$hex.	$T_m$sy.	$T_m$ha.	HP gas
1	51.1	104.3	193.2	175.8	176.1	116.9	169.3	293.2	+
2	71.1	155.4	183.1	/	175.9	113.9	/	292.4	–
	73.1	176.3	180.8	175.7	176.6	112.6	/	297.4	+
	74.1	161.5	181.2	171.2	175.7	113.3	/	292.9	+
3	78.1	172.9	179.6	173.9	175.1	112.6	/	287.8	+
	80.1	174.8	180.1	165.2	175.9	110.5	/	282	+
4	81.1	176.5	182.8	162	175.8	115.0	225	291.6	+

Comments on table 12

General comments. The solid:liquid ratio is extremely large before the first heating run. Grains of halite were in suspension in the trapped solutions in all the inclusions. With the exception of x-71.1, the melting of the halite released high-pressure gas. All the inclusions are modified negative crystals and the total melting temperatures of the tetrahydrate, which are minimum trapping temperatures, are practically the same (Discussion).

During the cooling periods bischofite formed in all inclusions.

1. After total melting of E (193.2°C) in the first heating run, only solution was left. The run was interrupted, and halite and two small grains of sylvite formed spontaneously at 159.5°C. Therefore, E consisted of much $MgCl_2 \cdot 4H_2O$, less NaCl and a small amount of KCl. E did not re-form in the succeeding runs.
2. E re-forms during the cooling periods in first and second heating runs. Also tetrahydrate and bischofite formed. In the second and third run, where E was present, the bischofite melted at 116.8°C in both runs. In the following three runs, where no E was present, the bischofite melted at 114.6, 114.3, 112,7°C, respectively. As KCl in solution lowers the melting temperature of bischofite with 1°C per 1.5 mol K_2Cl_2, E consisted of $MgCl_2 \cdot 4H_2O$, less NaCl and a very little amount of KCL.
3. E re-formed after the first heating run. The composition is slightly different, because tetrahydrate and bischofite also crystallized. The total melting temperature in the second run of the re-formed E is slightly lower than in the first run.
4. The heating runs of x-81.1 are expounded in detail below.

Heating runs of x-81.1, table 13

The long axis of the kidney shaped, faceted inclusion deviates c. 45° from the c-axis of the quarts crystal, maybe "twinning" according to the Zwickauer law (Zyndel 1914, figs. 1,2).

The solid:liquid ratio is extremely large with the liquid and a small bubble gathering in a small void in the surface of the solid chemical combination E.

In table 13 are noted the temperatures measured during the heating runs.

Table 13. Measured temperatures on x-81.1.

Com.	Events	1st run	2nd run	3rd run	4th run	5th run
1	T_b	178.8	/	175.9	176.1	175.3
2	T_mE,tot.	182.8	181.7	/	/	/
	$T_r$hex.	80	85.8	/	85.4	88.8
3	$T_m$hex.	/	117.0	114.9	115.1	115.0
4	$T_m$tet.tot.	/	/	175.9	176.1	175.4
5	$T_r$tet.	/	159.6	161.8	160.5	160.2
6	$T_m$ha.	/	290	/	/	291.6

Comments on table 13

1. No bubble nucleated after the first heating run, i.e. "stretched" fluid (Roedder 1967). The disappearence temperatures T_b in runs 1, 3, 4, and 5 show a minor amount of high-pressure gas in the vapour bubble.
2. After melting of the chemical combination E in the first and second runs, a thin crystal of halite, 22 x 20 μm, was discovered. E did not re-form after the second run.
3. In the second run, the bischofite melted in the presence of E, i.e. less KCl in the solution and therefore higher melting temperature of the bischofite than in the following runs.
4. The mean melting temperature of the tetrahydrate is 175.8°C, c. 6°C below the melting temperature of pure tetrahydrate under atmospheric pressure. This difference corresponds to c. 9 mol K_2Cl_2 /1000 mol H_2O in the equilibrium solution (fig. 6A).
5. The re-formation of tetrahydrate is spontaneous but incomplete. More tetrahydrate precipitates during the further cooling. In the fourth run, the tetrahydrate forms grains of a hexagonal shape, the length of an edge being 5-6 μm.
6. High-pressure gas was released during the total melting of the grain of halite in the second run. In the second and the fourth runs, the halite recrystallized into an octahedron with the length of an edge of 19 μm, maybe caused by a too fast cooling rate of some reason. In the fifth run the halite re-forms spontaneously in the characteristic reticulate pattern with a few very small "pearls" of sylvite, which melt from 216.2°C to c. 225°C.

Discussion

The quartz crystals

The deck halite-salt clay transition, Na2r – T3, is repeated at a depth of c. 2890 – 2900 m in the Erslev-1 well (fig. 5B). The insoluble residue from 500 g of salt clay from core No. 32 was separated. The clay is far more silty than the clay from core No. 30 at a depth of 2800 m (fig. 13). The number of quartz crystals is many times larger than the number from the studied core No. 30, and the number of usable crystals runs up to several thousands per 500 g. of core material. The formation of the quartz crystals is clearly connected with the clayey and silty material in the salt.

The salt clay member T3 of the German Zechstein evaporites is mainly composed of koenenite and quartz that formed concurrently (Sonnenfeld 1984, p. 263). Koenenite, $2MgCl_2 \cdot 3Mg(OH)_2 \cdot 2Al_2O_3 \cdot 3H_2O$, represents an exchange reaction between clay detritus and salt solution, taking up the Al component. Quartz in direct association with the koenenite must be considered of detrital origin only (Kühn 1968, p. 444).

It is a distinctive feature of the quartz crystals from Na2r – T3, in contrast to the quartz crystals from the grey salt Na1 and Na2, that clastic quartz grains as solid inclusions in the crystals are very rare. This means that the quartz precipitated from a solution saturated with silica, but barren of visible crystallization seeds. The silica-saturated solutions may derive from dissolved clastic quartz or from the alteration of the clay (Stewart 1956, p. 133, Harder 1966, p. 441, Hower et al. 1976, p. 733). The addition of small quantities of magnesium or aluminium ions to the solution drastically reduces the solubility of silica (Weaver and Pollard 1973, p. 170). Therefore, the quartz crystals possibly formed after mixing of the silica-rich solutions and the $MgCl_2$-rich solutions.

Many scientists consider the crystallization of the euhedral quartz in evaporites to be synsedimentary or early diagenetic (e.g. Grimm 1962a, p. 884, Demangeon 1966, p. 485, Nachsel 1966, p. 326, Arbey 1980, p. 316). The crystallization temperatures (c. 180°C) and pressures (c. 100 MPa) measured and calculated by Fabricius (1987) clearly show that the quartz crystals of the present work crystallized after the metamorphism of the potash zone K2, long time after the end of the diagenesis. The metamorphism of evaporites takes place at considerably lower temperatures and pressures than the metamorphism of silicate and carbonate rock (Winkler 1967, p. 1, Hodenberg et al. 1987, p. 90).

Holes after grains of carnallite

The holes in some crystals after now dissolved carnallite (pl. I, II, and III) may be caused by a grain of carnallite, which was either suspended in the solvent and then adhering to the growing face of the quartz crystal, or the carnallite nucleated on the growing crystal face (Smith 1954, p. 206). Or, reversely, the quartz may have nucleated on the surface of a grain of carnallite, the so-called *induced nucleation* (Fyfe et al. 1978, p. 104).

A possible explanation of the irregular holes after carnallite, the "front" of fluid inclusions, and the trapped dry grains of carnallite is given by Roedder (1979, p. 691): Solid particles are by far the most common source of interference, causing trapping of primary inclusions. The solid particle may be pushed along during the growth of the quartz crystal, leaving a trail of inclusions behind it. But generally the crystal grows over the solid particle, thus trapping a solid inclusion with or without some of the surrounding fluid medium.

The possibility of nucleation and crystallization of carnallite on the growing quartz crystal is strongly supported by the presence of the fluid inclusion front, combined with the quartz crystallization process (Roedder 1981b, p. 10).

Pl. III, fig. 1 shows a quartz crystal in a 1 mm thick section of the deck halite Na2r. In the upper pyramid of the quartz a grain of carnallite is trapped, partly in the quartz and partly in the surrounding halite. In connexion with the carnallite is seen high-pressure gas bubbles on the grain boundaries.

When the quartz crystallized combined with grains of carnallite of the first generation (Sub-section: Veggerby Potash Zone K2 and deck halite Na2r), inclusions of the surrounding solutions were trapped by the growing quartz. The solutions were in equilibrium with the grains of carnallite and with the host halite. Concequently, the melting/dissolving temperature of the carnallite in the inclusions of group A, B, and C, found in the laboratory, are minimum trapping temperatures. And the estimated pressures are minimum trapping pressures. The maximum melting temperature T_m car

= 178.9°C is measured on x-48.1 (table 8, pl. I). The trapping pressure of this inclusion must necessarily be higher than c. 110 MPa, because the quartz crystallized in connexion with a grain of carnallite of the first generation. P_t = (T_m car – 167.5°C)10 MPa = 114 MPa.

A few other crystals without a hole after carnallite, contain inclusions with carnallite having a higher T_m car, e.g. x-35.1: T_m car = 182.8°C, (table 6). These crystals possibly crystallized at later events with higher temperatures than the T_m car mentioned above.

The same kind of arguments cannot be used on crystals with holes after carnallite combined with inclusions of group D: tetrahydrate, but no carnallite present. The reason is that the melting temperature of tetrahydrate is highly dependent on the concentration of KCl in the trapped solution as opposed to carnallite.

The holes after carnallite combined with the melting temperatures of the carnallite in the inclusions, i.e. minimum trapping temperatures, proves that the melting temperature of carnallite is dependent on the pressure.

Stability, metastability, and crystallization

After total melting/dissolving of a solid phase, the rate of crystallization (re-formation) depends on

i. the ratio of supersaturation,
ii. the viscosity governing the rate of diffusion,
iii. the temperature,
iv. the rate of building-in of the solvates into the lattices.

The rate of crystallization is extremely large for halite and sylvite, somewhat smaller for carnallite and very small for kieserite and anhydrite (d'Ans and Kühn 1960, pp. 74-75).

The rates of crystallization of halite, sylvite, and carnallite noticed in the present work, correspond perfectly to the statement mentioned above.

The ratio of supersaturation is measured by means of the supercooling from the melting/dissolving temperature to the re-formation temperature. The ratio of supersaturation is very high for halite and much lower for sylvite, carnallite, and bischofite. The rate of crystallization of tetrahydrate is much slower than that of carnallite, and the crystallization is incomplete, as opposed to carnallite despite the same ratio of supercooling. This reaction of tetrahydrate may possibly be due to a somewhat slower formation of crystallization nuclei and a much slower growth of these nuclei. The nuclei must achieve a critical size before they are able to grow (Fyfe et al. 1978, pp. 90, 95, 103). The tetrahydrate nuclei possibly have difficulties in reaching the necessary critical size.

The diffusion of molecules and ions through liquids or solids is a very important process concerning the crystallization rate. The rate of diffusion is governed by the viscosity of the trapped solutions. The viscosity of the solutions (c. 5 poises at 20°C) increases with increasing pressure, but decreases dramatically with increasing temperature, so the net result at the actual re-formation temperatures (160-125°C) is a much lower viscosity, which facilitates the diffusion.

The diffusion path goes along the mosaic structure, consisting of a mosaic of blocks or lineages (pl. III, fig. 4) bounded by submicroscopic cracks that originated thermally or by primary growth. Diffusion through crystal lattices proceeds in proportion to the concentration gradient and the diffusion coefficient, which depends on the state of aggregation (disorder or vacancies) of the host (Holser 1947, pp. 390, 391, 395).

In the actual, comparatively large, three-dimensional inclusions concentration gradients develop locally, due to the dissolving or re-formation of the different solids at different temperatures. When the dissolved salt reforms, the concentration of solution where crystallization takes place, will be less (Duffell 1937, p. 496, Holser 1947, p. 389).

Concentration gradients develop even in homogeneous solutions and are related to temperature gradients (Tollert 1950, Sonnenfeld 1984, p. 53). These concentration gradients are a prime factor in transfer by diffusion (Duffell 1937, p. 495).

In the laboratory a high degree of metastability is observed, primarily through the pronounced decrease of the solid: liquid ratio after total melting/dissolving of the solids. Obviously, this deceptive metastability is a matter of the rate of crystallization totally, rather than true chemical metastability. The rate of crystallization is governed by the factors mentioned above, but also "foreign" ions in the solutions may have a certain influence.

The only true chemical metastability observed is seen during the transition from tetrahydrate to bischofite, e.g. in inclusion x-82.1 (pl. III, figs. 13-16), and the provoked, unnatural metastability after the freezing runs in inclusion x-67.1 (pl. IV, figs. 10-16 and pl. V, figs. 2-8). Also in these cases it is believed that equilibration into natural conditions is a matter of time, because bischofite and sylvite eventually form carnallite.

The best example of mestability is demonstrated by the thermal behaviour of the chemical combination E. The composition of E varies from inclusion to inclusion depending on the amounts of NaCl, KCl and $MgCl_2$ in the inclusion. As time certainly works in the direction of obtaining the most stable mineral (Holser 1979, p. 248), it is believed that E is a stable phase in these chemically closed systems. Before and during the first heating run up to the incipient melting temperature, E is in equilibrium with the extremely small amount of solution present in the inclusion. This equilibrium is

interrupted, when E melts totally. And as the build-up of E possibly demands a very long time, maybe geologic time, E cannot be re-formed in the laboratory.

The influence of "foreign" ions and molecules

The solutions of the inclusions are not pure Na-K-Mg-Cl solutions. Other ions like calcium, iron, rubidium, strontium, boron, sulphate, bromide etc. may be present. The solutions derive from the original sylvite-carnallite rocks K2 (e.g. Braitsch and Herrmann 1964, p. 1083), and therefore contain approximately the same amounts of these ions as were present in the original solid carnallitite.

As calcium and magnesium have a higher affinity to sulphate than to chlorine, the calcium and magnesium sulphates already have precipitated as anhydrite and kieserite at the original place of K2. Neither anhydrite nor kieserite are found in the inclusions. Kieserite is very rare as solid inclusion in the quartz crystals and anhydrite precipitated in the deck halite long before the quartz crystals. Therefore, it is stated that the content of sulphate in the solutions is negligible.

The secondary iron mineral rinneite: $3KCl{\cdot}NaCl{\cdot}FeCl_2$ is sporadically found in the deck halite but is not detected in the inclusions. In one inclusion, x-79.1, two very small, angular, opaque grains were found. The grains dissolved at c. 270°C and reformed at c. 155°C. The grains might be pyrite, which in places is abundant in the salt but extremely rare as inclusions. And so is hematite, maybe due to the "self-cleaning effect" of quartz concerning bitumen, hematite, and clay (Grimm 1962b, p. 600). Therefore, iron is believed to be present in the solutions in negligible amounts only.

The mineral boracite, $(Mg,Fe,Mn)_3\ ClB_7O_{13}$, precipitates very late in the evaporitic cycle as an early diagenetic mineral in equilibrium with solutions rich in $MgCl_2$ (Borchert 1940). Boracite and kieserite form concurrently as secondary minerals in potash zones (Kokorsch 1960, p. 63).

Concretions of boracite (= stassfurtite) are abundant in the potash zone K2, fig. 5B, but absent in the deck halite Na2r. Concequently, the concentration of boron is negligible.

Bromine is the only foreign ion that may have a certain influence on the rate of crystallization. With increase in the concentration of magnesium chloride in the brine the degree of diadochy between chloride and bromine also increases (Myagkov 1961, p. 775). The ionic radius of chlorine is 0.181 nm and of bromine 0.195 nm, i.e. a difference of approximately 7% of the larger bromine ion. This diadochy illustrates Goldschmidt's first rule of camouflage of the trace element (Kühn 1968, table 3). Bromine occurs diadochically almost exclusively for Cl in chlorides, although most of it remains in the residual solution (Braitsch 1962, p. 101, 1971).

The net result of the building-in of the foreign ions into the lattices of the precipitates in the inclusions is a minor distortion of the lattices, whereby the rate of diffusion is increased to some extent.

Gas molecules also unlock the lattices (Kühn 1952, p. 149). As high-pressure gas is present in practically all the inclusions, the diffusion into the lattices is made essentially easier.

Formation of chemical combination E

As in some inclusions, especially in inclusion x-82.1 (table 9) and after melting/dissolving of the solids, E precipitates from the solution, and in the next heating run dissolves at a higher temperature than the other solids tetrahydrate and carnallite, E must be a chemical combination, not an epitaxial compound. The epitaxy depends on lattice similarities between the salts, e.g. sylvite-halite (Kühn 1955, p. 94). That carnallite, tetrahydrate, sylvite, and halite should have common lattice characteristics, resulting in epitaxy, is unimaginable.

After the total melting of E in the first heating run the solid:liquid ratio decreases remarkably. The ratio at 20°C is still very large, but the liquid is now visible. This feature indicates that E is a hydrated complex, because the complexing is accompanied by an increase in volume (Titov 1939, tables 1-5, fig. 1). Titov (1949, p. 459) found, by the aid of the volumetric method at 20°C, in concentrated $MgCl_2$ solutions, complexing with NaCl but not with KCl. The complex: Na_2MgCl_4 was not hydrated, but Titov notes (p. 458) that the hydrates $NaCl{\cdot}MgCl_2{\cdot}H_2O$ and $KCl{\cdot}MgCl_2{\cdot}H_2O$ are probable complexes.

Preferentially, E is found in inclusions of group C and D (tables 8, 12). Carnallite and/or tetrahydrate are by far the most important components, whereas halite and especially sylvite play a minor role.

A quantitative determination of the composition of E is not possible, in consequence of the uncertainty of the volume calculations of the inclusions and the solid phases (Roedder and Bodnar 1980, p. 267). One inclusion (x-71.1) is nearly a sphere, slightly faceted on one side, with a diameter of 32 μm. The contents of the inclusion are $MgCl_2{\cdot}4H_2O$, very little amount of KCl, and a crystal of NaCl, approximately 13x13x10 μm. The semiquantitative composition of E is calculated to $0.1KCl{\cdot}NaCl{\cdot}MgCl_2{\cdot}4H_2O$, taking into account the negative lens effect of the vaulted surface of the inclusion.

The grains of halite were in suspension in the trapped solutions, which is proved by the very high dissolving temperatures (275-300°C) of the grains in consequence of the low solubility of halite in highly concentrated $MgCl_2$ solutions. As halite is a component of E, E

cannot be a precipitate from the trapped solutions. The precipitation temperature of carnallite or tetrahydrate in the inclusions is 150-160°C (table 9 and 13), i.e. 20-30°C below the assumed trapping temperature. These precipitation temperatures were present in the salt body at a depth of 2600-3400 m., corresponding to pressures of 60-80 MPa (Fabricius 1984, fig. 9). Therefore, the formation of E is a chemical reaction between solid salts. The rates of solid-solid reactions are extremely slow, and they are unlikely to attain equilibrium in geological time scales under the P-T conditions mentioned, without the catalytic effect of fluid (Fyfe et al. 1978, pp. 117,119).

E may have formed by the aid of ion exchange between the solid phases and/or by the aid of the saturated dipole water film on the grain surfaces. The water film acts as a catalyst and a flux, and foreign elements or gasses, causing lattice distortions, accelerate the processes (Kühn 1952, pp. 149, 150).

Only in inclusion x-82.1, E partly re-formed after the first and the following heating runs. The amount of E decreases consecutively from the first to the fifth run. And so does the total melting temperature: from 182.5°C to 173.7°C. As E re-forms with no delay after all the heating runs on x-82.1, E in this inclusion possibly is the mineral almeraite: $KCl{\cdot}NaCl{\cdot}MgCl_2{\cdot}H_2O$.

In the beginning of the geologic cooling period comparatively much solution was present and the alteration of the precipitates and the trapped grain of halite took place by means of diffusion of ions or atoms through the fluid phase into the crystal lattice. After the liquid was practically used up, the chemical processes are reactions between solid phases, which are almost inextricably connected with diffusion of the exchanged matter (Holser 1947, pp. 391, 392).

The cooling period, from the trapping temperature (ca. 180°C) to the in situ temperature (55-60°C at a depth of 2800 m), had a length of more than 100 millions of years. Under these conditions in chemically closed systems, E may be a stable phase, which cannot be re-established in the laboratory due to the time required.

Melting temperatures of tetrahydrate and daughter bischofite

When melting incongruently in a closed system, the melting temperature of the hydrates bischofite and carnallite are pressure-dependent with a dT/dP value of 0.1°C/MPa (fig. 11). Hydrohalite, $NaCl{\cdot}2H_2O$, shows pressure-dependent melting temperatures: 0.15°C at atmospheric pressure and 25°C at 8000-12000 atm. (Jänecke 1949, p. 250). Also the hydrated sulphates kieserite and polyhalite, besides carnallite, show pressure-dependent melting temperatures, when melting in a closed system (Hinze et al. 1985, p. 98).

The inclusions noted in table 12 are all negative crystals containing much tetrahydrate, a small trapped grain of halite, and very little KCl, except x-81.1. The melting temperatures of the tetrahydrate are remarcably equal: $T_m$tet. = 175.9°C ± 0.4°C, 95% confidence limit, with a spread of 1.5°C. The shapes of the inclusions show trapping of a tetrahydrate-KCl solution saturated with respect to NaCl, and with a grain of halite in suspension. Obviously, the inclusions are trapped under equal conditions as far as pressure and temperature are concerned.

According to d'Ans and Sypiena (1942, p. 93), van't Hoff and Meyerhoffer (1899) stated the transition temperature tetrahydrate-dihydrate to be 176°C in an equilibrium solution saturated with KCl: 240 mol $MgCl_2$ + 20.5 mol K_2Cl_2 per 1000 mol H_2O at atmospheric pressure, i.e. 1°C per 3.7 mol K_2Cl_2/1000 mol H_2O. This drop of temperature from 181.5°C for pure $MgCl_2{\cdot}4H_2O$ is regarded to be too low by d'Ans and Sypiena, who argue in favour of a temperature drop of 1°C per 1.5 mol K_2Cl_2/1000 mol H_2O, based on an equilibrium solution of 249 mol $MgCl_2$ + 40 mol K_2Cl_2 per 1000 mol H_2O and saturated with NaCl (fig. 6A).

The solution of tetrahydrate in x-81.1 is saturated with NaCl and KCl: 250 mol $MgCl_2$ + c. 40 mol K_2Cl_2 + less than 1 mole Na_2Cl_2 per 1000 mol H_2O. The salinity is c. 63 weight%. The temperature difference 181.5°C – 175.9°C = 5.6°C corresponds to c. 8 mol K_2Cl_2/1000 mol H_2O. The remaining c. 32 mol K_2Cl_2 correspond to c. 21°C, which is an expression of the effect of the pressure in the inclusion during the melting of the tetrahydrate. The disappearance temperature T_b = 104.3°C of the liquid shrinkage vapour bubble in the inclusion x-51.1 is probably valid for all the inclusions noted in table 12. $T_m - T_b$ = 175.9 – 104.3 = 71.6°C. From fig. 12: dP/dT = 1.00 MPa/°C. P_m = c. 70 MPa.

Bischofite formed after melting of the tetrahydrate in all the inclusions noted in table 12, even in x-81.1 despite saturation with KCl. The melting temperature of bischofite, $T_m$hex. = 116.7°C, is lowered 1°C per 1.5 mol K_2Cl_2/1000 mol H_2O at atmospheric pressure (fig. 6B). The inclusions x-51.1 and x-81.1 have the highest contents of KCl in solution but the lowest deviation from 116.7°C. Carnallite was not observed in these inclusions. Concequently, a high degree of metastability is present concerning bischofite (Materials and methods, sub-section *Bischofite, hexahydrate*).

High-pressure gas, partial decrepitation, or stretched walls

The last solid phase – halite or, very rarely, sylvite – dissolves at temperatures between 275°C and 300°C. The heating run is interrupted as soon as the solid phase disappears. The pressure in the inclusion cannot be calculated due to the high dissolving temperature.

But the pressure must be high, the melting temperature being 150-200°C higher than the disappearance temperature T_h of the liquid shrinkage bubble. No signs of decrepitation like micro-fractures or escape of solution, or nucleation of a bubble, are observed.

During the cooling down from the total dissolving temperature, a bubble nucleates between 285°C and 250°C in a few inclusions. The vast majority of the bubbles nucleates between 110°C and 75°C, very often combined with the re-formation of bischofite in the interval 100-90°C. All these bubbles are much larger than the very small liquid shrinkage vapour bubbles before the first heating runs (e.g. pl. V, figs. 9 and 14). The disappearance temperatures of the bubbles nucleating in the interval 110-75°C is in the interval 174.9-177.8°C combined with the total melting of the carnallite component. The disappearance temperatures T_h of the shrinkage bubbles in the first heating runs are 20-70°C lower than the disappearance temperatures noted above. Some of these bubbles possibly contain a small amount of high-pressure gas before the first heating run.

In 10 inclusions containing carnallite as the main solid component, the carnallite melted incongruently in the interval 170.6-179.6°C. The mean melting temperature T_m car. = 175.1°C ± 1.8°C, 95% confidence limit. This temperature corresponds to a pressure of c. 80 MPa. The mean bubble disappearance temperature equals 175.8°C ± 1.1°C, 95% confidence limit, therefore also corresponds to a pressure of c. 80 MPa.

If a partial decrepitation took place, resulting in the formation of a bubble, when the halite dissolved, and no high-pressure gas was released, the pressure in the bubble equals the vapour pressure of the highly saline solution. The vapour pressure decreases with increasing salinity and increases with increasing temperature. The vapour pressure of a 25.0 weight% NaCl solution at 180°C is 0.80 MPa and at 300°C 6.86 MPa (Haas 1971, p. 943). Khaibullin and Borisov (1966, p. 491) note the corresponding pressures to be 0.868 MPa and 7.25 MPa. The vapour pressure of a solution containing 25.0 wt.% Na_2O + 5.9 wt.% Al_2O_3 at 200°C is approximately 0.9 MPa and at 300°C c. 5 MPa (Potter and Haas 1978, fig. 5). The vapour pressures of bitterns containing 45 to 80 wt.% totally dissolved salts range from 0.7 MPa to a few hundredths MPa at 200°C (Stewart and Potter 1979, p. 303). Consequently, it is postulated that high-pressure gas is released when the trapped grain of halite dissolves in the highly saline K-Mg-Cl solution.

Possible nature of high-pressure gas

According to Kühn (1955, p. 70) *H_2S* gas is observed in coarse crystalline sylvite (Knistersalz = popping salt) from the Stassfurt Potash Zone (K2) in Germany. The gas occurs, microscopically visible, as dry bubbles and as bubbles in fluid inclusions in the crystals. This and other similar occurrences are always restricted to tectonic or transformation zones, i.e. bounded to non-primary salt formations.

Liquid and gaseous *hydrocarbons* are common in relatively undisturbed salt and potash sequences, being evidently formed *in situ* (Peterson and Hite 1969, p. 905). Interstitial and intercrystalline quantities of hydrocarbons are much greater than in underlying halite and anhydrite sequences.

The solubility of *methane* in aqueous solutions of NaCl and $CaCl_2$ is relatively low and decreases with increase in salt concentration at room temperature. The solubility increases with pressure (Duffy et al. 1961, pp. 30-31).

According to Sonnenfeld (1984, p. 277) increasing salinity of brines and formation waters decreases the solubility of *hydrocarbons* (Faingersh 1977), since nearly saturated levels of solute content alter the water structure to promote hydrophobic interactions of macromolecules (Borowitzka 1981).

Nitrogen gas very often occurs in halite and potash salts, mainly as inclusions and along crystal faces, always under high pressure. *Ammonia* reaches its maximum – up to 77 ppm – in carnallite (Sonnenfeld 1985, p. 256).

Oxygen solubility decreases markedly as the brine in seawater-fed lagoons is concentrated. At a seven-fold brine concentration (salinity: c.25 weight%), oxygen solubility drops to one-third of its value in seawater (Peterson and Hite 1969, p. 906). The solubility of oxygen is less than 2 ppm at 50°C, because the solubility decreases with increasing temperature (Kinsman et al. 1974, fig. 3).

The solubility of *carbon dioxide* in salt solutions markedly depends on the concentration of salt, and solubility decreases rapidly as the amount of salt increases (Takenouchi and Kennedy 1965, p. 451). Prutton and Savage (1945) found that the solubility of carbon dioxide in a 30 wt.% $CaCl_2$ solution at 121°C approximately is 1 wt.%, very weakly dependent on an increase in the pressure (Takenouchi and Kennedy 1965, fig. 1).

The composition of the released gas is unknown. CO_2 was not observed during the freezing runs. However, since magnesite is present in the water-insoluble residue and as solid inclusions in the quartz crystals, CO_2 might have been present in the salt before the formation of the quartz crystals. Therefore, traces of CO_2 in the gas cannot be excluded. As pyrite is abundant in the residue but extremely rare in the quartz crystals, H_2S was possibly present before and during the formation of the quartz. So, H_2S may be an appreciable part of the gas. This assumption is supported by a smell of mercaptane (-HS) combinations from the salt core when the core is crushed. The content of H_2S is a

characteristic feature of the Stassfurt series (Kokorsch 1930, p. 77).

Veggerby Potash Zone K2 and deck halite Na2r

The Danish Zechstein 2 evaporite cycle (table 1, fig. 5A) corresponds very well to the German Z2, except a very weakly developed deck anhydrite A2r at the top of the Danish Z2. The cycle represents a complete evaporite cycle beginning with carbonate-sulphate facies (Ca2), followed by halite facies (Na2) and ending upwith K-Mg facies (K2), expressed by sylvite and carnallite (Richter-Bernburg 1953). There are no signs of bischofite, but bischofite may be the final product of the cycle.

The Z2 cycle in NW Germany was brought to an end by a phase of remarcably rapid influx of sea water (Borchert and Muir 1964, p. 56). Also in the Norwegian-Danish basin this rapid influx must have happened, proved by the presence of the K-Mg-Cl mineralized deck halite Na2r. The presence of magnesite in the deck halite and as solid inclusions in the quartz crystals shows the formation of the deck halite in the deeper parts of the basin (Kühn 1968, p. 467), i.e. in the area south of the Mors dome (fig. 3). The so-called reversed profile above the potash zone K2: Ca2-Na2-K2-Na2r-A2r is a typical feature of potash zones precipitated in the deepest parts of the shallow basin, almost filled with halite (Waljaschko 1958, p. 226).

The brine above the precipitated potash zone was stratified with a bottom layer of the heavy $MgCl_2$ solution (d.: 1.34 g/cm^3 at 20°C), above which was situated a lighter layer of in-flowing sea water (d: 1.22 g/cm^3 at 20°C) (Raup 1970, table 2, fig. 7B). Due to the density gradient, the two layers did not mix, whereby the heavy bottom layer protected the precipitated potash deposit against solution and let pass the halite crystals snowing down from a higher level of the brine body, which was saturated mainly in NaCl (Richter-Bernburg 1972, p. 35, Harvie et al. 1980, p. 499). But also a slow diffusion of the lighter sodium-enriched brine into the heavier magnesium bittern in the interface zone leads to halite precipitation, i.e. to a salting-out effect (Raup 1970, pp. 2255-6).

The evaporation continues during the formation of the deck halite, resulting in further K-Mg concentration of the residual solutions. In (1 mm) thick sections of the studied deck halite are found many solid inclusions of carnallite with a very high S:L ratio (pl. III, figs. 2 and 3). Also many intergranular scales of hematite are present, sometimes within the grains of carnallite, but most frequently within sylvite, which has replaced carnallite, or within the halite. This carnallite is most likely the first generation, trapped in the halite during the compaction of the deck halite, possibly in the course of the remaining Zechstein times. This first generation of carnallite has no direct relation to the carnallite found in the quartz crystals.

Post-Zechstein sedimentation

The strong subsidence of the basin in Zechstein times continued throughout Triassic times. Approximately 5000 metres of Triassic sediments were accumulated in the central part of the basin (table 14).

The lithology comprises only the main rock types (Priisholm and Christensen 1985, p. 42). The depths of sediments/overburden are approximate (Priisholm et al. 1982, figs. 5, 6, 7).

The pressures of the overburden are calculated based on the bulk density to base of the column: from 2.18 g/cm^3 at a depth of 2 km to 2.33 g/cm^3 at a depth of 6 km (Dickinson 1953, fig. 14, Bodenlos 1970, table 1).

The Middle Jurassic sediments are not present. Instead erosional unconformities are found. So, depths of these sediments are unknown.

The temperatures noted are based on typical model temperatures related to bore hole temperatures for the central part of the Danish subbasin (Michelsen et al. 1981, fig. 6).

The value of the thermal conductivity for claystone equals 1-2 W/Km, for limestone 1.5-2.5, for sandstone 2.5-4, and for rock salt 5-7 W/Km (Michelsen et al. 1981, p. 14).

The geothermal gradient above Upper Permian va-

Table 14. Sedimentation centrally in the basin.

Epoch	Sediments		Overburden		Temperatures top U.P.,°C
	Lithology	Depth,km.	km.	MPa	
U.J.–L.C.	clay-, siltst.	1	6	140	155–240
L.J.	clay-, sandst.				
U.Tr.	clayst. salt	2	5	115	140–200
M.Tr.	clay-, limest.	1	3	70	100–140
L.Tr.	clay-, sandst.	2	2	45	70– 90
U.P.	evaporites	1	0	/	/

ries from 25 mK/m to 40 mK/m due to the high contents of claystone. The gradient in the salt formations is only 10 mK/m (Bachu 1985, fig. 9, p. 282).

These values show that layers of claystone are acting as insulating layers against heat from below. Therefore, a thermal build-up occurs in bedded rock salt below layers of claystone like the Lower Triassic Bunter Shale Formation (Talbot et al. 1982, p. 195).

In the deepest parts of the Polish Zechstein basin, the salt bearing rocks were subjected to the increasing pressure of the overlying rocks. Simultaneously, temperatures at these depths – 7000 m – reached more than 200°C (Kucha and Pawlikowski 1986, pp. 70, 75). The temperature of the German Zechstein salt rocks at a depth of 5000 m amounts to about 180°C (Richter-Bernburg 1977).

It is supposed that igneous intrusives, causing a high geothermal flux, are present in the basement below the sediments. Intrusives, enriched in U, Th, and K, are common in the Fennoscandian Border Zone, the northeastern border of the basin (Michelsen et al. 1981, p. 15).

The Early Permian volcanism in the basin is well documented: volcanics directly underlying the Zechstein sediments in well C-1, 30 km off the westcoast of N.Jutland, and in well D-1, 160 km west of the coast (Rasmussen 1974). The ages are 237 ± 16 m.y. and 276 ± 14 m.y., respectively. Volcanics from two wells onshore in the basin have the ages 250 ± 14 m.y. and 276 ± 12 m.y. (Larsen 1972, p. 92). Early Permian volcanism is also known in the southern border zone of the basin: the Ringkøbing-Fyn High, as well as the volcanism in the district of Oslo north of the basin.

For the reasons mentioned above it is supposed that the temperature at the top of Zechstein 2: K2 and Na2r, were markedly higher than the temperatures of the Lower Triassic clays, as long as the bedded salt was situated outside the salt pillow or diapir.

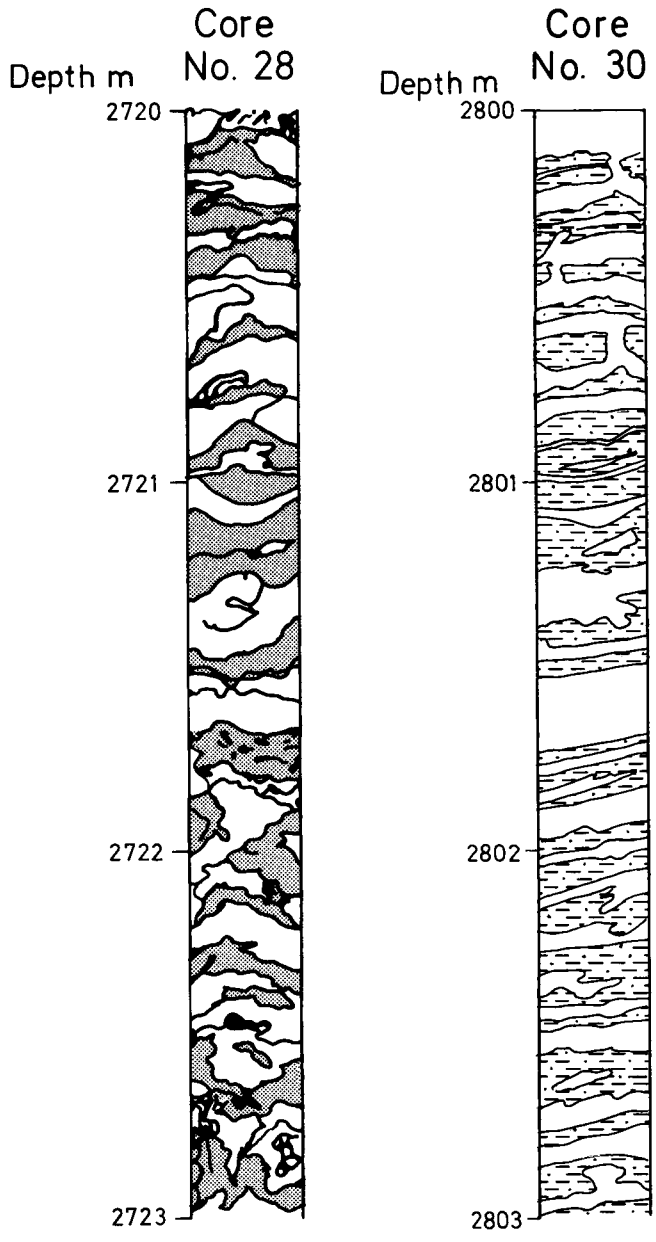

Fig. 13. Core No. 28. Veggerby Potash Zone K2 from drilled depth 2720 to 2723 m. Hard salt consisting of c. 30% kieserite, c. 30% sylvite, c. 30% halite, and less than 10% anhydrite. Lumps and thin bands of boracite. Disseminated small inclusions of carnallite. White to light grey kieseritel (mixed with salt: dotted), medium reddish orange to reddish brown halite and sylvite (white). The hard salt is strongly disturbed, mainly due to the large volume reduction of the original carnallite after geothermal metamorphism and squeezing out of the metamorphic lye.
Core No. 30. Deck halite Na2r from drilled depth 2800 to 2803 m. The core consists of dark yellowish orange to reddish brown halite (white) with strongly tectonized (brecciated and fractured) dusky brown to greyish black clayey siltstone. In the salt disseminated anhydrite, kieserite, secondary carnallite, and sylvite. In fractures and vugs primary carnallite with scales of hematite. In places rinneite.

Veggerby Potash Zone

The Veggerby Potash Zone K2, log depth 2691-2731 m, (figs. 5B and 13) is a kieseritic hard salt consisting of 54% halite, 34% kieserite, 8% sylvite, 1% anhydrite, and 2% clay and silt (Jacobsen 1984, p. 39). Concretions of boracite are common (Jacobsen and Christensen 1980, p. 27).

As kieserite can never precipitate from sea water (Borchert and Muir 1964, p. 174), and as boracite occurs in $MgCl_2$-rich solutions as a secondary mineral, but not post-diagenetic in origin (Braitsch 1962, 1971, p. 216), the kieseritic hard salt K2 must be a metamorphism product of the originally precipitated potassic rocks.

The halite-kieserite-sylvite hard salt may derive from progressive geothermal metamorphism of the evaporite assemblage halite-sylvite-epsomite, ($MgSO_4 \cdot 7H_2O$). During increasing temperature from 11°C up to 72.5°C, this assemblage is altered to the hard salt in question over different stages. Thereby is released a metamor-

phic lye, the so-called Q-lye (d'Ans and Kühn 1960, p. 73).

Q is the common corner of the stability fields kieserite, carnallite, and sylvite close to the Mg corner in the triangle diagram SO_4-Mg-K_2 (e.g. Borchert and Muir 1964, figs. 8.2-8.7).

Kieserite (+ sylvite) may form from alteration at 72°C of the primary paragenesis carnallite-halite-kainite, ($KCl \cdot MgSO_4 \cdot 2.75H_2O$) (Braitsch 1971, p. 110).

But other models are also conceivable:

i. A kieseritic halite-carnallite rock influenced by a saturated NaCl solution at 83°C, resulting in a Q-lye (Braitsch 1962, 1971, p. 180). The Q-lye at 83°C consists of 1.6 wt.% NaCl, 5.2 wt.% KCl, 29.2 wt.% $MgCl_2$, and 1.1 wt.% $MgSO_4$, giving a salinity of 36.9 wt.% (Baar 1952, p. 144).
ii. The paragenesis kieserite-carnallite-halite or kieserite-halite-carnallite, which is the most important potash salt paragenesis of ocean salt deposits, is altered to the hard salt in question by solution metamorphism, caused by percolating NaCl-$CaSO_4$ solutions at temperatures higher than 72°C, resulting in a Q-lye (Borchert 1958, p. 22, 1972, p. 64).
iii. The primary paragenesis halite-carnallite-hexahydrate (sakiite, $MgSO_4 \cdot 6H_2O$) is geothermally metamorphosed, ending up with release of a Q-lye, which causes precipitation of carnallite in fractures and pores of the hanging wall (Kokorsch 1960, p. 62, 67).
iv. The paragenesis kieserite-halite-carnallite or kieserite-carnallite-halite is altered to the hard salt in question through progressive geothermal metamorphism. The carnallite component melts incongruently, forming solid sylvite and an H-lye, consisting of 20.85 mol K_2Cl_2 + 166.7 mol $MgCl_2$ per 1000 mol H_2O, corresponding to 42.9 wt.% $MgCl_2$ + 8.4 wt.% KCl (Braitsch 1962, 1971 p. 112, Knipping and Hermann 1985, p. 115).

There is every probability that the latter model (iv.) is most likely to be the true one, because the metamorphic lye is highly concentrated in $MgCl_2$, and because the metamorphic temperature necessarily must be high.

Moreover, solution metamorphism is not so probable as progressive geothermal metamorphism, because the distances to solution producing layers like Ca2 (gypsum/anhydrite-dolomite), are large within the bedded rock salt.

According to Kern and Franke (1980, figs. 5 and 6), carnallite in a closed space begins dehydration at c. 85°C under atmospheric pressure, c. 140°C at 4 MPa, and c. 150°C under a pressure of 10 MPa. The dehydration is controlled by the water vapour pressure.

Supposing a bottom temperature of 10°C in the basin after precipitation of the carnallite, the temperature increase of 75°C demands a sedimentary column of c. 2 km, corresponding to a pressure of c. 45 MPa (table 14). The temperature 150°C is reached, when the pressure exceeds 70 MPa.

Kern and Franke (1986, p. 8) note that carnallite in a closed space is thermally stable close to the melting temperature 167.5°C under a pressure of c. 24 MPa. The carnallite studied in the present work is regarded to be situated in a closed space, surrounded by impermeable salt. Consequently, the carnallite concerned does not dehydrate with increasing temperature. But incongruent melting occurs at a temperature higher than 167.5°C due to the pressure-dependence (fig. 11).

At a depth of somewhat less than 5000 m the pressure is 80-90 MPa, giving a melting temperature of about 175°C (table 14).

Mineralization of deck halite Na2r

After the progressive geothermal melting of the primary carnallite, the equilibrium solution, i.e. the metamorphic $MgCl_2$-lye, which dissolved comparatively much KCl due to the high temperature, moved updip away from contact with the remaining reaction sylvite (Hentschel 1961, p. 147, fig. 7, Wardlaw 1968, pp. 1287, 1288).

The intercalated clayey layers in the deck halite (fig. 13) and the salt clay are compact and therefore competent compared with the grey salt. So, fissures, faults, and collapse cavities are generated within the hanging wall caused by the movements within the salt. The metamorphic lye is squeezed out from the potash zone into the hanging wall along these fractures and faults (Jänecke 1915, p. 75, Baar 1958, fig 4., 1960, p. 131, Goldsmith 1969, p. 795).

Table 15. Trapping conditions of the inclusions.

Group	T_t, °C appr.	P_t, MPa appr.	Epoch	Concentrations mol/1000 mol H_2O			Salinity wt.%
				$MgCl_2$	K_2Cl_2	Na_2Cl_2	
A	170–175	75–80	U.Tr.-J.	167	25	1.5	52
B	175–185	125	M.J.-L.C.	167	83	3	62
C	170–180	75–80	U.Tr.-J.	190	25	0	55
D	175–185	125	M.J.-L.C.	250	5	0	58

In table 15 is noted the results of the microthermometry. The trapped solutions are rich in $MgCl_2$, far less in KCl, and very poor in NaCl. The trapping temperatures T_t , i.e. the crystallization temperatures of the host quartz, are approximate, because no true measurements are possible due to the lack of daughter halite. The interpretation of T_t is partly based on the measured melting temperatures of carnallite and partly on experiences from earlier works (Fabricius 1984, table I, 1987, table 4). The estimated trapping pressures

P_t are based on the trapping temperatures combined with the depths of the overburden (table 14).

The post-Zechstein high below the Mors dome is situated at a depth of c. 5.5 km (fig. 4). So, the salt, feeding the dome from the south, moves updip horizontally c. 8 km and vertically c. 2.5 km (fig. 3).

The differential stress, i.e. the geostatic load combined with the bottom relief of the basin, is the prime motivating force on the bedded salt. The effectiveness of the differential stress depends on such factors as temperature, confining pressure, and the presence of solutions, which increase diffusive flow, or nonevaporites such as silt and clay, which reduce plasticity (Jackson and Talbot 1986, p. 306).

Richter-Bernburg (1970, p. 145) states that the pressure required for viscous salt flow is about 40 MPa. In the beginning the salt flow takes place in the lower parts of the bedded salt, i.e. preferentially in the grey salt Na1 and later also in Na2 (Jackson and Talbot 1986, p. 316). The upper 250-300 m of the Zechstein column (fig. 5A) may be retarded to some extent due to the high contents of clay or silt, and the frictional drag of the country rock.

The inclusions (table 15) are trapped by the quartz crystals outside the diapir during the salt flow. Or, more likely, the trapping may occur inside the diapir later than Late Triassic times, if the tectonic pressure during the initial diapirism in Early Jurassic or during the penetration phase in Late Jurassic-Early Cretaceous times is able to counterbalance the pressure of a sedimentary column of a depth of 1.5-2 km, see depth of overburden, fig. 4.

The bedded salt begins the flow late in Early Triassic in direction of the post-Zechstein high. The studied deck halite was drilled at a depth of 2.8 km, c. 3 km above the bottom of the dome. So, the salt concerned covers 8-12 km in a span of time of 220 m.y., which makes an average velocity of 0.05 mm/annum, including the high velocity 0.1-0.3 mm/annum during the diapiric penetration phase (Richter-Bernburg 1981, p. 29).

The temperature of the deck halite decreases during the uplift of the salt. The carnallite precipitates from the solutions, forming fracture fillings and disseminated grains, when the temperature drops below the pressure-dependent melting temperature.

Summary of the proposed mineralization model

The studied Zechstein 2 potash salt, consisting of the paragenesis kieserite-halite-carnallite or kieserite-carnallite-halite, was sedimented in the deeper parts of the basin, 6-10 km south of the later Mors dome.

The potash salt was altered by means of progressive geothermal metamorphism into the present kieseritic hard salt K2, the Veggerby Potash Zone.

The rock salt began viscous flow in direction of the post-Zechstein high in Early Triassic times when the geostatic pressure reached c. 40 MPa.

The metamorphic melting of the carnallite component took place at temperatures of c. 175°C under pressures of 80-90 MPa. The resulting, highly saline $MgCl_2$ solutions moved updip into the hanging wall – the deck halite – through fractures and along faults.

In Late Triassic times or maybe later during the diapiric penetration phase, the crystallizing quartz trapped solution and formed fluid inclusions as crystallographically orientated negative crystals.

When the temperature decreased during the uplift of the salt, the carnallite precipitated as fracture fillings and disseminated grains in the deck halite.

Conclusions

The formation of the quartz crystals in the deck halite is closely connected to the alteration of intercalated clay, combined with highly saline $MgCl_2$ solutions, which derive from progressive geothermal metamorphism of the original carnallitic potash bed, stratigraphically below the deck halite.

During the formation of the quartz crystals, solution with grains of halite in suspension was trapped, forming large faceted negative crystals, crystallographically orientated with the host quartz.

In several of these inclusions a chemical combination, named E, is found before the first heating run. E consists of carnallite, sylvite, halite, and, in some inclusions, also of tetrahydrate. Even though the composition of the various inclusions is different, E must be a stable phase, stabilized through millions of years. Therefore, E cannot re-form in the laboratory.

As the solid:liquid ratio is very large even after the heating runs, the solution represents a melt, often with a grain of halite in suspension. The compositions of the trapped solutions vary from a melt of carnallite: 167 mol $MgCl_2$ + 83 mol K_2Cl_2 + 3 mol Na_2Cl_2 per 1000 mol H_2O to a melt of tetrahydrate: 250 mol $MgCl_2$ + 5 mol K_2Cl_2 + 0 mol Na_2Cl_2 per 1000 mol H_2O. The salinity varies from 52 to 62 weight%.

Due to the highly complex solutions, a high degree of metastability during and after the heating runs must be expected. Therefore, much patience is needed, because normal heating runs up to 200°C and back to 20°C may rest for hours. Especially the phase transitions, e.g. bischofite-tetrahydrate or melting of the solid phases, are crtitical. So, a very small heating rate is necessary. Also the equilibration time after the heating runs is critical. Very often an equilibration time of 24 hours or some days must be spent. Equilibration during the runs, especially when the solid phases re-form, is often a necessity.

In a few cases solid grains of carnallite were trapped. The melt of these grains shows much higher metastability than did melts of daughter carnallite. But also inclusions, containing the complex solutions/melts of carnallite, tetrahydrate, and sylvite with a grain of halite in suspension, show high metastability, especially concerning the melting of the tetrahydrate and the carnallite components. Therefore, several heating runs on these inclusions are a necessity.

High-pressure gas is released, when trapped grains of halite or carnallite are dissolved. Thereby it is proved that the gas is dissolved in the solids, not in the solutions. It is advisable no to dissolve the trapped grains of halite (dissolving temperature: 275–300°C) if not needed, because the bubble of the released high-pressure gas covers large parts of the solid phases after the heating runs.

By the aid of the holes after now dissolved carnallite in the pyramids of some crystals, combined with carnallitic inclusions in the same crystals, it is proved that the melting temperature of carnallite depends on the prevailing pressure.

Based on the results of the microthermometry, the recent paragenesis of the Veggerby Potash Zone, and the $MgCl_2$–KCl mineralization of the deck halite used in the present work, a model of the geological events is proposed:

i. At the end of Zechstein 2, the deck halite Na2r sedimented in the deeper parts of the basin, south of the later Mors dome.
ii. The salt began viscous flow updip in the direction of the later Mors dome, when the lithostatic load exceeded 40 MPa in Early Triassic time.
iii. The original potash bed, consisting of the paragenesis kieserite-carnallite-halite, was subject to progressive geothermal metamorphism in Upper Triassic. The lithostatic load was approximately 70 MPa and the temperature c. 175°C.
iv. The metamorphic $MgCl_2$–KCl lye was squeezed out from the potash bed into the hanging wall, the deck halite. The quartz crystals formed in Late Triassic-Early Cretaceous times under pressures of 75–125 MPa and temperatures in the interval 170–185°C.
v. The salt possibly entered the diapir in Jurassic. During the diapiric penetration phase in Upper Jurassic-Lower Cretaceous times, the deck halite possibly was overrun by the Zechstein 1 and 2 grey salt, resulting in many overthrusts and faults, and a reversed stratigraphic position of the entire Zechstein column.

Acknowledgements

The author wishes to thank Fritz Lyngsie Jacobsen, Geological Survey of Denmark, for invaluable discussions on salt chemistry and related subjects and for critical review of this manuscript. John Rose-Hansen and Jens Konnerup-Madsen, University of Copenhagen, are gratefully acknowledged for critical review and constructive comments. The author would like to thank Kerstin Kåla, Geological Survey of Denmark, for her valuable translations of the Russian papers used. This work was supported by a grant from the Ministry of Energy (EFP-84).

Reference list

d'Ans, J., 1933: Die Lösungsgleichgewichte der Systeme der Salze ozeanischer Salzablagerungen. Ackerbau Verlag, Berlin: 254 pp.

d'Ans, J., 1961: Über Die Entwässerung der Magnesiumchloridhydrate und des Carnallites. Kali u. Steinsalz. 3.4: 126–129.

d'Ans, J., and Sypiena, G., 1942: Löslichkeiten im System KCL-$MgCl_2$–H_2O und NaCl–$MgCl_2$–H_2O bei Temperaturen bis etwa 200°C. Kalivervandte Salze und Erdöl. 36: 89–95.

d'Ans, J., and Kühn, R., 1960: Bemerkungen zu Bildungen Ozeanischer Salzlagerstätten. Kali u. Steinsalz. Band 3, Heft 3: 71–84.

Arbey, F., 1980: Les formes de la silice et l'identification des évaporites dans les formations silicifiées. Bull. Centre Rech. Explor.-Prod. Elf-Aquitaine, 4: 309–365.

Baar, A., 1952: Entstehung und Gesetzmässigkeiten der Fazieswechsel im Kalilager am Südharz (II). Bergakademie. Vol. 4. 138–150.

Baar, A., 1958: Über Gebirgsverformungen durch bergmännischen Abbau von Kaliflözen bzw. durch chemische Umbildungen von Kaliflözen in geologischer Vergangenheit. Freib. Forsch.-H., A 123: 137–159.

Baar, A., 1960: Über die fazielle Entwicklung der Kalilagerstätte des Stassfurtflözes N.Jb. Geol. Palaont. Abh. 111.1: 111–135.

Baar, C. A., 1977: Applied salt-rock mechanics 1; the in-situ behavior of salt rocks. Elsevier Sci. Pub. Co. Amsterdam. 283 pp.

Bachmann, K., 1985: Mineralogische und geochemische Untersuchungen an Bohrkernen des Stassfurt-Steinsalzes im Salzstock Asse. Kali u. Steinsalz. 9.4: 132–138.

Bachu, S., 1985: Influence of lithology and fluid flow on the temperature distribution in a sedimentary basin: A case study from the Cold Lake Area, Alberta, Canada. Tectonophysics. 120: 257–284.

Bain, G. W., 1936: Mechanics of Metasomatism. Econ. Geol. 31: 505–526.

Bergman, A. G. and Luzhnaya, K. P., 1951: The physicochemical basis for the study and use of chloride-sulfate salt deposits. Zzd. Akad. Nauk. SSSR, Moscow (in Russian).

Bodenlos, A. J., 1970: Cap-rock development and salt-stock movement. In: D. H. Kupfer (Editor), Geology and Technology of Gulf Coast Salt. Sch. Geosci., LSU: 73–86 c.

Bodnar, R. S. and Bethke, P. M., 1984: Systematics of stretching of fluid inclusions I: Fluorite and Sphalerite at 1 atmosphere confining pressure. Econ. Geol. 79: 141–161.

Borchert, H., 1940: Die Salzlagerstätten des deutschen Zechsteins, ein Beitrag zur Entstehung ozeaner Salzablagerungen. Arch. f. Lagerstättenforsch., H.67. Berlin.

Borchert, H., 1958: Grundzüge der Entstehung und Metamorphose ozeaner Salzlagerstätten. Freib. Forsch.-H., A 123: 11–40.

Borchert, H., 1972: Secondary replacement processes in salt and potash deposits of oceanic origin. Unesco, 1972. Geology of saline deposits. Proc. Hannover Symp. 1968. (Earth Sciences 7): 61–68.

Borchert, H. and Muir, R., 1964: Salt Deposits. D. Van Nostrand Company, Ltd. London: pp. 338.

Borisenko, A. S., 1978: Study of the salt composition of solutions of gas-liquid inclusions in minerals by the cryometric method. The Allerton Press Journal Program: 11–19.

Borowitzka, L. S., 1981: The microflora. Adaptions to life in extremely saline lakes. Hydrobiologia 81: 33–46.

Braitsch, O., 1962: Entstehung und Stoffbestand der Salzlagerstätten. Springer-Verlag, Berlin-Göttingen-Heidelberg: 232 pp.

Braitsch, O., 1971: Salt deposits. Their origin and composition. Springer-Verlag. Berlin-Heidelberg-New York: 297 pp.

Braitsch, O. und Herrmann, A. G., 1964: Zur Geochemie des Broms in salinaren Sedimenten. Teil II: Die Bildungstemperaturen primärer Sylvin- und Carnallit-Gesteine. Geochim. Cosmochim. Acta, 28: 1081–1109.

Buckley, H. E., 1934: On the Mosaic Structure in Crystals. Zeitschr. Kristallographie, 89: 221–241.

Buerger, M. J., 1932: The significance of "Block Structure" in crystals. Am. Min., 17: 177–191.

Campbell, A. N., Downes, K. W., and Samis, C. S., 1934: The system $MgCl_2$–KCl–$MgSO_4$–K_2So_4–H_2O at 100°. J. Am. Chem. Soc., 56.12: 2507–2512.

Crawford, M. L., 1981: Phase equilibria in aqueous fluid inclusions. In: L. S. Hollister and M. L. Crawford (Editors), Short Course in Fluid Inclusions, Vol. 6: Applications to Petrology. Mineral. Assoc. Can., Calgary, Alta.: pp. 75–99.

Demageon, P., 1966: A propos des quartz authigènes des terrains salifères. Bull. Soc. Franc. Miner. Crist., 89: 484–487.

Dickinson, G., 1953: Geological aspects of abnormal reservoir pressures in Gulf Coast Louisiana. Bull. Amer. Assoc. Petrol. Geol. 37.2: 410–32.

Dietzel, H., 1959: Die Dichten im System $MgCl_2$–H_2O zwischen 20° und 160°C. Freib. Forsch.-H., A132: 21–32.

Dietzel, H. und Serowy, F., 1959: Die Lösungsgleichgewichte des Systems $MgCl_2$–H_2O zwischen 20° und 200°C. Freib. Forsch.-H., A132: 1–19.

Duffell, S., 1937: Diffusion and its relation to Ore Deposition. Econ. Geol., 32.4: 494–510.

Duffy, S. R., Smith, N. O., and Nagy, B. 1961: Solubility of natural gases in aqueous salt solutions – I. Liquidus surfaces in the system CH_4–H_2O–NaCl–$CaCl_2$ at room temperatures and at pressures below 1000 psi. Geochim. et Cosmochim. Acta, 24: 23–31.

Eekelen, H. A. van, Hulsebos, T., and Urai, J. L., 1981: Creep of Biochofite. First Conference on the Mechanical Behaviour of Salt: 389–405.

Fabricius, J., 1984: Formation temperature and chemistry of brine inclusions in euhedral quartz crystals from Permian salt in the Danish Trough. Bull. Mineral., 107: 203–216.

Fabricius, J., 1985: Studies of fluid inclusions in halite and euhedral quarz crystals from salt domes in the Norwegian-Danish basin. In: B. C. Schreiber and H. L. Harner (Editors), Sixth International Symposium on Salt, Toronto, 1983. The Salt Institute, Alexandria, Virginia, USA, 1: 247–255.

Fabricius, J., 1987: Natural Na–K–Mg–Cl solutions and solid derivatives trapped in euhedral quartz from Danish Zechstein salt. In: E. E. Horn and H.-J. Behr (Guest-Editors), Current Research on Fluid Inclusions. Chem. Geol., 61: 95–112.

Fabricius, J. and Rose-Hansen, J., in prep.: Pressure-dependent melting of carnallite, $KMgCl_3 \cdot 6H_2O$, in a closed system. Bull. Mineral.

Faingersh, L. A., 1977: Particularities of gas accumulations in Paleozoic subsalt deposits of the Arctic syneclise (in Russian). In: "Problems of Salt Accumulation" (L. A. Yanshiw and M. A. Zharkov, eds.), Izd. Nanka, Akad. Nank SSSR, Sib. Otd., Novosibirsk, vol. 2: 308–311.

Findlay, X., 1907: Einführung in die Phasenlehre. Ambrosius Barth, Leipzig.

Fyfe, W. S., Price, N. S., and Thompson, A. B., 1978: Fluids in the Earth's crust. Elsevier, Amsterdam, vol. 1: 383 pp.

Geller, A., 1930: Das Schmelzen von Salzen bei hohen Drucken in seiner Bedeutung für den Vorgang der Salzmetamorphose. Fortschr. d. Min.: Bd. 14: 143–166.

Giesel, W., 1968: Kohlensäureausbrüche im Kohlbergbau an der Werra – Grundlagen und Prognosemöglichkeiten. Kali u. Steinsalz, 5: 103–108.

Giesel, W., 1972: Outbursts of carbon dioxide in potash mines – fundamentals and possibilities of forecast. Geology of saline deposits. UNESCO: 235–239.

Goldsmith, L. H., 1969: Concentration of Potash Salts in Saline Basins. Am. Ass. Petr. Geol. Bull. 53.4: 790–797.

Grimm, W.-D., 1962a: Idiomorphe Quarze als Leitmineralien für salinare Fazies. Erdöl und Kohle, 11: 880–887.

Grimm, W.-D., 1962b: Ausfällung von Kieselsäure in salinar beeinflussten Sedimenten. Z. deutsch. geol. Ges., 114: 590–619.
Grube, G. und Bräuning, W., 1938: Über die Entwässerung von Magnesium-Chloridhexahydrat und Carnallit. Ztschr. Elektrochem., 44: 134–143.
Haas, J. L., 1971: The Effect of Salinity on the Maximum Thermal Gradient of a Hydrothermal System at Hydrostatic Pressure. Econ. Geol., 66: 940–946.
Harder, H., 1965: Experimente zur "Ausfällung" der Kieselsäure. Geochim. Cosmoschim. Acta, 29: 429–442.
Harvie, C. E., Weare, J. H., Hardie, L. A., and Eugster, M. P., 1980: Evaporation of seawater: Calculated mineral sequences. Science, 208: 498–500.
Harville, D. G. and Fritz, S. J., 1986: Modes of diagenesis responsible for observed succession of potash evaporites in the Salado Formation, Delaware Basin, New Mexico. Jour. Sed. Petr. 56, No. 5: 648–656.
Haug, R., 1933: Ueber den tensiendiometrischen Abbau des Bischoffits. Adolf Remppis, Marbach a. Neckar: 53 pp.
Hentschel, J., 1961: Die Faciesunterschiede im Flöz Stassfurt des Kalisalzbergwerkes Königshall-Hindenburg. Kali u. Steinsalz 3: 137–157.
Herrmann, A. G., 1980: Geochemische und mineralogische Grundlagen für die Endlagerung radioaktiver Substanzen in Salzdiapiren Norddeutschlands. Fortschr. Miner., 58.2: 169–211.
Hinze, E., Will, G., Jockwer, N. und Gies, H., 1985: Entwässerungsverhalten von hydratisierten Salzphasen als Funktion des Drucks. Fortschr. Minera., 63, Beiheft 1: p. 98.
Hodenberg, R. v., Fischbeck, R., Kühn, R., 1987: Beitrag zur Kenntnis der Salzminerale, Salzgesteine und Salzlagerstätten, insbesondere im deutschen Zechstein. Aufschluss, 38: 77–92.
van't Hoff, J. H. und Meyerhoffer, W., 1898: Z. phys. Chemie, 27: 81.
van't Hoff, J. H. und Meyerhoffer, W., 1899: Über Anwendung der Gleichgewichtslehre auf die Bildung ozeanischer Salzablagerungen mit besonderer Berücksichtigung des Stassfurter Salzlagers. Z. phys. Chemie, 30: 64–88.
Holser, W. T., 1947: Metasomatic processes. Econ. Geol., 42: 384–395.
Holser, W. T., 1979: Mineralogy of Evaporites. In: R. G. Burns (Editor), Marine Minerals, Mineral. Soc. Am. Short Course Notes Vol. 6: 211–294.
Hower, J., Eslinger, E. V., Hower, M. E., and Perry, E. A., 1976: Mechanism of burial metamorphism of argillaceous sediment: 1. Mineralogical and chemical evidence. Geol. Soc. Am. Bull., 87: 725–737.
Jackson, M. P. A. and Talbot, C. J., 1986: External shapes, strain rates, and dynamics of salt structures. Geol. Soc. Am. Bull. 97: 305–323.
Jacobsen, F. L., 1984: Lithostratigraphy of the Zechstein salts in the Norwegian-Danish basin. DGU series C No. 1, 2: 7–70.
Jacobsen, F. L. and Christensen, O. W., 1980: Erslev No. 1. Well Completion Report. DGU Well File No. 37.882: 145 pp.
Jänecke, E., 1915: Die Entstehung der deutschen Kalisalzlager. Friedr. Vieweg & Sohn, Braunschweig: 109 pp.
Jänecke, E., 1949: Über das inkongruente Schmelzen von Salzhydraten bis zum Auftreten von Eis VI, insbesondere von $NaCl{\cdot}2H_2O$. Z. Elektrochem. angew. phys. Chem., 53.4: 250–254.
Khaibullin, I. Kh. and Borisov, N. M., 1966: Experimental investigation of the thermal properties of aqueous and vapor solutions of sodium and potassium chlorides at phase equilibrium. Teplofizika Vysokikh Temperatur, 4.4: 518–523. Translated in High Temperature, 4: 489–494.
Kern, H. und Franke, J.-H., 1980: Thermische Stabilität von Carnallit unter Lagerstättenbedingungen. Glückauf-Forschungshefte, 6: 252–255.
Kern, H. und Franke, J.-H., 1986: Carnallit – thermisches und thermomechanisches Verhalten in Endlager-Salzstöcken. Z. dt. geol. Ges., 137: 1–27.
Kinsman, D. J. J., Boardmand, M., and Borcsik, H., 1974: An experimental determination of the solubility of oxygen in marine brines. In: A. H. Coogan (Editor), Fourth Symposium on Salt. Northern Ohio Geol. Soc. 1: 325–327.
Klockmann, 1978/1980: Lehrbuch der Mineralogie. P. Ramdohr und H. Strunz, eds. Ferdinand Enke, Stuttgart: 876 pp. + 55 pp.
Knipping, B. and Herrmann, A. G., 1985: Mineralreaktionen und Stofftransporte an einem Kontakt Basalt-Carnallit im Kalisalzhorizont Thüringen der Werra-Serie des Zechsteins. Kali und Steinsalz, 9.4: 111–124.
Kokorsch, R., 1960: Zur Kenntnis von Genesis, Metamorphose und Faziesverhältnissen des Stassfurtlagers in Grubenfeld Hildesia-Mathildenhall, Diekholzen bei Hildesheim. Beih. Geol. Jb., 41: 140 pp.
Kucha, H. and Pawlikowski, M., 1986: Two-brine model of the genesis of strata-bound Zechstein deposits (Kupferschiefertype), Poland. Mineral. Deposita, 21: 70–80.
Kühn, R., 1950/51: Nachexkursion im Kaliwerk Hattorf, Philippsthal – als Beitrag zur Kenntnis der Petrographie des Werra-Kaligebietes. Fortschr. d. Miner, 29/30: 101–114.
Kühn, R., 1952: Reaktionen zwischen festen, insbesondere ozeanischen Salzen. Heidelberger Beiträge zur Mineralogie und Petrographie, 3: 147–168.
Kühn, R., 1968: Geochemistry of the German Potash Deposits. Geol. Soc. Am. Special Paper, 88: 427–504.
Larsen, O., 1971: Kalium/argon datering af prøver fra danske dybdeboringer. Dansk geol. Foren. Årsskrift for 1971: 91–94.
Larson, L. T., Miller, J. D., Nadeau, J. E., and Roedder, E., 1973: Two sources of Error in Low Temperature Inclusion Homogenization Determination and Corrections on Published Temperatures for the East Tennessee and Laisvall Deposits. Econ. Geol., 68: 113–116.
Lee, W. B. and Egerton, A. C., 1923: Heterogeneous Equilibria between the chlorides of Calcium, Magnesium, Potassium, and their aqeous solutions. Part I. J. Chem. Soc.: 706–716.
Lepeschkow, I. N., 1958: Untersuchungen der Schule N. S. Kurnakows zur physikalischen Chemie der natürlichen Salze und Salzsysteme. Freib. Forsch.-H., A 123: 105–118.
Lightfoot, W. S. and Prutton, C. F., 1948: Equilibria in saturated solutions. III. The Quaternary System $CaCl_2$–KCl–H_2O at 35°. J. Am. Chem. Soc., 70: 4112–4115.
Luzhnaya, N. P. and Verescetina, I. P., 1946: Sodium, Calcium and Magnesium Chlorids in Aqueous Solutions of −57° to +25° (Polythermic Solubility). (in Russian). Journal of applied Chemistry, 19, No. 7: 723–733.
Maar, U., 1958: Die Bildung des Stassfurt-Flözes unter Berücksichtigung geochemischer Untersuchungen. Freib. Forsch.-H., A. 88: 85–96.
Meyer, T. A., Prutton, C. F., and Lightfoot, W. J., 1949: Equilibria in saturated salt solutions. V. The quinary system $CaCl_2$–$MgCl_2$–KCl–NaCl–H_2O at 35°. J. Am. Chem. Soc., 71: 1236–1237.
Michelsen, O., Saxov, S., Leth, J. A., Andersen, C., Balling, N., Breiner, N., Holm, L., Jensen, K., Kristiansen, J. I., Laier, T., Nygaard, E., Olsen, J. C., Poulsen, K. D., Priisholm, S., Raade, T. B., Sørensen, T.R. and Wurtz, J., 1981: Kortlægning af potentielle geotermiske reservoirer i Danmark. DGU serie B nr. 5: 96 pp.
Myagkov, V. F., 1961: Distribution of bromine in the sylvinites of the Upper Kama deposit. Geochemistry, 8: 772–776.
Müller, P. und Heymel, W., 1956: Verfahren zur Bestimmung der Gaskonzentrationen des Südharz- und Werrakalibergbaus. Bergbautechnik, 6: 313–318.
Nachsel, G., 1966: Quarz als Faziesindikator. Zeitschr. angew. Geol., 12: 322–326.
Naumow, V. B., 1982: Possibilities of determination of pressure and density of mineralforming substances based on inclusions in minerals. (in Russian) N. P. Laverorv ed. Nedra, Moscou: 85–94.
Peterson, J. A. and Hite, R. J., 1969: Pennsylvanian Evaporite-Carbonate Cycles and Their Relation to Petroleum Occurrence, South Rocky Mountains. Am. Ass. Petr. Geol. Bull., 53.4: 884–908.
Pichavant, M., Ramboz, C., and Weisbrod, A., 1982: Fluid immiscibility in natural processes: Use and misuse of fluid inclusion data. I., Chem. Geol., 37: 1–27.
Potter, R. W. II and Clynne, M. A., 1978: Solubility of Highly Soluble Salts in Aqueous Media. – Part I, NaCl, KCl, $CaCl_2$, Na_2SO_4 and K_2SO_4 Solubilities to 100°C. Jour. Research U.S.G.S., 6, No. 6: 701–705.
Potter, R. W. II and Haas, J. L. jr., 1978: Models for calculating density and vapor pressure of geothermal brines. Journal of Research, U.S.G.S., 6, No. 2: 247–57.
Priisholm S. Frandsen N., Fine, St., Abatzis, I., Balling, N., Friis, H., Gosk E., Holm, L., Kristiansen, J. I., Laier, T., Michelsen, O.,

Nielsen, A. I., and Nygaard, E., 1982: Geothermal reservoirs in Denmark. Geol. Surv. Denmark. 3 volumes.
Priisholm, S. and Christensen, S., 1985: Assesment of geothermal resources and reserves in Denmark. DGU series C, No. 2: 54 pp.
Prutton, C. F. and Savage, R. L., 1945: The solubility of carbon dioxide in calcium chloride-water solutions at 75, 100, 120° and high pressures. Am. Chem. Soc. Jour., 67: 1550–1554.
Ramboz, C., Pichavant, M., and Weisbrod, A., 1982: Fluid immiscibility in natural processes: Use and misuse of fluid inclusion data II. Chem. Geol. 37: 29–48.
Rasmussen, L. B., 1974: Some geological results from the first five Danish exploration wells in the North Sea. Geol. Surv. Denmark, III. ser. No. 42: 42 pp.
Raup, O. B., 1970: Brine mixing: an additional mechanism for formation of basin evaporites. Am. Ass. Petr. Geologists Bull. 54,12: 2246–2259.
Richter-Bernburg, G., 1953: Stratigraphische Gliederung des deutschen Zechsteins. Z. deutsch. geol. Ges. 105: 843–854.
Richter-Bernburg, G., 1955: Geologische Voraussetzungen für die Genese von Kalisalzlagerstätten. Kalium-Symposium 1955: 19 pp. (Separatdruck), Internationales Kali-Institut, Bern.
Richter-Bernburg, G., 1960: Zeitmessung geologischer Vorgänge nach Warven-Korrelationen im Zechstein. Geol. Rundschau, Bd. 49/1: 132–148.
Richter-Bernburg, G., 1962: Geologische Stellungnahme zum Ergebnis der Bohrung Suldrup 4A und zur Frage weiterer Salzbohrungen. In: Kaliboringerne ved Suldrup 1959–1961, Bind I, bilag 4. Egnsudviklingsraadets Boreudvalg.
Richter-Bernburg, G., 1970: Contribution to discussion. In: Geology and Technology of Gulf Coast Salt (Kupfer, D. H., ed.), A symposium 1967. School of Geoscience. Louisiana. USA.
Richter-Bernburg, G., 1972: Saline deposits in Germany: a review and general introduction to the excursions. Unesco 1972, Geology of saline deposits. Proc. Hannover Symp., 1968 (Earth Sciences, 7.): 275–287.
Richter-Bernburg, G., 1977: Sicher im Salz. Bild der Wissenschaft, 12: 81–100.
Richter-Bernburg, G., 1981: Geological remarks about the North Jutland Salt Domes in respect on their suitability for radioactive waste disposal. 39 pp. Unpublished.
Richter, A. und Klarr, K., 1984: Bischofit im Stassfurtflöz der Asse. Kali u. Steinsalz, 9: 94–101.
Roedder, E., 1967: Metastable Superheated Ice in Liquid-Water Inclusions under High Negative Pressure. Science, 155, II: 1413–1417.
Roedder, E., 1971: Metastability in fluid inclusions. Soc. Mining Geol. Japan, Spec. Issue, 3: 327–34.
Roedder, E., 1972: Composition of fluid inclusions. Data of Geochemistry, Geol. Surv. Prof. Paper: 440–JJ.
Roedder, E., 1979: Fluid Inclusions as Samples of Ore Fluids. In: Geochemistry of Hydrothermal Ore Deposits. John Wiley & Sons: 798 pp.
Roedder, E., 1981a: Natural occurrence and significance of fluids indicating high pressure and temperature. Physics and Chemistry of the Earth, Vol. 13/14: 9–14.
Roedder, E., 1981b: Origin of fluid inclusions and changes that occur after trapping. In: L. S. Hollister and M. L. Crawford (Editors), Short Course in Fluid Inclusions, Vol. 6: Applications to Petrology. Mineral. Assoc. Can., Calgary, Alta.: pp. 101–137.
Roedder, E. and Bodnar, R. J., 1980: Geologic pressure determinations from fluid inclusion studies. In: Annual Review of Earth and Planetary Sciences (ed. Donath, F. A. et al), vol. 8: 263–301.
Roedder, E. and Skinner, B. J., 1968: Experimental evidence that Fluid Inclusions do not leak. Econ. Geol., vol. 63, No. 7: 715–730.
Sasvari, K. and Jeffrey, G. A., 1966: The crystal structure of Magnesium Chloride Dodecahydrate, $MgCl_2 \cdot 12H_2O$. Acta Cryst., 20: 875–881.
Schwerdtner, W. H., 1964: Genesis of Potash rocks in Middle Devonian Prairie Evaporite Formation of Saskatchewan. Am. Ass. Petr. Geol. Bull, 48.7: 1108–1115.
Serowy, F. and Tittel, M., 1959: Zur Frage der thermischen Behandlung von Carnallit und Bischofit. Freib. Forsch.-H., A 128: 1–88.
Skinner, B. J., 1953: Some considerations regarding liquid inclusions as geologic thermometers. Econ. Geol., vol. 48, No. 7: 541–550.
Smith F. G., 1954: Composition of vein-forming fluids from inclusion data. Econ. Geol., Vol. 49, No. 2: 205–210.
Sonnenfeld, P., 1984: Brines and Evaporites. Academic Press, Inc.: 613 pp.
Sonnenfeld, P., 1985: Evaporites as oil and gas source rocks. J. Petr. Geol., 8.3: 253–271.
Sterner, S. M. and Bodnar, R. J., 1984: Synthetic fluid inclusions in natural quartz I. Compositional types synthesized and applications to experimental geochemistry. Geochim. Cosmochim. Acta, 48: 2659–2668.
Stewart, F. H., 1956: Replacements involving early carnallite in the potassium-bearing evaporites of Yorkshire. Mineralogical Magazine, 31: 127–135.
Stewart, D. B. and Potter, R. W., 1979: Application of Physical Chemistry of Fluids in Rock Salt at elevated Temperature and Pressure to Repositories for Radioactive Waste. Scientific Basis for Nuclear Waste Management, Plenum Press, vol. 1: 297–311.
Strakhov, N. M., 1962: Principles of Lithogenesis. Vol. 3. (in Russian). Translated 1970, Plenum Publishing Corporation, New York, Vol. 3, Chapter 2.
Swanenberg, H. E. C., 1980: Fluid inclusions in high-grade metamorphic rocks from S. W. Norway. Geologica Ultraiectina No. 25. 147 pp.
Takenouchi, S. and Kennedy, G. C., 1965: The solubility of Carbon Dioxide in NaCl solutions at high temperatures and pressures. Am. Jour. Sci., 263: 445–454.
Talbot, C. S., Tully, C.P., and Woods, P. J. E., 1982: The structural geology of Boulby (Potash) mine, Cleveland, United Kingdom. Tectonophysics, 85: 167–204.
Titov, A. V., 1939: Effect of temperature on the composition of complexes obtained by the interaction of chloride solutions. (in Russian). Tr. Ivanov. Khim. – Technol. Inst., 2: 12–24.
Titov, A. V., 1949: Complex compounds formed by magnesium chloride in aqueous solutions. Zh. Obshch. Khim., 19.3: 458–461 (in Russian).
Tollert, H., 1950a: Über den Nachweis von Molekülen höherer Ordnung in Mischungen verdünnter wässeriger Elektrolyt-Lösungen und über einen neuen Trenneffekt. Z. Phys. Chem., 195: 237–243.
Tollert, H., 1950b: Über die Verteilung der Temperatur, der Konzentration und der Strömungsgeschwindigkeit in dynamisch-polythermen Systemen. Z. Phys. Chem., 195: 281–294.
Tollert, H., 1956: Die kinetische und stationäre Bestimmung von Lösungsgleichgewichten leichtlöslicher Salze und deren thermodynamische Grundlagen zur Deutung des metastabilen Sättigungszustandes mit Hilfe der Hydratationsenthalpien. Zeitschrift für Physikalische Chemie, Neue Folge, 6: 242–260.
Tuttle, 0. F., 1949: Structural petrology of planes of liquid inclusions. Jour. Geol., 57.4: 331–356.
Urai, J. C., 1983: Water assisted dynamic recrystallization and weakening in polycrystalline Bischofite. Tectonophysics, 96: 125–157.
Urai, J. L. and Boland, J. N., 1985: Development of microstructures and the origin of hematite in naturally deformed carnallite. N. Jb. Miner. Mh. H2: 58–72.
Waljaschko, M. G., 1958: Die wichtigsten geochemischen Parameter für die Bildung der Kalisalzlagerstätten. Freib. Forsch.-H., A 123: 197–235.
Waljaschko, M. G., 1972: Scientific works in the field of geochemistry and the genesis of salt deposits in the U.S.S.R. Geology of saline deposits. UNESCO: 289–301.
Wardlaw, N. C., 1968: Carnallite-Sylvite relationships in the Middle Devonian Prairie Evaporite Formation, Saskatchewan. Geol. Soc. Am. Bull., 79: 1273–1294.
Wardlaw, N. C., 1970: Effects of fusion, rates of crystallization and leaching on bromide and rubidium solid solutions in halite, sylvite and carnallite. In: J. L. Rau and L. F. Dellwig (Editors), Third Symposium on Salt. Northern Ohio Geol. Soc. 1: 223–231.
Weaver, C. E. and Pollard, L. D., 1973: The Chemistry of Clay Minerals. Elsevier, Amsterdam, London, New York: 213 pp.
Winckler, H. G. F., 1967: Petrogenesis of metamorphic rocks. Revised second edition. Springer-Verlag, Berlin, Heidelberg, New York: 237 pp.
Zdanovskij, A. B., 1949; The use of Secenov's formula on strong electrolyte solutions. Zh. Obshch. Khim, 19.4: 577–592. (in Russian).
Ziegler, P. A., 1981: Evolution of Sedimentary Basins in North-West Europe. Petr. Geol. of the Continental Shelf of North-West Europe. London: 3–39.
Zyndel, F., 1914: Über Quarzzwillinge mit nichtparallelen Hauptaxen. Zeitschr. Krystallogr., 53: 15-52.

The natural Na-K-Mg-Cl-H_2O system is present in the Zechstein 2 evaporite cycle in the well Erslev-1, Mors. The system is studied in detail by means of microthermometry on solid inclusions in quarts crystals from the very top of the Zechstein 2 cycle. The measurements give rise to a model in time and space of the metamorphism of the originally sedimented K-Mg zone, resulting in the present Veggerby Potash Zone.

ISBN 87-421-0751-2
ISSN 0901-0270